

**UNIVERSITY OF CRETE
DEPARTMENT OF CHEMISTRY**

GENERAL POSTGRADUATE PROGRAMME



MASTER THESIS

**MECHANICALLY-INDUCED MAIN CHAIN SCISSION
OF POLYACETALS FOR CONTROLLED DRUG
RELEASE**

MARIA PSARROU

Supervisor: Prof. SPIROS ANASTASIADIS

HERAKLION 2018

ΠΑΝΕΠΙΣΤΗΜΙΟ ΚΡΗΤΗΣ

ΤΜΗΜΑ ΧΗΜΕΙΑΣ

ΓΕΝΙΚΟ ΜΕΤΑΠΤΥΧΙΑΚΟ ΠΡΟΓΡΑΜΜΑ ΣΠΟΥΔΩΝ



ΜΕΤΑΠΤΥΧΙΑΚΟ ΔΙΠΛΩΜΑ ΕΙΔΙΚΕΥΣΗΣ

**ΜΗΧΑΝΙΚΑ ΕΠΑΓΟΜΕΝΗ ΔΙΑΣΠΑΣΗ ΤΗΣ ΚΥΡΙΑΣ
ΑΛΥΣΙΔΑΣ ΠΟΛΥΑΚΕΤΑΛΩΝ ΓΙΑ ΤΗΝ
ΕΛΕΓΧΟΜΕΝΗ ΑΠΟΔΕΣΜΕΥΣΗ ΦΑΡΜΑΚΩΝ**

ΜΑΡΙΑ ΨΑΡΡΟΥ

Υπεύθυνος Καθηγητής: ΣΠΥΡΟΣ ΑΝΑΣΤΑΣΙΑΔΗΣ

ΗΡΑΚΛΕΙΟ 2018

Στους γονείς μου

Εξεταστική Επιτροπή

Σπύρος Αναστασιάδης
Καθηγητής, Τμήμα Χημείας, Π.Κ

Μαρία Βαμβακάκη
Καθηγήτρια, Τμήμα Επιστήμης και Τεχνολογίας Υλικών, Π.Κ

Σταυρούλα Μπαριτάκη
Επίκουρη Καθηγήτρια Πειραματικής Ογκολογίας, Ιατρική Σχολή, Π.Κ

ACKNOWLEDGMENTS

I would like to thank all the people that have supported me and helped in the fulfillment of this thesis during these 2 years.

First, I would like to express my very great appreciation to my supervisor Professor Maria Vamvakaki for giving me the opportunity to carry out this master thesis. I want to thank her for her guidance, advice and the opportunity to participate in conferences and learn more about research and science throughout these years. I would also like to thank Professor Spiros Anastasiadis for his willingness to supervise this thesis and Assistant Professor Stavroula Baritaki for participating in my committee.

I would also like to express my gratitude to my co-supervisor Dr. Theodore Manouras for the collaboration, for his guidance and for all these things that I have learned from him in the lab through these years.

I want to thank my colleagues at the polymer lab Lefteris, Eva, Lucille, Dr. Maria Kaliva, Nicky, Kostas, Sophia and Elmina for their support and their collaboration.

A huge thank you goes to my friends outside the lab, for understand my “no time” but being always next to me to support me.

And finally the biggest thank you goes to my parents, my brother and all my beloved family for supporting and encouraging me everyday all these years.

Thank you all!!!

ΒΙΟΓΡΑΦΙΚΟ ΣΗΜΕΙΩΜΑ

Όνοματεπώνυμο
Διεύθυνση κατοικίας
Τηλέφωνο επικοινωνίας
E-mail
Υπηκοότητα
Ημερομηνίας γέννησης
Τόπος γέννησης
Οικογενειακή κατάσταση

ΨΑΡΡΟΥ ΜΑΡΙΑ

Θερίσου 24, Ηράκλειο Κρήτης, Ελλάδα, ΤΚ 71304
6949522720

psarroum@iesl.forth.gr

Ελληνική
6 Οκτωβρίου 1994
Μυτιλήνη, Λέσβος
Άγαμη

ΕΚΠΑΙΔΕΥΣΗ-ΣΠΟΥΔΕΣ

9/2016 έως 11/2018

Μεταπτυχιακές σπουδές στη Σύνθεση και Χαρακτηρισμό Πολυμερών

Πανεπιστήμιο Κρήτης, Ηράκλειο, Τμήμα Χημείας, Τομέας Φυσικοχημείας

Τίτλος πτυχιακής εργασίας: «Μηχανικά επαγόμενη διάσπαση της κύριας αλυσίδας πολυακετάλων για ελεγχόμενη αποδέσμευση φαρμάκων»

Υπεύθυνος Καθηγητής: Αναστασιάδης Σπύρος

Συνυπεύθυνη Καθηγήτρια: Βαμβακάκη Μαρία

9/2012 έως 9/2016

Πτυχίο στην Επιστήμη και Τεχνολογία Υλικών

Πανεπιστήμιο Κρήτης, Ηράκλειο

Βαθμός πτυχίου: Λίαν καλώς (6,8)

Τίτλος διπλωματικής εργασίας: «Σύνθεση και χαρακτηρισμός πολυμερών αποικοδομίσιμων με χρήση φωτός και υπερήχων»

Υπεύθυνη Καθηγήτρια: Βαμβακάκη Μαρία

Μαθήματα Ειδικότητας: Φυσική πολυμερών, Χημεία πολυμερών, Κolloειδή συστήματα, Σύνθετα Βιοϋλικά, Βιο-οργανικές νανοδομές

6/2012

Απολυτήριο Γενικού Λυκείου

Μανταμάδος, Λέσβος

ΕΠΑΓΓΕΛΜΑΤΙΚΗ/ ΕΡΕΥΝΗΤΙΚΗ ΕΜΠΕΙΡΑ

9/2016 έως σήμερα

Ερευνήτρια

Εργαστήριο Συνθετικής Χημείας Υλικών, Πανεπιστήμιο Κρήτης

Κύρια θέματα-Επαγγελματικές δεξιότητες

- Σύνθεση και χαρακτηρισμός ομοπολυμερών και συμπολυμερών πολυακετάλων με αντίδραση πολυσυμπύκνωσης.
- Αυτό-οργάνωση (self-assembly) αμφίφιλων πολυμερών σε νερό και ενκαψυλίωση δραστικών μορίων.
- Μελέτη του μηχανισμού διάσπασης της κύριας αλυσίδας

πολυακετάλων με χρήση μηχανικής ενέργειας. Εφαρμογές στην ελεγχόμενη αποδέσμευση φαρμάκων.

- Σύνθεση και χαρακτηρισμός γραμμικών και αστεροειδών (star-like polymers) πολυμερών μέσω αντίδρασης μεταφοράς ομάδας (Group Transfer Polymerization).
- Μελέτη και ανάπτυξη νέου μηχανισμού για το ριζικό πολυμερισμό μεταφοράς ατόμου (Atom Transfer Radical Polymerization) βασισμένο σε υπερήχους. Σύνθεση και χαρακτηρισμός ακρυλικών και μεθακρυλικών πολυμερών.
- Ανάπτυξη ενός καινοτόμου φώτο-ελεγχόμενου συστήματος απελευθέρωσης φαρμάκων από νανομεταφορείς βασισμένους σε πολυακετάλες μέσω ενεργειακά «ασυνήθιστων» φωτοχημικών διεργασιών.

Τεχνικές χαρακτηρισμού πολυμερών:

- Φασματοσκοπία πυρηνικού μαγνητικού συντονισμού (NMR).
- Φασματοφωτομετρία υπεριώδους-ορατού (UV/Visible).
- Φασματοσκοπεία φθορισμού.
- Χρωματογραφία αποκλεισμού μεγεθών (GPC or SEC).
- Δυναμική σκέδαση φωτός (Light scattering).

7/2015-9/2015

Πρακτική Άσκηση

Ινστιτούτο Ηλεκτρονικής Δομής και Λείζερ, Ίδρυμα Τεχνολογίας και Έρευνας, Ηράκλειο Κρήτης, Ελλάδα

Τίτλος άσκησης: «Σύνθεση και χαρακτηρισμός φώτο-αποικοδομίσιμων δισυσταδικών συμπολυμερών για εφαρμογές στην ελεγχόμενη αποδέσμευση φαρμάκων»

Βαθμός: Άριστα(10 στα 10)

ΞΕΝΕΣ ΓΛΩΣΣΕΣ

Ιταλικά

Μέτρια γνώση (B1 επίπεδο), Κρατικό Πιστοποιητικό Γλωσσομάθειας, Μάιος 2011

Αγγλικά

Καλή γνώση (B2 επίπεδο), Κρατικό Πιστοποιητικό Γλωσσομάθειας, Μάιος 2010

ΓΝΩΣΕΙΣ Η/Υ

Άριστη γνώση και χειρισμός Η/Υ

Κάτοχος ευρωπαϊκού διπλώματος ECDL

ΔΙΑΚΡΙΣΕΙΣ/ΥΠΟΤΡΟΦΙΕΣ

- 1^ο Βραβείο για τη καλύτερη παρουσίαση (poster presentation) στο 12^ο Συνέδριο Πολυμερών, 2018
- Υποτροφία για μεταπτυχιακές σπουδές από το Ινστιτούτο Ηλεκτρονικής Δομής και Λείζερ του Ίδρυματος Τεχνολογίας και Έρευνας Κρήτης. Υπότροφος στο ερευνητικό πρόγραμμα RESEARCH AGREEMENT L'OREAL του ιδρύματος.

ΑΝΑΚΟΙΝΩΣΕΙΣ ΣΕ ΣΥΝΕΔΡΙΑ

1. **Psarrou M.**, Manouras T., Vamvakaki M., «A novel visible-light photo-activated drug release system», 12^ο Διεθνές συνέδριο της Ελληνικής εταιρείας πολυμερών, 30 Σεπτεμβρίου-3 Οκτωβρίου 2018, Ιωάννινα, Ελλάδα.
2. **Psarrou M.**, Manouras T., Vamvakaki M., «A photo-

- activated drug delivery system based on an “unusual” electron transfer sensitization process» Διεθνές Συνέδριο Πολυμερών στο Μπορντώ, 28-31 Μαΐου 2018, Μπορντώ, Γαλλία.
3. Προφορική παρουσίαση με τίτλο « A photo-activated drug delivery system based on an “unusual” electron transfer sensitization process» σε Επιστημονική εσπερίδα για τα βλαστοκύτταρα, 24 Νοεμβρίου 2017, Ιατρική Σχολή Πανεπιστημίου Κρήτης, Ηράκλειο, Ελλάδα.
 4. **Psarrou M.**, Makris K. Manouras T. Mavrothalassitis G. Vamvakaki M., «PEG-b-polyacetal block copolymer micelles for the treatment of craniosynostosis», 28^ο Ευρωπαϊκό Συνέδριο Βιοϋλικών, 4-8 Σεπτεμβρίου 2017, Αθήνα, Ελλάδα.
 5. **Psarrou M.**, Manouras T., Vamvakaki M., «A photo-activated drug delivery system based on an “unusual” electron transfer sensitization» 11^ο Διεθνές συνέδριο Ελληνικής εταιρείας πολυμερών, 3-5 Νοεμβρίου 2016, Ηράκλειο, Κρήτη, Ελλάδα.
 6. 16^ο Διεθνές συνέδριο πολυμερών και οργανικής χημείας, 13-16 Ιουνίου 2016, Χερσόνησος, Κρήτη, Ελλάδα.

ΣΥΣΤΑΣΕΙΣ

Διαθέσιμες εφ’ όσον ζητηθούν

Curriculum Vitae

First name/ Surname **Maria Psarrou**
Address Therisou 24, 71304, Heraklion, Crete, Greece
Telephone (+30)6949522720
E-mail psarrou@iesl.forth.gr
Date of birth October 6, 1994
Place of birth Mytilene, Lesvos
Nationality Greek

EDUCATION

- 9/2016 – 11/2018** Master degree in Polymer Chemistry
University of Crete, Greece -Department of Chemistry
Dissertation title: “Mechanically-induced main chain scission of polyacetals for controlled drug release”
Supervisor: Prof. Spiros Anastasiadis, Department of Chemistry, University of Crete
Co-supervisor: Prof. Maria Vamvakaki, Materials Science and Technology, University of Crete
- 9/2012-9/2016** Bachelor degree in Materials Science and Technology
University of Crete, Greece –Department of Materials Science and Technology
Grade: Very good (6.7 out of 10)
Dissertation title: “Synthesis and characterization of photo-degradable and sono-degradable polymers”
Supervisor: Prof. Maria Vamvakaki, Materials Science and Technology, University of Crete
- 6/2012** General Lyceum of Mantamados, Lesvos, Greece

WORK EXPERIENCE

- 9/2016-today** Researcher
Lab of Materials Chemistry, University of Crete
Main responsibilities-Technical skills:
- Synthesis and characterization of homopolymer and block copolymer polyacetals via a step-growth reaction.
 - Self-assembly of amphiphilic block copolymers in water and encapsulation of hydrophobic molecules (e.g. drugs).
 - Study of the degradation mechanism of main chain polyacetals using mechanical energy. Application in controlled drug release.
 - Synthesis and characterization of linear and star-like polymers via group transfer polymerization.
 - Development of a novel ultrasound-induced Atom Radical Polymerization (ATRP) in organic media.
 - Development of a novel Near InfraRed (NIR) photoactivated drug release system.

Characterization Techniques:

- Nuclear Magnetic Resonance spectroscopy (NMR)
- Ultraviolet-Visible (UV/Vis) spectrophotometry
- Fluorescence spectrophotometry
- Gel Permeation Chromatography (GPC)
- Dynamic Light Scattering

7/2015-9-2015

Traineeship

Institute of Electronic Structure and Laser-Foundation of Research and Technology (IESL-FORTH)

Dissertation title: “Synthesis and characterization of photo-degradable block copolymers for controlled drug delivery”

Grade: Excellent (10 out of 10)

LANGUAGES

Greek (Native language)

Italian

Average level, State Certificate of Foreign Language Proficiency, May 2011

English

Vantage level, State Certificate of Foreign Language Proficiency, May 2010

COMPUTER SKILLS

10/2008

European Computer Driving Licence (ECDL)

SCHOLARSHIPS-
AWARDS

- 1st Best Poster Presentation Award , 12th Hellenic Polymer Society International Conference 2018, Ioannina, Greece
- Fellowship from the Institute of Electronic Structure and Laser-Foundation of Research and Technology (IESL-FORTH) for master studies in the scientific program RESEARCH AGREEMENT L’OREAL

PRESENTATIONS AT
SCIENTIFIC
CONFERENCES

1. **Psarrou M.**, Manouras T., Vamvakaki M., «A novel visible-light photo-activated drug release system», 12th Hellenic Polymer Society International Conference 2018, September 30-October 3 2018, Ioannina, Greece
2. **Psarrou M.**, Manouras T., Vamvakaki M., «A photo-activated drug delivery system based on an “unusual” electron transfer sensitization process», International Bordeaux Polymer Conference, May 28-31 2018, Bordeaux, France
3. Oral presentation « A photo-activated drug delivery system based on an “unusual” electron transfer sensitization process», scientific meeting for stem cells, November 24 2017, Medical School, University of Crete, Heraklion, Greece
4. **Psarrou M.**, Makris K. Manouras T. Mavrothalassitis G. Vamvakaki M., «PEG-b-polyacetal block copolymer micelles for the treatment of craniosynostosis», 28^o European Conference on Biomaterials, September 4-8

2017, Athens, Greece

5. **Psarrou M.**, Manouras T., Vamvakaki M., «A photo-activated drug delivery system based on an “unusual” electron transfer sensitization» 11^o Hellenic Polymer Society International Conference 2016, Heraklion, Crete, Greece
6. 16^o International Polymer Conference and Organic Chemistry, June 13-16 2016, Chersonissos, Crete, Greece

Table of contents

ACKNOWLEDGMENTS.....	5
ABSTRACT.....	15
ΠΕΡΙΛΗΨΗ.....	16
Chapter 1.....	18
1.1 Controlled Drug Delivery.....	18
1.2 Tumor targeting.....	20
1.2.1 Passive targeting: Enhanced Permeability and Retention (EPR) effect.....	20
1.2.2 Active tumor targeting.....	20
1.3 Types of nanocarriers in drug delivery.....	21
1.3.1 Inorganic nanocarriers.....	21
1.3.2 Organic nanocarriers.....	22
1.3.2.1 Liposomes.....	22
1.3.2.2 Polymeric nanoparticles.....	23
1.3.2.3 Dendrimers.....	24
1.4 Polymer micelles.....	24
1.4.1 Amphiphilic block copolymers and self-assembly.....	25
1.4.2 Micelle preparation process.....	27
1.5 Stimuli-degradable polymers for controlled drug delivery.....	28
1.5.1 Polyacetals: A conventional family of acid-degradable polymers.....	29
1.6 Novel photodegradable polyacetals.....	32
1.7 Ultrasounds: An emerging external stimulus for biomedical use.....	33
1.7.1 Basic principles of ultrasound.....	33
1.7.2 Ultrasounds in polymer mechanochemistry.....	35
1.7.3 Ultrasound-triggered release from polymer micelles.....	38
1.8 Current study.....	42
Chapter 2.....	44

Experimental	44
2.1 Materials	44
2.2 Characterization methods	44
2.2.1 Gel Permeation Chromatography (GPC).....	44
2.2.2 ¹ H NMR spectroscopy	45
2.2.3 Ultraviolet/Visible spectroscopy	45
2.2.4 Field emission scanning electron microscopy (FE-SEM)	45
2.2.5 Dynamic Light Scattering (DLS)	45
2.3 Ultrasound apparatus.....	45
2.4 Synthesis of the polyacetal homopolymers	47
2.4.1 Sono-degradation experiments of the polyacetal homopolymers followed by GPC	49
2.4.2 Sono-degradation experiments of the polyacetal homopolymers followed by ¹ H-NMR spectroscopy	49
2.5 Synthesis of PEG- <i>b</i> -polyacetal di-block copolymers	50
2.5.1 Sono-degradation of the block copolymer polyacetals followed by GPC.....	51
2.5.2 Sono-degradation experiments of the block copolymer polyacetals by ¹ H-NMR spectroscopy	51
2.6 Preparation of PEG- <i>b</i> -polyacetal block copolymer micelles.....	51
2.7 Preparation of sudan red (SR)-loaded micelles	52
2.8 Ultrasound irradiation of the polyacetal-based micelles in water	52
2.9 Ultrasound-induced degradation of the PEG- <i>b</i> -polyacetal micelles and cargo release	53
2.10 pH- and ultrasound-triggered release of cargo from the polyacetal-loaded micelles ..	53
Chapter 3	54
Results and discussion.....	54
3.1 Synthesis and characterization of the polyacetal homopolymers.....	54
3.2 Sono-degradation study of the polyacetal homopolymers	56
3.2.1 Ultrasonic degradation of PA-benz-15k and PA-benz-5k.....	56

3.2.2 Ultrasonic degradation of PA-hex-15k and PA-hex-5k.....	66
3.2.3 Influence of the chemical structure on the ultrasonic degradation of the polyacetals	67
3.2.4 Proposed mechanism for the sono-degradation of the polyacetals.....	69
3.3 PEG- <i>b</i> -polyacetal diblock copolymers.....	70
3.3.1 Synthesis and characterization of the PEG- <i>b</i> -polyacetal diblock copolymers	71
3.3.2 Ultrasonic degradation of the block copolymers in organic media	73
3.4 Self-assembly of the PEG- <i>b</i> -polyacetal block copolymers in water	78
3.5 Ultrasound-induced morphological changes of the PEG- <i>b</i> -polyacetal block copolymer micelles.....	80
3.6 In vitro release studies.....	83
3.6.1 Influence of frequency on the ultrasound-induced disruption of the PEG- <i>b</i> -polyacetal micelles and the release of the encapsulated dye molecules.....	84
3.8 The synergistic effect of ultrasound and low solution pH on the degradation of the PEG- <i>b</i> -polyacetal micelles and the release of the encapsulated loads	89
Chapter 4	91
Conclusions	91
REFERENCES	94
APPENDIX: Characterization Techniques	99

ABSTRACT

Stimuli-controlled drug delivery has attracted enormous attention over the past decades. Several type of nanosized carriers including organic nanoparticles, inorganic nanomaterials or combinations of organic/inorganic materials have been extensively studied for the controlled delivery of active compounds at specific areas such as tumor tissues. The stimuli that trigger drug release from the nanocarriers can be broadly classified in two main classes: the internal stimuli such as pH, glutathione and enzymes and the external stimuli (physical stimuli) such as light irradiation, magnetic and electric fields and ultrasound. Ultrasound in particular is one of the most promising external triggers for controlled drug release from polymeric nanocarriers because it offers great spatiotemporal control, deep tissue penetration (deeper than light irradiation) and is a non-invasive and non-ionizing method.

Smart materials in the form of stimuli-responsive amphiphilic block copolymers are of great interest and have been widely used for the development of responsive drug nanocarriers. They can self-assembled into core-shell micelles in aqueous solution and can solubilize hydrophobic molecules (e.g. drugs) into their hydrophobic core. Herein, we present a new class of dual, ultrasound and pH, degradable drug carriers based on PEG-*b*-polyacetal block copolymers. For this study, the homopolymer polyacetals and the PEG-*b*-polyacetal copolymers were synthesized using a facile and scalable chemistries without incorporation of toxic reagents.

An extensive sono-degradation study of the polyacetal homopolymers using both low and high frequency ultrasound verified the main-chain degradation of the polyacetals due to the generation of elongation flows from cavitation setting the acetal bond a very “weak” mechano-labile group. Also, sono-degradation experiments in organic media proved the main-chain degradation of the PEG-*b*-polyacetal block copolymers into low molecular weight products. Next, the block copolymers were self-assembled into spherical micelles in water and Sudan Red was used as a model payload, to examine the release behavior of the micelles under different sonication conditions. The results showed that our system can be degraded into small hydrophilic and non-toxic molecules while releasing its cargo in the surrounding medium using medical ultrasound at 1 MHz frequency and extremely low irradiation energies. Moreover, the combination of low solution pH and ultrasound irradiation increased the release efficiency from the carriers suggesting, a particularly effective combinatorial dual stimuli induced release.

ΠΕΡΙΛΗΨΗ

Τις τελευταίες δεκαετίες, η ελεγχόμενη μεταφορά και αποδέσμευση φαρμάκων έχει προσελκύσει ιδιαίτερο επιστημονικό ενδιαφέρον. Διάφορα είδη νανομεταφορέων βασιζόμενων είτε σε οργανικά νανοσωματίδια είτε σε ανόργανα νανοϋλικά ή ακόμη και σε συνδυασμό οργανικών με ανόργανων υλικών έχουν εκτενώς μελετηθεί για την ικανότητά τους να μεταφέρουν ελεγχόμενα και στοχευόμενα δραστικές ουσίες (π.χ. αντικαρκινικά φάρμακα) σε συγκεκριμένες περιοχές του ανθρώπινου σώματος όπως για παράδειγμα στους καρκινικούς ιστούς. Τα ερεθίσματα που έχουν χρησιμοποιηθεί ευρέως για να διεγείρουν την απελευθέρωση ουσιών από φορείς μπορούν να χωριστούν σε δύο βασικές κατηγορίες: τα ενδογενή ερεθίσματα όπως για παράδειγμα μικρές αλλαγές στη τιμή του pH, αυξημένα επίπεδα γλουταθειόνης ή αλλαγές στη συγκέντρωση κάποιου ενζύμου και τα εξωγενή ή αλλιώς φυσικά ερεθίσματα στα οποία συμπεριλαμβάνονται η ακτινοβολία με φώς, η χρήση μαγνητικού ή ηλεκτρικού πεδίου και η έκθεση σε υπερήχους. Μεταξύ αυτών, ο υπέρηχος αποτελεί ένα πολλά υποσχόμενο φυσικό ερέθισμα καθώς μπορεί να χρησιμοποιηθεί για την ελεγχόμενη αποδέσμευση φαρμακευτικών ουσιών προσφέροντας μεγάλη ακρίβεια ως προς το τόπο και χρόνο της αποδέσμευσης, διεισδύει βαθειά στους ιστούς, είναι μια μη-επεμβατική μέθοδος και σε αντίθεση με άλλες μεθόδους (π.χ. ακτίνες X) δεν προκαλεί ιοντισμό.

Πληθώρα «έξυπνων» υλικών έχουν αποτελέσει τη βάση για την ανάπτυξη καινοτόμων αμφίφιλων συμπολυμερών τα οποία κατ' επέκταση έχουν χρησιμοποιηθεί για την ανάπτυξη νανομεταφορέων φαρμάκων. Τα αμφίφιλα συμπολυμερή, όταν βρεθούν σε υδατικό περιβάλλον αυτό-οργανώνονται σε μικκύλια αποτελούμενα από ένα υδρόφιλο κέλυφος και έναν υδρόφοβο πυρήνα στον οποίο μπορούν να δεσμευθούν υδρόφοβα μόρια. Στη παρούσα εργασία, παρουσιάζεται για πρώτη φορά μια νέα οικογένεια νανομεταφορέων αποκρινόμενων σε δύο ερεθίσματα, pH και έκθεση σε υπερήχους. Οι νανομεταφορείς βασίζονται σε υλικά αποτελούμενα από μια συστάδα πολυαιθυλενογλυκόλης (PEG) και μία συστάδα πολυακετάλης (PEG-*b*-polyacetal). Για την εργασία αυτή συντέθηκαν ομοπολυμερή πολυακετάλης και συμπολυμερή PEG-*b*-polyacetal μέσω εύκολων συνθετικών πορειών και απουσίας τοξικών αντιδραστηρίων.

Αρχικά, μελετήθηκε εκτενώς η διάσπαση των ομοπολυμερών πολυακετάλων υπό την επίδραση τόσο χαμηλής όσο και υψηλής συχνότητας υπερήχων και επαληθεύτηκε ο μηχανισμός διάσπασης των υλικών αυτών. Ο μηχανισμός που προτείνεται είναι η

διάσπαση της κύριας αλυσίδας των πολυακετάλων ως αποτέλεσμα των διατμητικών τάσεων που αναπτύσσονται λόγω του φαινομένου της σπηλαίωσης (cavitation effect) κατά μήκος της πολυμερικής αλυσίδας. Έτσι ο ακεταλικός δεσμός καθίσταται ως ο πιο μηχανικά-ασθενής δεσμός που υφίσταται διάσπαση. Επίσης, αποδείχθηκε η μηχανικά-επαγόμενη διάσπαση συμπολυμερών πολυακετάλης και πιστοποιήθηκε η παραγωγή χαμηλού μοριακού βάρους, υδρόφιλων και μη-τοξικών προϊόντων διάσπασης. Περαιτέρω, τα συμπολυμερή πολυακετάλης αυτό-οργανώθηκαν σε σφαιρικά μικκύλια σε νερό και στον υδρόφοβο ακεταλικό πυρήνα ενκαψυλιώθηκαν μόρια μίας χρωμοφόρας ένωσης (Sudan Red). Η αποδέσμευση του φορτίου από το πυρήνα των μικκυλίων μελετήθηκε σε διάφορες συνθήκες και ιδιαίτερα τα αποτελέσματα έπειτα από έκθεση σε ιατρικούς υπερήχους συχνότητας 1 MHz και εξαιρετικά χαμηλής ενέργειας, έδειξαν ότι οι νανομεταφορείς βασισμένοι σε πολυακετάλη μπορούν επιτυχώς να διασπώνται σε μικρά, μη-τοξικά μόρια καθώς απελευθερώνουν ελεγχόμενα το δεσμευμένο φορτίο. Τέλος, μελετήθηκε η επίδραση του ελαφρώς όξινου περιβάλλοντος του διαλύματος μικκυλίων σε συνδυασμό με έκθεση σε υπερήχους και βρέθηκε ότι η αποδέσμευση του φορτίου ήταν αρκετά πιο αποτελεσματική καθιστώντας τους πολυακεταλικούς νανομεταφορείς ιδανικούς για την ελεγχόμενη αποδέμευση δραστικών ουσιών υπό την επίδραση ενός ενδογενούς και ενός εξωγενούς ερεθίσματος.

Chapter 1

Introduction

1.1 Controlled Drug Delivery

According to the World Health Organization (WHO), cancer is the second leading cause of death worldwide and it will surpass cardiovascular disease to become the leading cause of death in the next decade. This is the reason why cancer is characterized as a devastating disease. It is estimated that 1 to 4 women and 1 to 3 men will develop a cancer case during their lifetime even in a very young age. In 2015, 17.5 million cancer cases and 8.7 million deaths from cancer were recorded, worldwide. The American Cancer Society estimated that in 2018, 1.73 million new cancer cases and 609 thousand cancer deaths will occur in the United States. These numbers clearly show the increasing need for improved anticancer treatments. Although major advances have been made in the successful prevention, diagnosis and treatment of several different cancer cases, the prognosis for many other types of cancer remain unsuccessful. Therefore, the need for improved cancer therapies is urgent [1].

Till today, the most commonly used method for the treatment of many cancer types, is the administration of free drugs, such as small chemotherapeutic molecules, via direct injection into the bloodstream. However, this method of anticancer drug administration has two main drawbacks, the nonspecific action of the drug and its nonspecific biodistribution. Many chemotherapeutic drugs act with preferential cytotoxicity on cancer cells as a result of their rapid proliferation compared to normal cells. Even in these cases, the cytotoxicity is not restricted only to cancer cells, but is often apparent in healthy tissues as well as the nervous system, the heart and the gastrointestinal tract. This nonspecific action in combination with the nonspecific accumulation of the drug in both healthy and non-healthy tissues results in side effects that limit the maximum tolerated drug dose and eventually hinder the efficacy of the drug. Unfortunately, apart from cancer which is a very serious illness, many other genetic diseases suffer from inefficient therapies because they face similar limitations [2].

In 1906, Paul Ehrlich, known as the founder of chemotherapy, received the Nobel Prize for Physiology or Medicine. With his revolutionary ideas and his ability to combine chemistry with biology and medicine, he was the first to imagine that somehow we could target the tumor tissues and exploit vascular abnormalities of tumors and physiological barriers by using specific molecular structures. This concept of targeting tumors was named Ehrlich's "magic bullet" concept and since then has inspired many generations of scientist to develop smart and powerful chemistries to overcome the drawbacks of conventional chemotherapeutic agents [3].

After the introduction of the "magic bullet" and based on this concept, a new field of medicine has been developed which is known today as nanomedicine. Nanomedicine is defined as the application of nanotechnology to medicine and specifically employs the use of nanosized materials (1-100nm) to treat diseases such as cancer and others [4]. Controlled drug delivery is a very challenging task in nanomedicine that aims to improve conventional therapy by delivering drugs and active compounds via smart nanocarriers to the diseased sites. This field is believed to contribute significantly to the human health and the treatment of serious diseases. As shown in Table 1, controlled drug delivery systems offer significant advantages compared to conventional methods of drug administration [5].

Table 1: Major advantages of controlled drug delivery systems in nanomedicine.

-
1. Increase drug concentration in the diseased site while decreasing drug concentration in healthy tissues
 2. Decrease side effects and toxicities
 3. Improve drug solubility
 4. Increase drug stability and reduce the degradation of the drug during circulation
 5. Decrease the number of dosages being less painful for the patient
 6. Co-delivery of multiple drugs to specific sites to improve the therapeutic efficacy
 7. Co-delivery of drugs and screening agents
-

1.2 Tumor targeting

1.2.1 Passive targeting: Enhanced Permeability and Retention (EPR) effect

The Enhanced Permeability and Retention (EPR) effect is a unique characteristic of the tumor tissues related to their anatomical and pathophysiological differences from healthy tissues. It was described in detail and validated by Maeda and colleagues in the late 80s [6]. Extensive angiogenesis and hypervascularity, lack of smooth-muscle layer (pericytes), defective vascular architecture (fenestrations), no constant blood flow and inefficient lymphatic drainage are some of the major characteristics of the tumor tissues. Passive targeting of tumors is based on these tissue abnormalities. Macromolecular structures such as nanocarriers in the size range of 20-200nm can extravagate and accumulate into tumors. Nanocarriers which enter the tumor sites are not removed efficiently due to the inefficient lymphatic drainage and are thus retained in the tumor where they release the chemotherapeutic drugs (**Figure 1.1A**). This phenomenon of passive accumulation of nanostructures and drugs in solid tumors has been called the EPR effect and serves as the key point for the development of new drug delivery systems for effective cancer therapy [7, 8]. However, according to recent clinical studies, the EPR effect is extremely heterogeneous in humans and tumor targeting has not been proved yet in the clinic [9, 10].

1.2.2 Active tumor targeting

In active tumor targeting, a certain ligand-target is covalently attached on the surface of the nanocarrier and specifically recognizes and binds to appropriate receptors at the target sites. The ligand chosen must be recognized by receptors that are over-expressed at the tumor sites and not in the normal tissues. The binding affinity of the ligands to the receptor is important for the penetration of the nanocarrier into the tumor because of the “binding-site barrier” [11]. This ligand-target is usually an antibody or a peptide. In active tumor targeting, there are two different cellular targets: (a) the targeting of cancer cells and (b) the targeting of the tumor endothelium (**Figure 1.1 B**) [8].

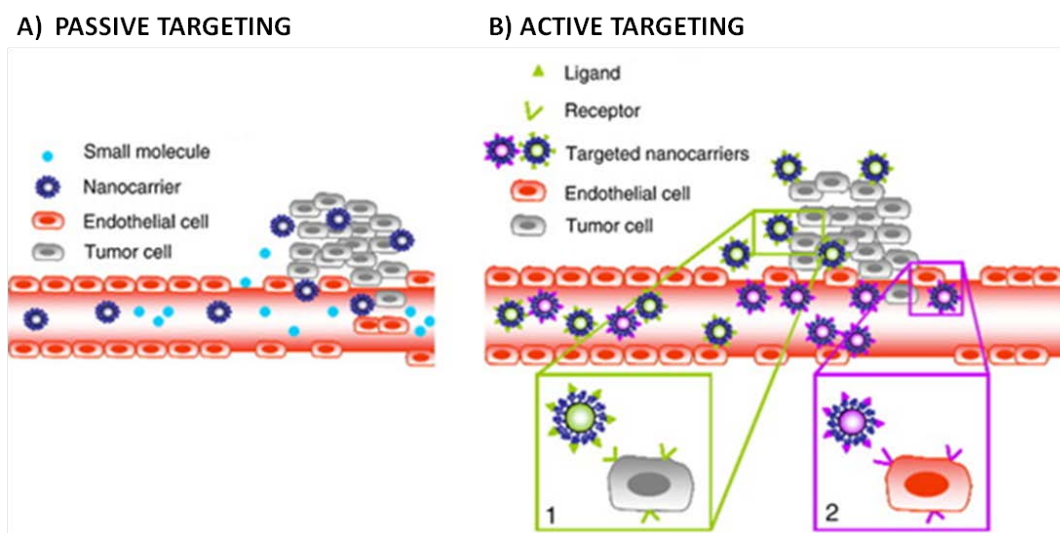


Figure 1.1: Schematic illustration of (A) passive tumor targeting through the EPR effect and (B) active tumor targeting of nanocarriers decorated with specific ligands on their surface for recognition of (1) cancer cells and (2) endothelial cells [8].

1.3 Types of nanocarriers in drug delivery

The enormously increasing need for more effective anticancer therapies has led to the design and development of several innovative drug delivery systems. Because of this urgent need, a wide range of different chemistries including lipids, synthetic and natural polymers, proteins, organic and inorganic materials have been employed for the development of novel drug carriers for the controlled and efficient delivery of payloads to target sites.

1.3.1 Inorganic nanocarriers

Quantum dots, mesoporous silica nanoparticles and magnetic nanoparticles are the most commonly used inorganic materials for such applications [12–14]. There are numerous studies based on these type of materials showing the effective delivery of bioactive compounds and minimum side effects and toxicity to healthy tissues. Moreover, it's worthwhile to mention that there are a few examples of inorganic-based drug delivery systems that have been approved by the Food and Drug

Administration (FDA) and have been used in clinic. For example, MagForce or NanoTherm (phospholipid-PEG coated superparamagnetic iron oxide nanoparticles), is the first magnetic nanoparticle used for chemotherapy and hyperthermia treatment of solid tumors. Another characteristic example of commercialized inorganic-based drug carrier are the mesoporous silica nanoparticles modified with azobenzene molecules for NIR-triggered release of anticancer drugs. However, the plethora of these inorganic drug delivery systems are still in very early, pre-clinical studies and important questions about the internalization of these materials into human tissues or their ejection from the body (as most of them are not biodegradable) must be answered. Therefore, their safety is still under discussion.

1.3.2 Organic nanocarriers

In contrast to inorganic nanocarriers, drug delivery systems comprising organic materials, either synthetic or natural, have attracted much more attention because in most cases they are based on biocompatible and biodegradable components. For the preparation of the organic nanocarriers, small organic molecules are self-assembled covalently or/and non-covalently to form three-dimensional structures such as liposomes, polymeric nanoparticles, dendrimers and polymeric micelles. These interesting structures provide a suitable environment for the encapsulation and transport of bioactive molecules including anticancer drugs, genes, antibodies and several other lipophilic or hydrophilic molecules. Their promising behavior as future theranostic agents, have been investigated for many years and some of these organic nanocontainers have been already introduced in the clinic [15- 17].

1.3.2.1 Liposomes

In 1964, the liposomal structure was published for the first time and right after it was used for the sustained delivery of low molecular compounds. Liposomes are characterized as the first generation drug delivery systems and comprise the most common and well-investigated carriers for targeted and controlled drug delivery of drugs and genes. They are phospholipid vehicles consisting of one or several concentric lipid bilayers. In the interior of their hydrophobic bilayer they can solubilize

and deliver hydrophobic drugs and compounds, while in the central aqueous lumen they can load hydrophilic drugs and molecules. Moreover, their surface can be modified with poly(ethylene glycol) (PEG) and grafted with targeting ligands (**Figure 1.2**). Their size ranges between 40-400nm. A large number of liposome-based delivery systems have been approved for cancer therapy in the clinic and even more are in phase II/III clinical studies. For example, Doxil, Myocet and Caelyx were the first class of liposomal therapeutics approved by FDA for cancer treatment [18].

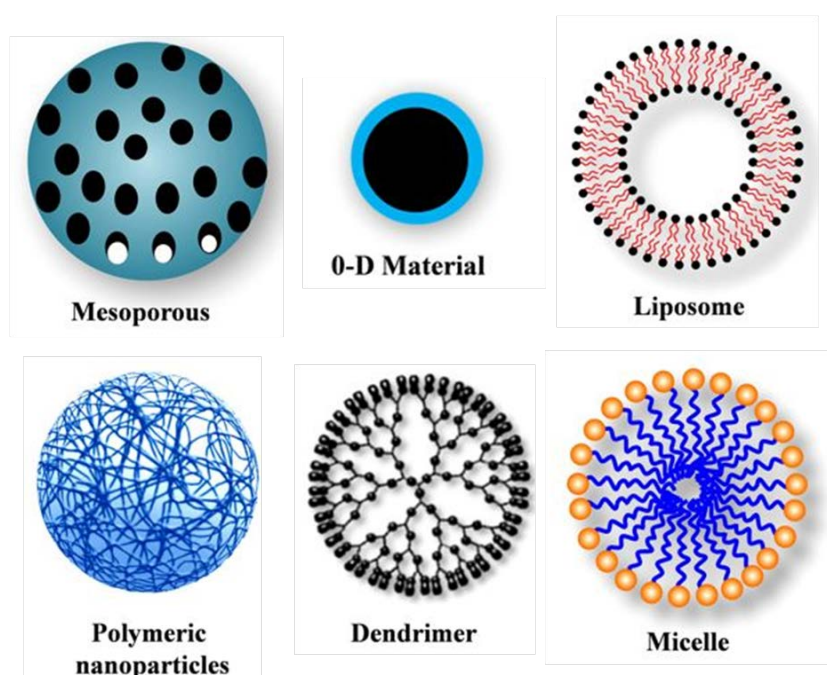


Figure 1.2: Schematic representation of the structures of the main inorganic and organic nanocarriers [19].

1.3.2.2 Polymeric nanoparticles

The application of polymeric nanoparticles as drug carriers has received great attention. They have been widely used as carriers for the delivery of drugs, genes and vaccines to the sites of interest with potential reduction of toxicity and increased therapeutic efficacy. Polymeric nanoparticles are divided into two categories: “nanospheres” in which the drug is dispersed inside the core of the particles and “nanocapsules” in which the drug is entrapped in a liquid cavity surrounded by a polymer membrane. They can also be PEGylated and decorated with ligands on their

surface. The most commonly used synthetic polymers are poly(lactic acid) (PLA), poly(glycolic acid) (PGA), poly(ϵ -caprolactone) (PCL) and the copolymer of PLA and PGA known as poly(lactic-co-glycolic acid) (PLGA). These polymers are known for their biocompatibility and biodegradability. On the other hand, natural polymers that have been used for the preparation of polymeric nanoparticles include chitosan, sodium alginate and gelatin. Most of these polymers are FDA approved materials and have been used for anticancer therapy. Some of them are known with the trade names Copaxone (Teva), Eligard (Tolmar), etc [20].

1.3.2.3 Dendrimers

Another attractive type of drug delivery systems are the polymeric dendrimers. Dendrimers are three-dimensional hyper-branched macromolecules with a tree-like structure (**Figure 1.2**). Their main structure consists of a core molecule and alternating layer of monomer repeat units which are known as “Generations” and are characterized as G1, G2, G3, etc. They have attracted a lot of attention as drug carriers due to their unique characteristics such as their well-defined size, shape and molecular weight, monodispersity and high degree of surface functionalities. The internal cavities of the dendritic structure, offer an appropriate environment for the physical entrapment or encapsulation of hydrophobic compounds, while the functional groups on the surface of the dendrimers can be used for the delivery of hydrophilic agents or genes. There are many different types of dendrimers such as peptide dendrimers (PPI), poly(l-lysine) dendrimers, polyamidoamine (PAMAM) dendrimers etc. Among these families of dendrimers, PAMAM dendrimers have been widely investigated as drug and gene carriers. However, the studies on these dendrimers are in a very early stage and potential undesirable toxicity and side effects of these dendrimers are unknown [21], [22].

1.4 Polymer micelles

Polymer micelles have been the topic of interest for many years and have been extensively explored as carriers for the delivery of bioactive compounds in a controllable manner. The term polymeric micelles, is referred to spherical or globular colloidal systems in nano-dimensions, formed by the self-assembly of amphiphilic block copolymers in an aqueous environment. The resulting system comprises a

hydrophobic core and a hydrophilic shell (**Figure 1.2**). The hydrophobic micellar core serves as a reservoir for the incorporation of hydrophobic drugs and active compounds, while the outer shell serves as a stabilizing interface between the hydrophobic core and the external aqueous medium. Although the formation of micelles from block copolymers is known for over 30 years, the majority of micelles were synthesized from non biocompatible polymers, thus their application in drug delivery was limited.

1.4.1 Amphiphilic block copolymers and self-assembly

Amphiphilic block copolymers have been at the focus of polymer science for many years because of their unique properties and potential applications in biology and medicine, in microelectronics and photoelectronic materials, in catalysis, etc. One of the most important features of amphiphilic block copolymers is their ability to self-assemble in solution to give a plethora of diverse morphologies such as spherical and cylindrical micelles, vesicles, lamellae, etc. A significant contribution in the scientific field of block copolymers, has been the development of “living” radical polymerizations which opened a new pathway for the preparation of a large variety of well-defined block copolymer structures. Linear block copolymers, graft copolymers and star-like polymers are a few examples of macromolecular structures that can self-assemble into several morphologies under certain conditions [23], [24].

Linear amphiphilic di-block (hydrophilic-hydrophobic) copolymers or tri-block (hydrophilic-hydrophobic-hydrophilic) copolymers are the most common and extensively used polymers for the preparation of micelles. These polymers are obtained by the polymerization of more than one type of monomer, typically one hydrophobic and one hydrophilic, so that the resulting macromolecule is composed of immiscible blocks. For biological applications such as drug delivery, the hydrophobic polymer is usually a non-toxic, biocompatible and biodegradable material whereas the hydrophilic segment, in almost all systems, is composed of low molecular poly(ethylene glycol) (PEG). PEG is the most known non-ionic hydrophilic polymer with stealth behavior (**Figure 1.3**). PEG-based micelles or other PEGylated nanocarriers are characterized by lower initial toxicities compared to the non-

PEGylated carriers, efficient blood circulation, reduced extraction by the kidney, reduced renal filtration, etc [25].

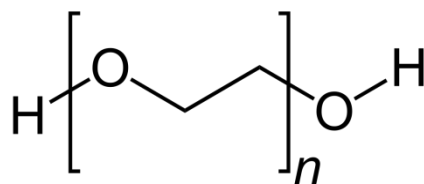


Figure 1.3: Chemical structure of poly(ethylene glycol).

As mentioned above, polymeric micelles from amphiphilic copolymers are formed through a procedure known as self-assembly. Self-assembly of amphiphilic macromolecules takes place when these macromolecules are dissolved in a selective solvent which is a thermodynamically good solvent, and completely dissolves one part of the molecule over another. In amphiphilic di-block copolymers, the lipophilic segments become packed together, as it is more entropically favorable and create a hydrophobic environment which is the core of the micelles. On the other hand, the hydrophilic parts are preferentially dissolved in water and create a flexible corona which is the outer shell of the micelles (**Figure 1.4**).

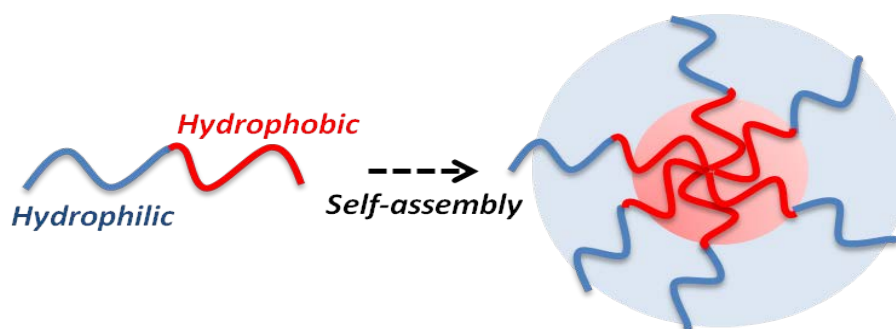


Figure 1.4: Self-assembly of amphiphilic di-block copolymers to core-shell micelles.

The self-assembly process can lead to different morphologies which results from the different relative sizes of the soluble and insoluble block and the inherent molecular curvature. The packing parameter, p , can be used to define the relative size of the insoluble region of a copolymer and is given by the equation below:

$$p = \frac{v}{a_0 l_c}$$

Where, (a_0) is an optimal surface that results from the solvophobic and solvophilic interactions of the insoluble block at the interface between the soluble and insoluble blocks, (l_c) is the length of the insoluble block and (v) is the volume of the insoluble block. According to a general rule, when $p \leq 1/3$ spherical micelles are formed, when $1/3 < p \leq 1/2$ the possible morphology is cylindrical micelles and polymersomes and when $1/2 \leq p \leq 1$ vesicles are formed (**Figure 1.5**) [26].

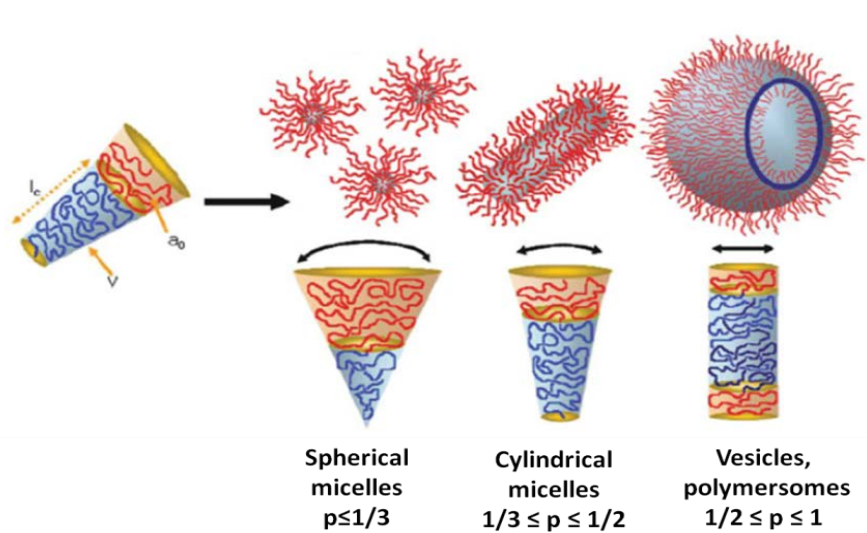


Figure 1.5: Different self-assembled structures formed by block copolymers in selective solvents. The morphology of the structure can be estimated by the packing parameter, p [27].

1.4.2 Micelle preparation process

The preparation of polymer micelles which are based on amphiphilic block copolymers can be achieved by using one of the following methods: (1) the direct dissolution method, (2) the non-selective selective solvent dissolution method. In the direct dissolution method, a solid sample of the block copolymer is directly dissolved in a good solvent for the one block and then the solvent is left to anneal by standing or via thermal annealing and this leads to the formation of the micellar solution. It

should be noted that this method is more suitable for low molecular weight block copolymers in which the insoluble block is shorter. The second technique is based on the dissolution of the block copolymer in a good solvent for both blocks, which results in completely dissolved polymer chains in the solution. The micelle formation in this method depends on the solvent-removal procedure. The most commonly used and thermodynamically favorable way to induce micelle formation is the addition of an aqueous solvent (e.g. water) into the solution of the block copolymer. This method is generally preferred because it leads to micelles with uniform size and low polydispersity. Another way to form micelles is to evaporate the organic phase in order to make a polymer film and then to rehydrate the film with an aqueous solvent. In this case the main disadvantage is that the resulting micelles are not uniform in size and usually large aggregates are formed. The last way to induce micelle formation in the second method is to remove the organic solvent against dialysis in water which will lead to micellization [28].

1.5 Stimuli-degradable polymers for controlled drug delivery

Stimuli-degradable polymers are defined as polymers that undergo abrupt changes, usually irreversible bond breakage, in response to small external changes in the environmental conditions. The cleavable bonds can be located in the main-chain of a polymer or in the side chain. In both cases, there are many different strategies to involve a degradable linkage into a polymer backbone. As shown in **Figure 1.6**, the degradable linkage can be located (i) in the center of a homopolymer chain, (ii) as a junction in a block copolymer chain (iii), as multi-cleavable bonds along the polymer backbone (iv) in every repeat unit of the polymer chain, or (v) in the case of a block copolymer as cleavable bonds in every repeat unit of the one block. In the case of polymers with side chains the degradable linkage can be located either (vi) in the middle of the side chain or (vii) as a junction between the main-chain and the side chain.

Stimuli that can be applied to trigger polymer degradation can be either (bio)chemical (e.g. pH, temperature, enzymes) or physical (e.g. light, ultrasound and magnetism). Polymer systems that response to one or more stimuli, have been extensively used for the development of novel “smart” drug delivery systems. These systems are

characterized as “smart” because they can release their cargo upon remote and spatiotemporal control in response to the applied stimulus. Moreover, nanocarriers that can be degraded into small and non-toxic molecules in the presence of an applied stimulus are even more attractive for biological use [29], [30].

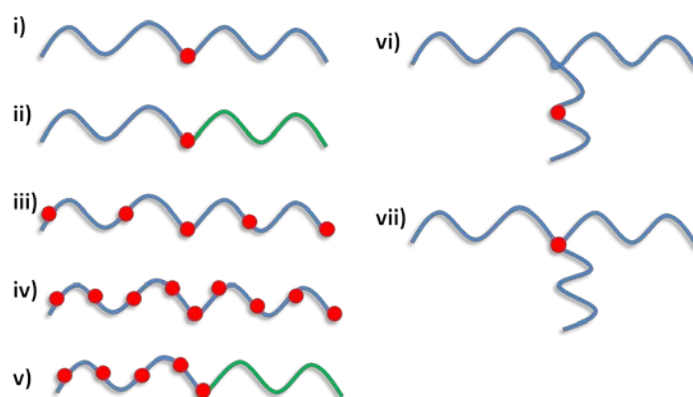


Figure 1.6: Different strategies for the incorporation of degradable groups in the main-chain (i-v) or the side chains (vi-vii) of a polymer.

1.5.1 Polyacetals: A conventional family of acid-degradable polymers

Among the various existing stimuli-degradable polymers, acid-degradable polymers have been widely studied and used for drug delivery applications. In general, we could say that pH is the most extensively studied stimulus in the literature. The increasing interest on pH-responsive systems is dated back to the period when the specific characteristics of the tumor microenvironment were determined. The mildly acidic pH of the tumor sites and of the inflammatory tissues (0.5-1.0 pH units lower than normal tissues), as well as of the intracellular compartments, such as endosomes and lysosomes (pH range from 4.0-6.5) of the cells, can be ideally exploited by acid-degradable carriers to trigger the selective release of anticancer drugs in tumor tissues or within the tumor cells [29], [31].

Acid-degradable polymers are those that contain in their polymer chain at least one acid-labile linkage. There is a wide range of chemical bonds that are known to be unstable under acidic solutions. However, only a few of them show an enhanced degradation or hydrolysis in the presence of slightly acidic conditions, while being

stable at neutral pH. This unique feature is determined by the chemical structure of the bond. Orthoesters, acetals or ketals, hydrazones and imines are the most commonly used acid-labile linkers. Among them, polymers that contain acetal bonds in their chemical structure have been of intense interest over the last two decades. The acetal bond comprises two single-bonded oxygen atoms attached to the same carbon atom. In an acidic environment, the one oxygen of the acetal bond is protonated and activates the neighbouring carbon. Then, in the presence of water molecules, the cleavage of the acetal bond occurs to produce an alcohol and an aldehyde molecule as the degradation products (**Figure 1.7**). In contrast to polyester based biomaterials, the hydrolysis of polyacetals does not generate acidic degradation products which are cytotoxic [32], [33]. Thus, polyacetals could be used for the development of novel non-toxic acid-degradable drug release systems.

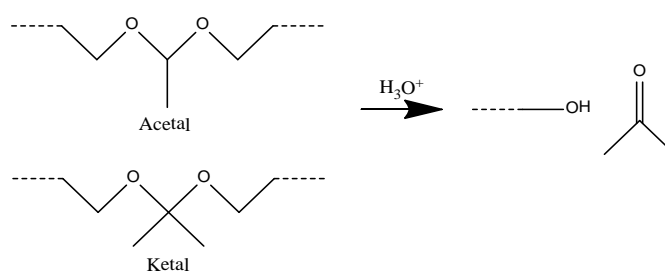


Figure 1.7: Chemical structure of the acetal and ketal bond and their degradation products upon exposure to acidic conditions.

In 1980, Heller et al. reported for the first time the synthesis of bioerodible linear and cross-linked polyacetals by the condensation of polyols with divinyl ethers (**Figure 1.8**) and claimed their potential application as drug-releasing depots [34]. Twenty years later, Tomilson et al. used the same synthetic reaction for the synthesis of novel main-chain water-soluble, amino-functionalized polyacetals with a pH-dependant degradation profile, being suitable for drug-conjugation [35]. Their preliminary cytotoxicity and body distribution studies have shown the lack of toxicity both in polyacetals and their degradation products and no significant accumulation in specific organs. In 2003, the same group reported the synthesis of a polyacetal-Dox conjugate (doxorubicin as a pendant group) and they performed a comparative study with an N-

(2-Hydroxypropyl)methacrylamide (HPMA) copolymer-Dox conjugate [36]. HPMA polymer is among the first synthetic polymers that were used for the preparation of the second generation polymer therapeutics and clinical studies have confirmed its safety. It was shown that the polyacetal-dox conjugate exhibits significant prolonged blood half-life and enhanced accumulation in tumors compared to the HPMA copolymer-dox conjugate. In another approach, Vincet et al. used the same reaction to synthesize a linear polyacetal and incorporate into the polymer backbone a drug with bis-hydroxyl functionality (diethylstilboestrol (DES)) [37]. These polyacetal-DES polymers were the first water-soluble anticancer polymeric drugs designed for acid-dependant release. In 2006, Schacht et al., also from Heller's group, reported the synthesis of graft copolymers comprising of a polyacetal backbone and pendant PEG side chains [38]. These graft polymers were used to prepare a series of thermogels with a lower critical solution temperature (LCST) ranging from 25 to 60 °C and at the same time the rate of hydrolysis of these gels could be controlled by adjusting the solution pH.

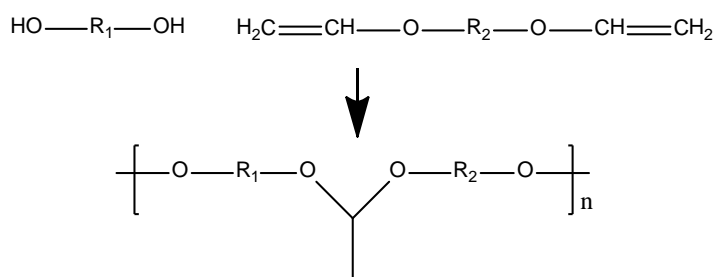


Figure 1.8: Synthesis of polyacetals by the condensation of diols with divinyl ethers.

Another interesting study based on polyketals was reported from Murthy's group in 2005 [39]. More specifically, they used a new acid-sensitive polymer, poly(1,4-phenylacetone dimethylene ketal), which has ketal bonds along the polymer backbone and formed microparticles, encapsulated with the antiinflammatory drug dexamethasone, via an emulsion procedure. From the same group, Khaja et al, proposed a new strategy for the preparation of polyacetals based on the acyclic diene metathesis (ADMET) polymerization [40]. They synthesized a series of new polyketals and polyacetals with this method and used an anthracene-based polyacetal to form microparticles for the delivery of the therapeutic protein catalase.

Finally, Frechet's group synthesized eight different acid-degradable polymers, based on polyurethanes and polyureas, bearing the same acid-labile ketal bond in their main chain [41]. All polymers were synthesized using a step growth polymerization between a bis(*p*-nitrophenyl carbamate/carbonate) or diisocyanate monomer with an acid-degradable, ketal-containing diamine. Significant differences were observed both in the hydrolysis rate of the polymers and in the release profile of the polyacetal-based microparticles at pH 5.0, indicating that the chemical structure of the synthesized polyacetal plays a major role in the polymer degradation.

1.6 Novel photodegradable polyacetals

Recently, our group, reported for the first time the photo-degradation of novel linear main-chain polyacetals under very low irradiation energies [42–44]. The degradation threshold for these polymers was two orders of magnitude lower than that of other photodegradable materials such as poly(methyl methacrylate). A zwitterionic photodegradation mechanism was proposed eliminating the production of free-radical intermediates which are usually toxic for the human body. Moreover, a great advantage of these polymers was the facile tuning of the irradiation wavelength depending on the chromophore moiety that was located next to the acetal unit. Hence, the photodegradation process was triggered by using either ultraviolet-visible (193 nm, 248 nm, 365 nm and 532 nm) near infrared (1,064 nm) light sources via single or multi-photon excitation, respectively. These polymers served as excellent carriers for the co-delivery of an anticancer drug, camptothecin (CPT) and a phototoxic drug, hematoporphyrin (HP) to HeLa cancer cells. The cytotoxicity studies showed the enhanced cell death rates due to the combination of phototherapy (production of reactive oxygen species (ROS) upon irradiation of HP) with chemotherapy using clinically relevant light dosage for the activation of the system. More importantly, the cytotoxicity of both the nanocarriers and their degradation products was lower than 10%. Finally, a significantly increased cell uptake of the drugs when loaded into the nanocarriers was observed compared to the free drugs alone. This study use in the potential of main-chain polyacetals for light-triggered drug release applications.

1.7 Ultrasounds: An emerging external stimulus for biomedical use

The last 10 years, the concept of ultrasound-triggered drug release from nanocarriers has attracted great attention. In contrast to other external stimuli, ultrasound have major advantages. Apart from their unique and precise way for achieving spatiotemporal control of the drug release at the desired sites, ultrasounds are also attractive because of their noninvasiveness, the absence of ionizing irradiations, their cost effectiveness and their facile regulation of tissue penetration by tuning the irradiation characteristics (frequency, intensity, continuous or pulsed exposure). Ultrasound irradiation is often compared with light irradiation because they both offer great advantages for spatiotemporal control of the drug release. However, light cannot penetrate deep into the tissues as ultrasound can and most photo-degradable systems are activated in the UV-visible region which is a harmful irradiation for living organisms.

In general, low frequency ultrasounds can penetrate deep into the body tissues, but their beam cannot be focused at a local focal spot because of their longer wavelength. On the other hand, high frequency ultrasounds have less tissue penetration depth due to scattering, but the ultrasonic beams can be focused at a tiny area and thus the intensity becomes higher at the focal spot while in other surrounding areas the intensity is low and acceptable for use in the human body. For this reason, high-intensity focused ultrasound (HIFU) technology is a powerful and emerging tool in medicine not only for the triggered release of drugs from nanocarriers, but also for the direct ablation of tumor tissues. It should be noted that HIFU technology is already being used in the clinic for tumor ablation in cancer treatment [29], [45–47].

1.7.1 Basic principles of ultrasound

Ultrasound is a sound wave that transports energy through a medium and is created by the mechanical oscillations of a piezoelectric crystal or transducer. This results in alternating compression and rarefaction of the medium through which the sound propagates with a certain amplitude and frequency. The type of sound wave is determined by its frequency. The word “ultrasound” refers to sound waves which are above the threshold of audible human hearing (~20 kHz). Ultrasounds are classified

into two main categories: low or power ultrasounds with a frequency range from 20 kHz to around 1 MHz and high or diagnostic with frequencies above 1 MHz (**Figure 1.9**).

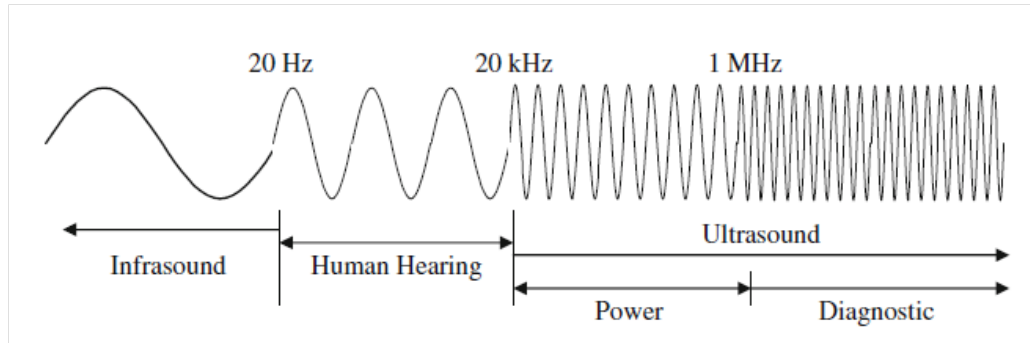


Figure 1.9: The sound wave [48].

Both low and high frequency ultrasounds are characterized by chemical and mechanical events caused via the unique phenomenon of acoustic cavitation. Cavitation is characterized by three steps. The first step is the formation of tiny gas bubbles or nucleation of pre-existing bubbles in the liquid. At a second step, the bubbles grow in every cycle of rarefaction and compression of the oscillating sound wave until they reach a critical size. The critical size of the bubbles depends on the frequency of the ultrasound wave. In general, low frequency ultrasonic waves generate larger bubbles. For the third step there are two possible scenarios. When bubbles reach their critical size they either become unstable and collapse violently within a single acoustic cycle, this is the so-called transient cavitation, or the bubbles are oscillating for many cycles near their critical size which is called stable cavitation (**Figure 1.10**). In transient cavitation, the collapsing bubble can be considered as a microscopic implosion that generates hot-spots with very high temperatures and pressures due to local turbulence. These high temperatures are responsible for the chemical effects such as radical formation, while the strong shear gradients caused by the bubble collapse induce the mechanical effects. Acoustic cavitation is a phenomenon that is more dominant at low ultrasound frequencies, while at frequencies above 2 MHz cavitation it becomes weaker. In biological systems, a high cavitation effect in combination with non-focused ultrasonic beams of low frequency result in irreversible changes of human tissues. Cavitation induces the cell membrane

lysis which results to cell necrosis. This limitation renders low frequency ultrasounds unsuitable for clinical use [48], [49] [50].

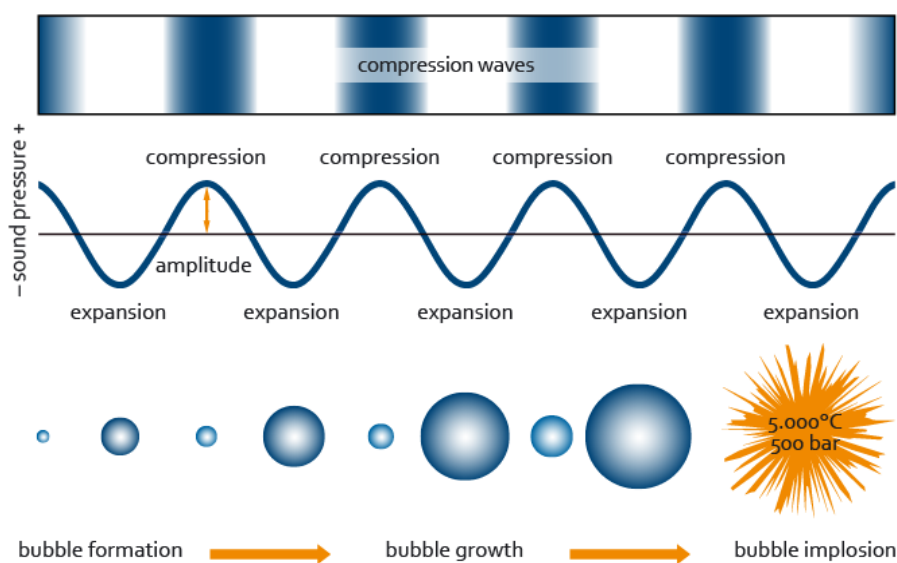


Figure 1.10: A graphical explanation of the generation, growth and collapse of bubbles over several acoustic cycles.

1.7.2 Ultrasounds in polymer mechanochemistry

One of the most unique and exciting effect of ultrasonic cavitation is the mechanical effect, which is attributed to the shear forces, elongation flows and shock waves produced by the collapsing bubbles. Especially, in the field of materials chemistry these mechanical forces have been used for the synthesis of polymeric materials by initiating polymerization reactions and for the degradation of polymers by elongating the polymer chain, leading to irreversible scission of its chemical bonds [51].

The destructive character of the ultrasonic cavitation on polymers was first reported by Flosdorf and Chambers in 1933 [52]. They applied high-frequency ultrasounds in solutions of natural polymers and observed a decrease in the viscosity of the solution after the treatment. They attributed their observation to a breakdown of the polymer chain to smaller chains. After this observation, several other groups investigated the degradation of polymers in solution and their results indicated that cavitation is the most crucial parameter for the scission of the polymer chains. However, none of these

groups has reported the nature of the new chain ends formed after the chain scission. Later, in 1950, Melville and Murray elucidated the nature of ultrasonic degradation of polymers in solution [53]. They sonicated solutions of poly(methyl methacrylate) and polystyrene and observed events of the initiation of a polymerization process they suggested the homolytic bond rupture and the generation of radicals

To date, a large number of studies have reported the degradation of polymers in solution both in organic and aqueous media. The solvent, the applied frequency and the intensity of the ultrasound, the solution concentration and the temperature are the most crucial parameters that have been extensively studied in different polymer systems to obtain insights on the mechanism of polymer degradation under ultrasonic irradiation. Most of these cases concluded that solvents of low viscosity and low solution concentrations increased the degradation rate because the polymer chains diffuse faster in the solution. Alike, faster degradation was also observed in polymer systems at higher solution temperatures. Nevertheless, the effect of the applied ultrasound frequency is not very clear. For polymers such as carboxymethyl cellulose, polyvinyl alcohol and polystyrene the degradation rate was significantly faster at low frequencies than at frequencies above 1 MHz. On the other hand, the degradation of starch, chitosan, dextran and poly(ethylene oxide) was more efficient at high sonication frequencies (350-500 kHz) compared to low frequencies (20 kHz) [54].

Although there are still questions about the precise mechanism of polymer chain scission under ultrasonication, it is generally accepted that the polymer chains breakdown due to solvodynamic shear forces created by the collapsing bubbles. Polymer segments near the field of bubble collapse move at a higher velocity compared to the segments that are further away from the cavity. This phenomenon causes the elongation of the polymer chain and the development of tension along the polymer backbone which finally leads to chain scission. Collectively, it has been concluded that the chain scission is a non-random process and preferentially occurs near the mid-point of the chain, due to greater stretching at this site (**Figure 1.11a**). Moreover, it has been accepted that polymers with higher molecular weights degrade faster than those with lower molecular weights and that there is a limiting molecular weight (M_{lim}) below which no more chain scission can occur [55]. Schaefer et al. confirmed that there is a cutoff degree of polymerization below which the polymer chains cannot degrade, by demonstrating an extensive study on the effect of the

contour length of the polymer chain and the polymer molecular weight on the chain scission of PS and poly(norbornene) homopolymers [56].

More recently, Moore and his group introduced for the first time the concept of site-specific bond cleavage upon sonication. More specifically they proposed that they can control the degradation of a polymer by placing a force-labile moiety along the polymer backbone. In their first study, they incorporated an azo linkage, as a labile bond for specific cleavage, in the center of a PEG backbone [57]. This study triggered the research for new ultrasound or mechano-labile units that could afford novel functional materials. In 2006, Ken Caster from the Army Research Office (ARO) introduced the term “mechanophore” to characterize all the labile bonds that undergo physicochemical changes in response to an exogenous mechanical stimulus such as ultrasound. To date, several different chemical groups have been recognized as mechanophores and have been proposed for site specific activation of chemical bonds (**Figure 10B**). The mechanochemical reactions that can take place are classified into three categories which include bond scission (homolytic, heterolytic or coordinate bond), pericyclic reactions and isomerizations [58].

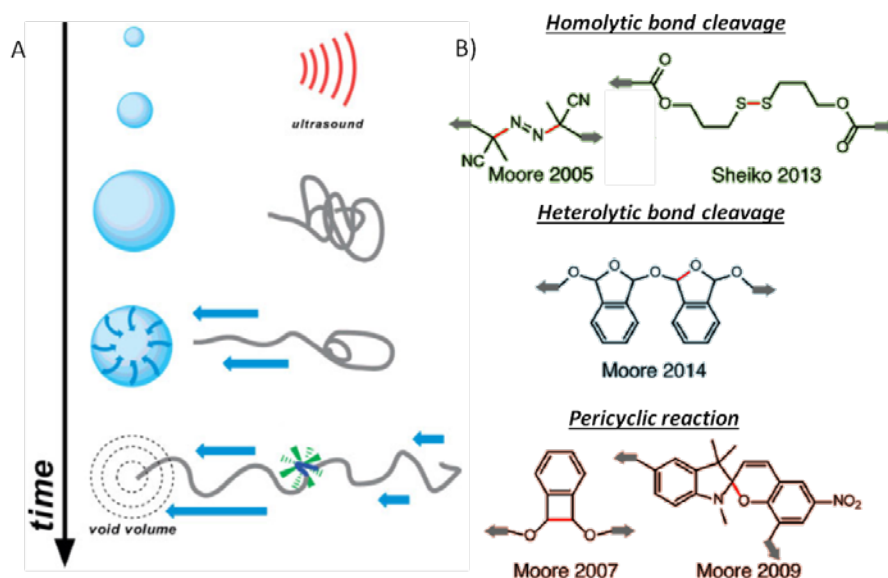


Figure 1.11: a) Cavitation results in elongation of a coiled polymer chain and cleavage of the weaker bond along the polymer backbone, b) Examples of mechanophore structures reported to date [58], [59].

Among them, a very interesting example is the ultrasound-triggered cleavage of poly(o-phthalaldehyde) (PPA) proposed by Moore's group [60]. In this study they demonstrated the mechanochemically triggered depolymerization of linear and cyclic PPA and proposed a heterolytic scission mechanism for these polymers. Their results were also supported by molecular dynamic calculations that confirmed the heterolytic unzipping of the polymer chain. It was also presented for the first time that extensive sonication leads to complete depolymerization and generation of the initial monomers that can further be further re-polymerized under suitable conditions. The reusable character of this synthetic polymer and the unique ability of remodeling are of significant interest for the development of adaptive and sustainable material systems for a plethora of applications.

1.7.3 Ultrasound-triggered release from polymer micelles

Ultrasound-triggered drug release from polymeric micelles was first investigated by Rapoport et al. [58–60]. They used a Pluronic P-105 copolymer to prepare micelles loaded with Dox and they investigated the effect of ultrasound on the drug release profile of the micelles. The micelles were incubated in several cell lines including promyelocytic leukemia HL-60, drug-sensitive A2780 and ovarian carcinoma A2780/ADR cells and they concluded that ultrasound irradiation not only triggers drug release from the micelles but also enhances the intracellular uptake of both the released and the micellar encapsulated drug. However, the mechanism of drug release from the pluronic micelles was not very clear. Rapoport reported that the released drug was quickly re-encapsulated into the micelles when sonication was ceased therefore its release was mostly attributed to the diffusion of the drug from the micelles due to their destabilization upon sonication rather than the degradation of the micellar structures.

In another example Zhang et al., prepared an amphiphilic block copolymer comprising a hydrophilic PEG block and a hydrophobic poly(lactic acid) (PLA) block which is known for its biodegradability and biocompatibility and formed polymeric micelles loaded with the hydrophobic dye Nile Red [64]. They successfully verified the controlled release of the dye from the hydrophobic core of the micelles by employing HIFU irradiation at different intensities and at different focal points of

irradiation. The irreversible release of Nile Red from the PEG-*b*-PLA micelles was attributed to the disruption of the micelles due to the degradation of the block copolymer rather than the destabilization of the micelles.

The same group, inspired by the concept of “mechanophore” and site-specific bond cleavage, prepared the same amphiphilic block copolymer bearing a weak mechano-labile bond in the middle of the polymer chain [65]. More specifically, they introduced a disulfide (S-S) linkage between the PEG and the PLA blocks (PEG-S-S-PLA) in order to achieve a faster degradation profile as the disulfide bond has a lower dissociation energy ($E_{S-S}=268 \text{ kJ mol}^{-1}$) and longer bond length ($l_{S-S}=2.03 \text{ \AA}$) compared to the C-C bond ($E_{C-C}=347 \text{ kJ mol}^{-1}$, $l_{C-C}=1,54 \text{ \AA}$). As a result of this, the PEG-S-S-PLA copolymer micelles were more sensitive to HIFU irradiation (1.1 MHz) and at the same time the disulfide junction introduced a redox response to the polymer (**Figure 1.12**). Thus, the combinatorial use of HIFU and a redox agent (GSH) allowed the fine-tuning of the release kinetics of the encapsulated cargo and the site-specific fast release.

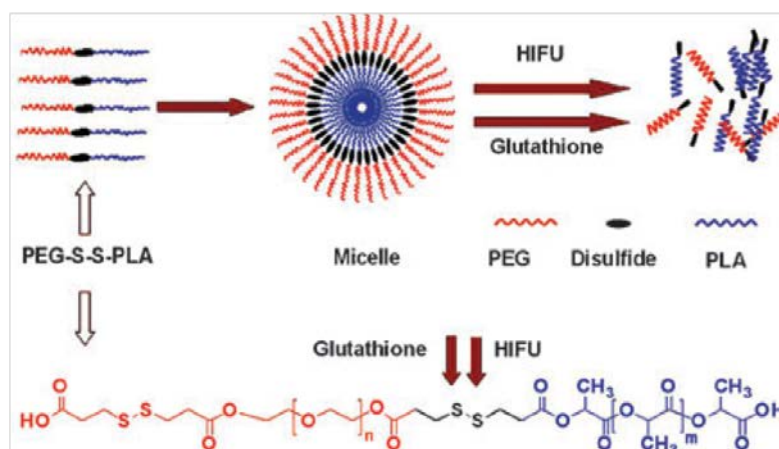


Figure 1.12: Schematic illustration of a HIFU and redox dual responsive release process from PEG-S-S-PLA block copolymer micelles [65].

Another ultrasound and redox responsive drug delivery system was proposed by Tong et al. [66]. They prepared an ABA triblock copolymer using poly(ethylene glycol) methyl ether as the hydrophilic block and polyurethane as the hydrophobic block and incorporated different number of disulfide bonds (PEG-PU(50%SS)-PEG and PEG-PU(100%SS)-PEG) along the copolymer backbone. They found that the number of

disulfide bonds resulted in small differences in the release rates with the PEG-PU(100%SS)-PEG copolymer releasing the cargo approximately 10mins faster than the PEG-PU(50%SS)-PEG copolymer micelles. However, the effect of the combined HIFU and redox stimulus enhanced significantly the release rate. Following the same concept of ultrasound/redox responsive systems, the same group reported a novel copolymer based on a PEG block and a poly(propylene glycol) (PPG) block bearing a central ester bond and a disulfide bond (PEG-COO-SS-PPG) [67]. The new finding in this system was that the mechano-chemical cleavage caused by HIFU irradiation occurs preferentially at the central ester bond rather than the disulfide linkages despite the higher bond energy of the former (358 kJ mol^{-1}).

In a different approach, Zhao et al. reported on the HIFU (1.1 MHz) response of an amphiphilic diblock copolymer comprising of a poly(ethylene oxide) (PEO) block as the hydrophilic part and a poly(tetrahydropyranyl methacrylate) (PThPMA) as the hydrophobic block [68]. They used the PEO-*b*-PThPMA block to form micelles in water loaded with the hydrophobic dye Nile Red and they employed HIFU irradiation to disrupt the micellar structures and release the dye molecules loaded in the assemblies. The mechanism proposed was based on the cleavage of the labile acetal bonds located in the side-chain of the polymer, leading to the transformation of PThPMA to hydrophilic poly(methacrylic acid) (PMAA) which results in the destruction of the micelles (**Figure 1.13**). The same group also performed a comparative study on the disruption of block copolymer micelles composing of a PEO block and different polymethacrylate blocks [69]. They found that the poly(ethylene oxide)-block-poly[1-(isobutoxy)ethyl methacrylate] (PEO-*b*-PIBMA) and PEO-*b*-PThPMA micelles with hydrophobic blocks bearing labile acetal bonds in their side-group are more sensitive to HIFU irradiation and release their cargo more efficiently compared to micelles formed by PEO-*b*-PMMA.

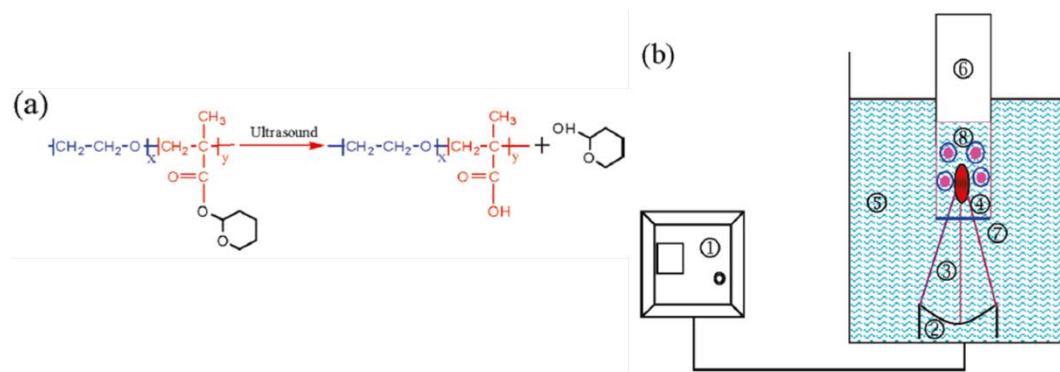


Figure 1.13: (a) Proposed mechanism of the HIFU-triggered cleavage of the tetrahydropyranyl groups of the PEG-*b*-PTHMPMA copolymer to produce methacrylic acid moieties. (b) Schematic diagram of the HIFU apparatus used in most studies: 1) ultrasound generator, 2) acoustic lens transducer, 3) ultrasonic beam, 4) focal spot, 5) water bath, 6) tube reactor, 7) latex membrane and 8) micelles solution [68].

Another example was reported by Lee and co-workers [70]. They synthesized a redox- and ultrasound-triggered thermo-responsive amphiphilic copolymer comprising of a poly(*N*-isopropylacrylamide) (PNiPAAm) block which is a water soluble polymer with lower critical solution temperature (LCST) around 32°C, close to body temperature and a poly(4-substituted- ϵ -caprolactone) (PXCL) block. The two blocks were linked via a disulfide bond (S-S) to afford the redox and ultrasound response to the final PNiPAAm-S-S-PXCL block copolymer. The copolymer formed spherical micelles in aqueous solutions which were loaded with the hydrophobic dye Nile Red. The release profile of the micelles was studied separately and in combination of the three stimuli. It was found that the dye molecules were effectively released from the assemblies under the combined stimulation of temperature, the redox agent and HIFU (20 kHz) irradiation. The cytotoxicity of the polymer and the Dox-loaded PNiPAAm-S-S-PXCL copolymer micelles in the presence of a redox agent (DTT) was tested on HeLa cancer cells. The results showed that the polymer is slightly cytotoxic even at very low concentrations and there are no significant differences in the cell death for the Dox-free and Dox loaded micelles.

1.8 Current study

Ultrasound-degradable polymeric nanocarriers have lately attracted great scientific interest. However, the ultrasound-responsive polymer systems reported to date suffer from major drawbacks. The most important limitations of these systems are 1) the high irradiation energies required for their degradation and the release of their cargo and 2) the high molecular weight degradation products which are often toxic to cells. These drawbacks limit their use in clinical applications. In response to this demand, the current work presents the development of a novel ultrasound and pH, dual responsive drug release system based on PEG-*b*-polyacetal diblock copolymer micelles (**Figure 1.14**). Encouraged by our previous results which proved the high sensitivity of polyacetals to light irradiation at low energies, we envisaged the use of ultrasound as an external stimulus to cleave mechanochemically the polymer chains of block copolymer polyacetals under clinically relevant ultrasound irradiation.

The present study is divided into three parts. In the first part of this work, an extensive study on the degradation profile of homopolymer polyacetals upon exposure to ultrasound was carried out. Two different homopolymer polyacetals, one aliphatic and one aromatic, were synthesized via a step-growth polycondensation reaction of a diol with a divinyl ether. Both homopolymers were synthesized at low (5000 gr/mol) and high (15000 gr/mol) molecular weight. The parameters which affect polymer sono-degradation in solution, such as the molecular weight of the polymer chain, the type of the solvent, the ultrasound frequency (42 kHz and 1 MHz) and the chemical structure of the polymer were investigated. The degradation kinetics were studied by GPC and the degradation products were analyzed by ¹H-NMR spectroscopy. The proposed mechanism of the sono-degradation of the polyacetals is discussed.

In the second part of the thesis, three different amphiphilic PEG-*b*-polyacetal diblock copolymers were synthesized following a two step polycondensation reaction. The copolymers that were synthesized were the PEG-*b*-PA-benz, PEG-*b*-PA-hex and PEG-*b*-PA-nitro. The degradation profile of the block copolymers under ultrasound irradiation at 1 MHz, was studied in organic media. The degradation kinetics were monitored by GPC and ¹H-NMR spectroscopy and the proposed mechanism for the degradation of the block copolymers is presented.

In the last part of this work, the self-assembly of the synthesized amphiphilic block copolymers was studied in water. PEG-*b*-polyacetal micelles were prepared and were

characterized by Dynamic Light Scattering (DLS) and Scanning Electron Microscopy (SEM). Furthermore, one of these block copolymers was selected to study 1) the possible changes on the micellar structure following exposure to ultrasound irradiation and 2) the release profile of a model dye from the micelles upon sonication at different conditions. Finally, the synergistic effect of ultrasound and pH stimuli on the release profile of hydrophobic molecules from the micellar cores was investigated.

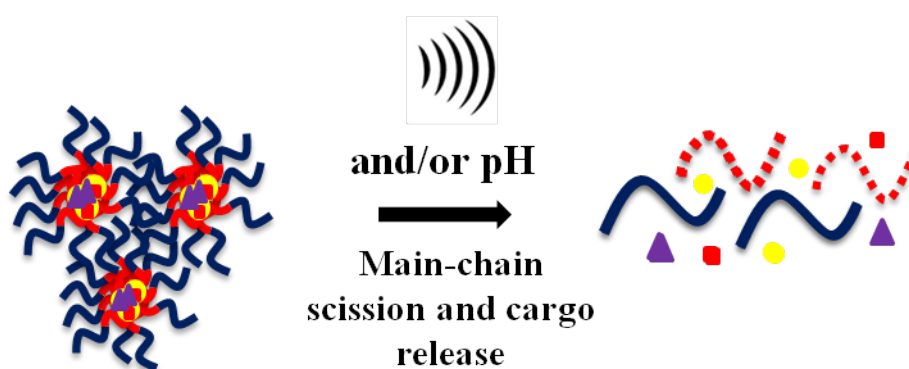


Figure 1.14: Schematic illustration of the proposed release system.

Chapter 2

Experimental

2.1 Materials

1,4-benzenedimethanol (99%) was purchased from Alpha Aesar. 1,6-cyclohexanedimethanol divinyl ether (98%) and 1,6-hexanediol were purchased from Sigma Aldrich. 2-nitro-1,4-benzenedimethanol was obtained from Tokyo Chemical Industry (TCI). All the diol monomers were dried under vacuum overnight before use. Poly(ethylene glycol) mono methyl ether (MePEG, Mw=5000gr/mol) was purchased from Polysciences, Inc. and was freeze dried before use. Pyridinium p-toluenesulfonate (PPTS) (98+%) was obtained from Alpha Aesar and was used as received. Sudan Red 7B (95%) was obtained from Sigma Aldrich. Triethylamine (TEA) (99,8%), tetrahydrofuran (THF) (HPLC grade), hexane (99,9%), petroleum ether and methanol (99,8%) were purchased from Sigma Adrich.

2.2 Characterization methods

2.2.1 Gel Permeation Chromatography (GPC)

The molecular weights and the molecular weight distributions of the polymers were determined by GPC utilizing a Waters-515 isocratic pump equipped with two columns, Mixed-D and Mixed-E (Polymer Labs), a Waters 2745 Dual Absorbance detector and a Waters 410 refractive index (RI) detector. THF with 2% TEA was used as the eluent at a flow 1ml/min and the column temperature was set at 40°C. The molecular weights of the polymers were determined by the universal calibration method using eight narrow molecular weight PMMA standards ranging from 875 to 138,600gr/mol. In a typical measurement, 20 mg of the polymer were dissolved in 1ml THF (HPLC), filtered through a PTFE filter with pore size 0.45 μm and was injected to the system (20 μL).

2.2.2 ¹H NMR spectroscopy

¹H Nuclear Magnetic Resonance (NMR) spectra were recorded on an Avance Bruker 300MHz spectrometer. CDCl₃ and d8-THF were used as the solvents.

2.2.3 Ultraviolet/Visible spectroscopy

UV/Vis absorption spectra were recorded on a Lambda 25 spectrophotometer (Perkin Elmer) in the wavelength range 200-900nm. All the samples were measured using quartz cuvettes.

2.2.4 Field emission scanning electron microscopy (FE-SEM)

FESEM images were obtained from a JEOLJSM-7000F microscope. For each measurement one drop of a dilute suspension of the sample was deposited on a silicon substrate and was allowed to dry overnight at room temperature.

2.2.5 Dynamic Light Scattering (DLS)

The size of the micelles was measured using a Malvern Zetasizer Nano ZS instrument equipped with a 4 mW He-Ne laser operating at $\lambda = 632.8$ nm. The scattered light intensity was measured at a scattering angle of 90°. The reported data are average values of three runs.

2.3 Ultrasound apparatus

In this study, two different ultrasound apparatus were used. The first was a commercially available ultrasound machine for physical therapy (Globus Medisound 3000, Italy) with a double-frequency ultrasound transducer at 1 MHz and 3 MHz and with an option for continuous wave (cw) or pulsed wave use (**Figure 2.1**). According to the manufacturer, the maximum intensity output was 3 Watt/cm². For the degradation experiments the parameters that selected were 1 MHz or 3 MHz, 3 Watt/cm² at cw application. The ultrasound head was immersed in a water bath to a)

avoid overheating of the head and b) maintain a constant temperature during the experiment. In this case, a large amount of the output energy was lost due to absorption from the medium (water) so the final intensity was calculated from the above equation:

$$Q = mC_v \frac{\Delta T}{dt}$$

Where m is the mass of water in kilograms, C_v is the heat capacity of water and $\Delta T/dt$ is the fluctuation of the temperature to a constant time dt . From this equation the calculated intensity of our system was found 0.083 Watt/cm^2 . The samples were placed at the middle of the ultrasound head at a constant distance of around 2-3 cm.

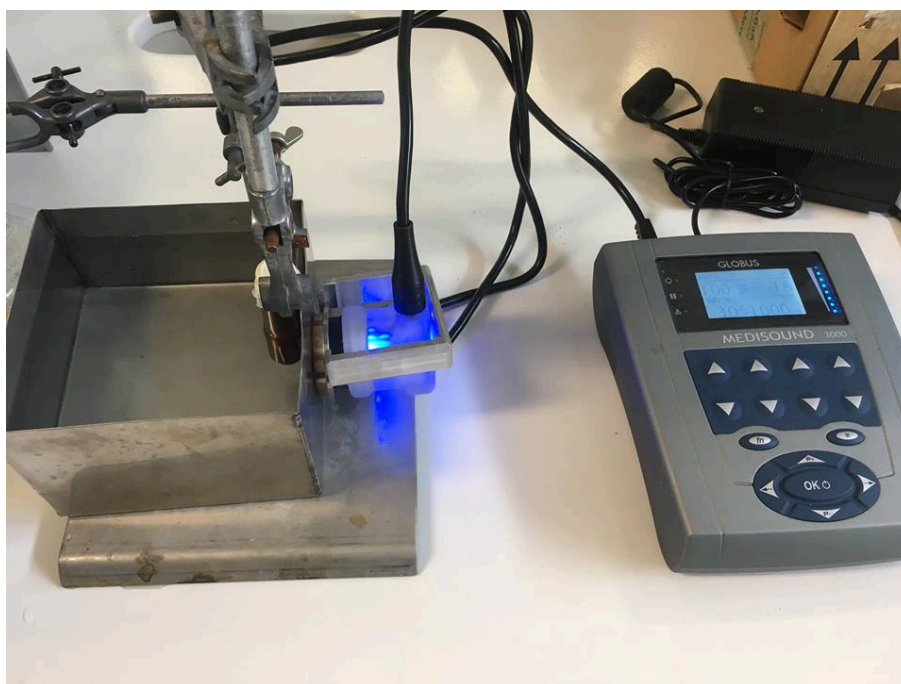


Figure 2.1: Ultrasound set up at 1 MHz and 3 MHz used in this study.

The second set up used for the sonication experiments was an ultrasound bath (Cole-Parmer 8891) with frequency 42 kHz and maximum water capacity 2 Lt (**Figure 2.2**). Under the sonic bath there are two piezoelectric transducers which create the ultrasound waves. The output intensity was calculated from the same equation as

above and it was found 0.24 Watt/cm^2 . In this case, the samples were immersed in the bath at a distance 10 cm from the bottom. In both experimental set ups, the water medium was changed every hour of sonication in order to prevent overheating and maintain similar conditions for all the experiments.



Figure 2.2: Ultrasonic bath used at 42 kHz in this study.

2.4 Synthesis of the polyacetal homopolymers

The synthesis of the polyacetal homopolymer was achieved following an acid-catalyzed polycondensation reaction of a divinyl ether with a diol under mild conditions. Three different homopolymers were synthesized by varying the diol monomer (**Figure 2.3**). In each case, one homopolymer of low molecular weight (5000gr/mol) and one of higher molecular weight (15000gr/mol) were prepared.

For the synthesis of the different polyacetals, slightly different reaction conditions were chosen to obtain the final product with the desired molecular characteristics. In brief, the diol monomer was dissolved in anhydrous THF under mild stirring at room temperature. Subsequently, the second monomer, 1,4-cyclohexanedimethanol divinyl

ether (CHDE), was added at a diol:ether molar ratio 1:1.1 and was allowed to react in the presence of an acid catalyst (1% PPTS with respect to the diol monomer). The polymerization kinetics were followed by GPC. Aliquots of the reaction mixture were collected and diluted in THF (HPLC) at predetermined time intervals. The solutions were filtered through 0.45 μm PTFE filters and were injected into the GPC. The reaction was left under stirring until the desired molecular weight was obtained and then a few drops of dry MeOH were added to terminate the polymer. Next, a few drops of triethylamine were added to quench the acid catalyst. The polymers were recovered by precipitation in cold petroleum ether or dry MeOH. The obtained products were dried under vacuum overnight, were purged with nitrogen and were stored at 4°C until use. The amounts of the reagents used for the synthesis of the polyacetals are summarized in Table 2.1.

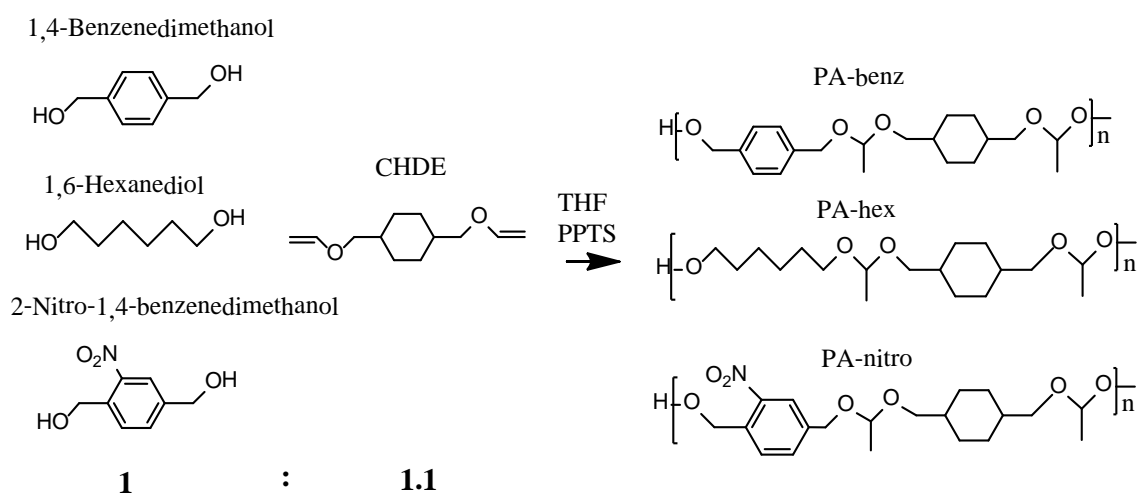


Figure 2.3: Synthetic procedure followed for the preparation of polyacetal homopolymers.

Table 2.1: Amounts of the reagents and reaction times used for the synthesis of the polyacetals PA-benz, PA-hex and PA-nitro.

	Diol	Divynyl ether (10% excess)	Anhydrous THF	PPTS 1%
1,4-Benzenedimethanol	0.5gr, 3.6mmol	0.85ml, 3.9mmol	3.6ml	0.009gr, 0.036mmol
1,6-Hexanediol	1 gr, 8.46mmol	2ml, 9.35mmol	4.2ml	0.02gr, 0.085mmol
2-Nitro-1,4-Benzenedimethanol	0.5gr, 2.72mmol	0.63ml, 3mmol	1.36ml	0.0067gr, 0.026mmol

*All reactions were carried out at RT

2.4.1 Sono-degradation experiments of the polyacetal homopolymers followed by GPC

For the sono-degradation experiments followed by GPC, samples of the synthesized polyacetals were prepared by dissolving 100mg of the polymer in 5ml THF (HPLC) to obtain 20 mg/ml final polymer concentration. The polymer solutions were filtered through hydrophobic PTFE filters with pore size 0.45 μm before being exposed to ultrasound irradiation. 20 μL of the irradiated samples were collected at predetermined time intervals and were injected into the GPC system.

2.4.2 Sono-degradation experiments of the polyacetal homopolymers followed by $^1\text{H-NMR}$ spectroscopy

The polymers were dissolved in CDCl_3 or $d_8\text{-THF}$ at a final polymer concentration of 10-15 mg/ml and a solution volume of 2ml. All the samples were filtered through hydrophobic PTFE filters with pore size 0.45 μm before being placed in NMR tubes. The polymer solutions were exposed to ultrasound irradiation and NMR spectra were recorded at predetermined time intervals.

2.5 Synthesis of PEG-*b*-polyacetal di-block copolymers

The synthesis of the block copolymer polyacetals was carried out in two steps. In the first step, the polyacetal homopolymer was synthesized as described above (section 2.4). In the second step, a solution of the second block, MePEG (5000 gr/mol) in anhydrous THF was heated at 40°C (to facilitate the dissolution of PEG in THF) and was added in the reaction mixture (**Figure 2.4**). 1% PPTS was added to initiate the reaction. The polymerization kinetics were followed by GPC. Aliquots of the reaction mixture were collected and diluted in THF (HPLC) at predetermined time intervals. The solutions were filtered through 0.45 μm PTFE filters and were injected into the GPC. The reaction was stopped after a certain time by adding a few drops of triethylamine to quench the catalyst. The polymer mixture was precipitated into cold petroleum ether or hexane and dried under vacuum overnight. The final polymer was stored under N_2 atmosphere at 4°C until use. Three different block copolymers were synthesized based on the three polyacetals, PA-benz, PA-hex and PA-nitro. Table 2.2 summarizes the amount of reagents used for the synthesis of the block copolymers.

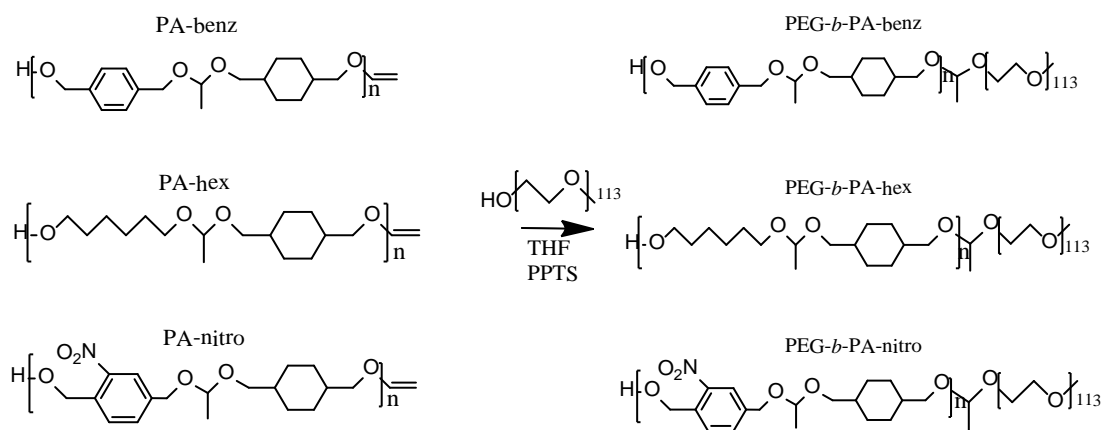


Figure 2.4: Synthetic procedure followed for the preparation of the block copolymers from the precursor polyacetals.

Table 2.2: Amount of the reagents and reaction conditions for the synthesis of the block copolymer polyacetals.

	Reaction time prior to the addition of the second block	MePEG	Anhydrous THF	PPTS 1%
PEG-<i>b</i>-PA-benz	2h	0.15gr, 0.03mmol	3.5ml	0.009gr, 0.036mmol
PEG-<i>b</i>-PA-hex	2h	0.4gr, 0.08mmol	4.2ml	0.02gr, 0.085mmol
PEG-<i>b</i>-PA-nitro	3h	0.2gr, 0.04mmol	1.36ml	0.0067gr, 0.026mmol

*All reaction were carried out at RT.

2.5.1 Sono-degradation of the block copolymer polyacetals followed by GPC

The degradation kinetics of the block copolymers were studied by GPC. Fresh copolymer solutions in THF with concentration 20 mg/ml and final volume 5ml were prepared and passed through 0.45 μm pore size filters before being subjected to ultrasound irradiation. 20 μL of the irradiated samples was collected at predetermined time intervals and were injected for analysis to the GPC system.

2.5.2 Sono-degradation experiments of the block copolymer polyacetals by ^1H -NMR spectroscopy

The degradation experiments were also followed by ^1H -NMR spectroscopy. Samples were prepared in deuterated CDCl_3 at a final concentration of 10-15 mg/ml and at a total volume of 2 ml. The polymer solutions were passed through 0.45 μm pore size filters and were transferred in NMR tubes. The samples were subjected to ultrasonication and NMR spectra were recorded at predetermined time intervals.

2.6 Preparation of PEG-*b*-polyacetal block copolymer micelles

For the preparation of the block copolymer micelles, 20 mg of the block copolymers were dissolved in 5 ml anhydrous THF and were left under stirring for 1-2 h at room temperature. Next, 15 ml of nanopure water at pH 7.5 were added dropwise under vigorous stirring at a 0.2 ml/min rate to induce the aggregation of the hydrophobic

blocks and lead to the micelle formation. Subsequently, another 5 ml of neutral water were added rapidly to freeze the micellar structures. The THF was removed from the micellar solution under vacuum in the rotavap at 40°C. The final micellar solution was passed through a 0.22 µm pore size filter to isolate the micelles as a nearly monodisperse suspension which was stored in the fridge at 4°C until use. A similar procedure was followed for all the synthesized block copolymers. The size, the shape and the morphology of the copolymer micelles were determined by DLS and FESEM.

2.7 Preparation of sudan red (SR)-loaded micelles

Polyacetal micelles loaded with a model dye, SR, were prepared using the block copolymer PEG-*b*-PA-benz. The loaded copolymer micelles were formed following a similar procedure to that described above in section 2.6. First, a stock solution of the dye in anhydrous THF was prepared at a final concentration of 1 mg/ml. Next, 50 mg of block copolymer were dissolved in 3 ml anhydrous THF and 2 ml of the dye solution were added in the polymer solution. The solution was left under stirring at room temperature for 1-2 h and next 20 ml water at pH 7.5 were added slowly to induce the formation of the micelles and simultaneously the encapsulation of SR. After that, another 5 ml of water were added rapidly to stabilize the micellar structure. THF was removed from the micellar solution under vacuum in the rotavap at 40°C. Upon the removal of THF, unloaded SR was precipitated in the water medium and was removed by filtration using a 0.22 µm pore size hydrophilic filter. In addition, the final micellar solution was dialyzed against a large excess of water at pH 7.5 for 2-3 h using a dialysis bag with molecular weight cut off 7000 gr/mol, to remove any traces of unloaded dye molecules and PEG homopolymer contamination. The final micellar solution was stored in the fridge at 4°C until use.

2.8 Ultrasound irradiation of the polyacetal-based micelles in water

In order to investigate the ultrasound-triggered degradation of the copolymer micelles and determined changes in the morphology and the size of the nanocarriers, a solution of the micelles (0.2 mg/ml) was sonicated at 1 MHz ultrasound frequency and 0.085

Watt/cm² intensity. Changes in the hydrodynamic diameter of the micelles were recorded by DLS. SEM images were obtained before and after ultrasound treatment.

2.9 Ultrasound-induced degradation of the PEG-*b*-polyacetal micelles and cargo release

In vitro release studies were performed on the dye-loaded PEG-*b*-polyacetal block copolymer micelles. A stock solution of the PEG-*b*-polyacetal loaded micelles was divided in three different parts and was diluted to a final concentration of 0.2 mg/ml, 1 mg/ml and 2 mg/ml, respectively. Each part was transferred into three different vials (4-5 ml solution in each vial). The first sample was used as a control (untreated), the second sample was sonicated with an ultrasound frequency of 1 MHz and 0.083 Watt/cm² intensity and the third sample was sonicated with applied ultrasound frequency of 3 MHz and 0.083 Watt/cm² intensity. Moreover, a micellar solution (0.2 mg/ml) was irradiated with a maximum intensity 3 Watt/cm². At predetermined time intervals the sonicated solutions were transferred into quartz cuvettes and the absorbance of the loaded-dye was monitored by UV-Visible spectroscopy.

2.10 pH- and ultrasound-triggered release of cargo from the polyacetal-loaded micelles

The synergistic effect of a low solution pH and ultrasound irradiation on the degradation profile of the polyacetal micelles was studied. A solution of dye-loaded nanoparticles at a 0.2 mg/ml concentration was prepared and was divided into three parts. The first sample was used as a control and was not subjected to ultrasound treatment. In the second part the pH was dropped to 5.0 using 0.1M HCl and in the third sample the pH was dropped at 5.0 and immediately it was transferred into the sonication bath for ultrasound treatment. The absorbance of the dye which remained in the hydrophobic core of the micelles following the application of the different stimuli for the same exposure time (1, 2, 3 and 4 hours) was monitored by UV-Visible spectroscopy.

Chapter 3

Results and discussion

3.1 Synthesis and characterization of the polyacetal homopolymers

Three polyacetal homopolymers were successfully synthesized by an acid-catalyzed polycondensation reaction of a diol with a divinyl ether under certain conditions. The progress of the polycondensation reaction and the increase of the molecular weight of the polymers were monitored by recording the GPC chromatograms at different polymerization times (1, 2, 3, 4, 6 and 24 hours). Typical chromatograms for the PA-benz, PA-hex and PA-nitro are shown in **Figure 3.1**. Typical for a step-growth reaction, the monomers react to form dimers, the dimers form trimers and tetramers and so forth. As the molecular weight increases, the GPC curve is shifted to lower elution times until an almost constant molecular weight is obtained due to the excess of the divinyl ether monomer.

As observed from the kinetics of the three polyacetals, the molecular weight gradually increased during the first 6 h of reaction for PA-benz and PA-hex and up to 4 h of reaction for the PA-nitro until a maximum of around 25000 gr/mol and 20000 gr/mol, respectively. It is noted, that in contrast to traditional step-growth polymerization in which the polymer chains become longer with reaction time, in this case a decrease in the molecular weight was found after 24 hours reaction time indicating that slight degradation of the polymer. This was attributed to the presence of the acid-catalyst, PPTS, in the reaction mixture [71].

In a polycondensation reaction, the monomers react in a non-controlled manner to form oligomers and the oligomers react to form the polymer chains. Due to the non-controlled character of this polymerization the final polymers have high polydispersity indices ($M_w/M_n > 1.5$). The molecular characteristics of the synthesized polyacetals are shown in Table 3.1. An aromatic, PA-benz, and an aliphatic, PA-hex, polyacetal of two different molecular weights, 5k and 15k, were synthesized. The number average molecular weights, determined by GPC, were in good agreement with the theoretical values, whereas the polydispersity indices ranged from 1.5-2.0. Finally, a PA-nitro of 5k with number average molecular weight (M_n) of 4600 gr/mol and $M_w/M_n = 1.97$ was synthesized.

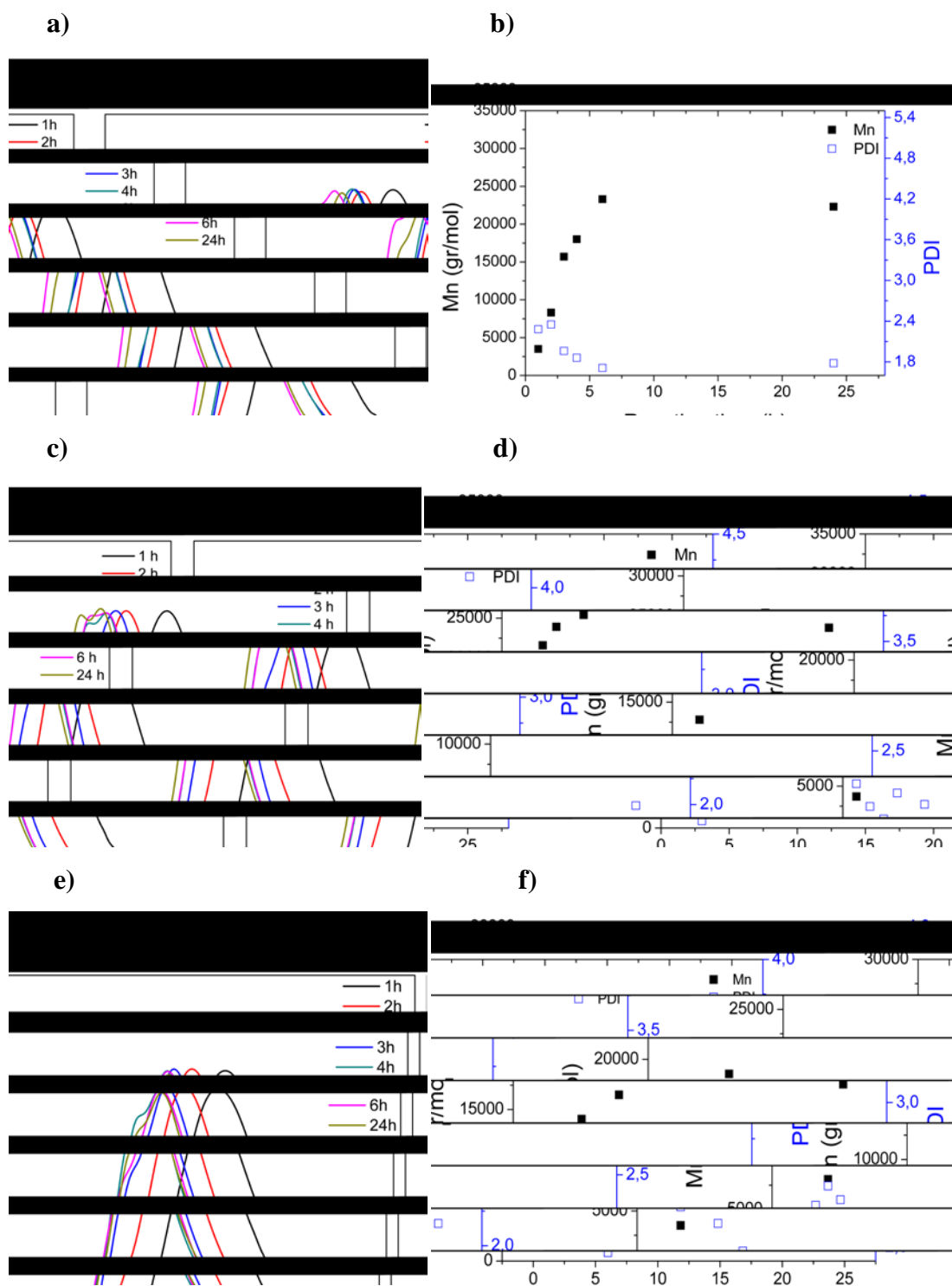


Figure 3.1: a) and b) GPC curves and kinetics data of PA-benz, c) and d) GPC curves and kinetics data of PA-hex and e) and f) GPC curves and kinetics data of PA-nitro.

Table 3.1: Synthesized polyacetal homopolymers and their molecular weight characteristics.

Polymer		Mn (gr/mol)	Mw (gr/mol)	Mw/Mn
PA-benz	15k	15000	30900	2.06
	5k	5000	7250	1.45
PA-hex	15k	14700	25800	1.75
	5k	5000	9050	1.81
PA-nitro		4600	9100	1.97

3.2 Sono-degradation study of the polyacetal homopolymers

3.2.1 Ultrasonic degradation of PA-benz-15k and PA-benz-5k

A freshly prepared sample of PA-benz, with average molecular weight (Mn) 15000 gr/mol, in THF (20 mg/ml) was used for the degradation study. The degradation kinetics of the polymer under ultrasound irradiation at 42 kHz frequency and 0.23 Watt/cm² ultrasound intensity was monitored by GPC. During ultrasound treatment, the shear forces created by cavitation are responsible for the disaggregation of possible polymer clusters in solution especially in the initial exposure times. Intramolecular interactions between the same polymer chain and between different chains are destroyed leading to swollen polymer chains whereas prolonged sonication gives extended chains in the solution that can break into shorter chains.

Figure 3.2a shows the characteristic GPC trace of the initial untreated polymer (black line) which shifts to higher elution volumes and broadens with sonication time indicating that chemical changes occurs on the polymer chains. The intensity of the main peak gradually decreases with irradiation time whereas the intensity of the peaks at high elution volumes which correspond to oligomers (13-16 minutes elution time) and to the initial monomers (16-19 minutes elution time) increases. Extensive sonication resulted in a limiting average molecular weight (Mn_{lim}) around 1000

gr/mol which corresponds to 3 monomer repeat units. It is also worth mentioning that the rate of polymer degradation is faster during the first 6 hours of sonication with an amazing decrease of the molecular weight from 15000 to 4000 gr/mol. However, the degradation rate significantly decreased after this time and extended irradiation was required (~25 h) to reduce the molecular weight from 4000 to 1000 gr/mol (**Figure 3.2b**). Based on these results, the overall polymer degradation was calculated ~94% which indicates that the polymer was successfully degraded into small molecules upon ultrasonication.

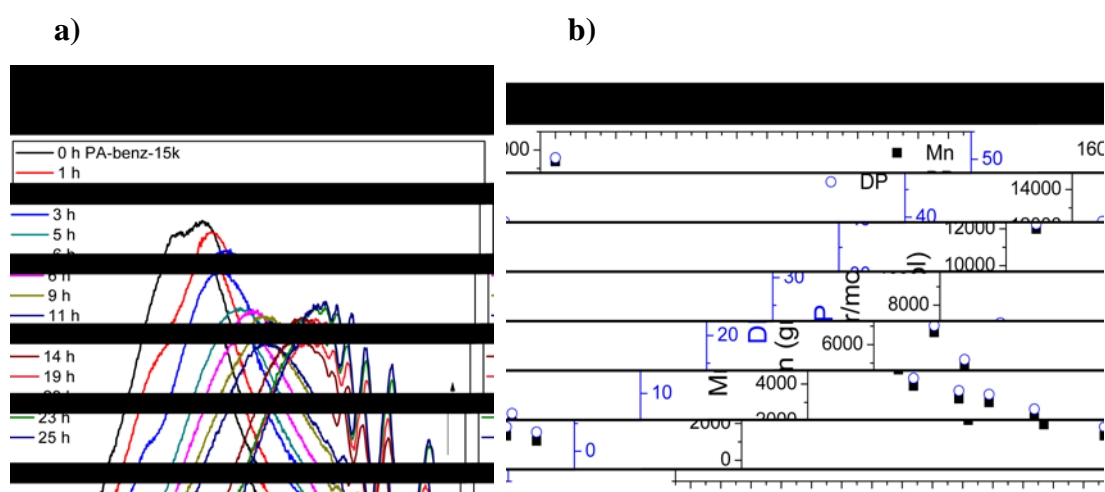


Figure 3.2: Ultrasonic degradation of PA-benz-15k in THF at 42 kHz and 0.23 W/cm² a) Degradation kinetics followed by GPC and b) the change in Mn and degree of polymerization (DP) as a function of sonication time.

The effect of the initial molecular weight of the polymer on the sonodegradation profile was also studied. A solution of low molecular weight PA-benz-5k was prepared in THF (20 mg/ml) and was subjected to ultrasonic irradiation under the same conditions (42 kHz). The degradation profile, as well as the polymer molecular weight obtained by GPC are presented in the **Figure 3.3**. The initial curve (black line) in **Figure 3.3a** corresponds to the untreated polymer chains, gradually shifted to higher elution times with sonication time. Simultaneously, four new peaks appeared at elution times above 16 mins and their intensity gradually increased indicating the formation of low molecular weight chains and monomers. The degradation rate is in good agreement to that found for PA-benz-15k. Extensive irradiation of 18 h was

applied in order to reach a limiting molecular weight which was again around 1000 gr/mol (**Figure 3.3b**).

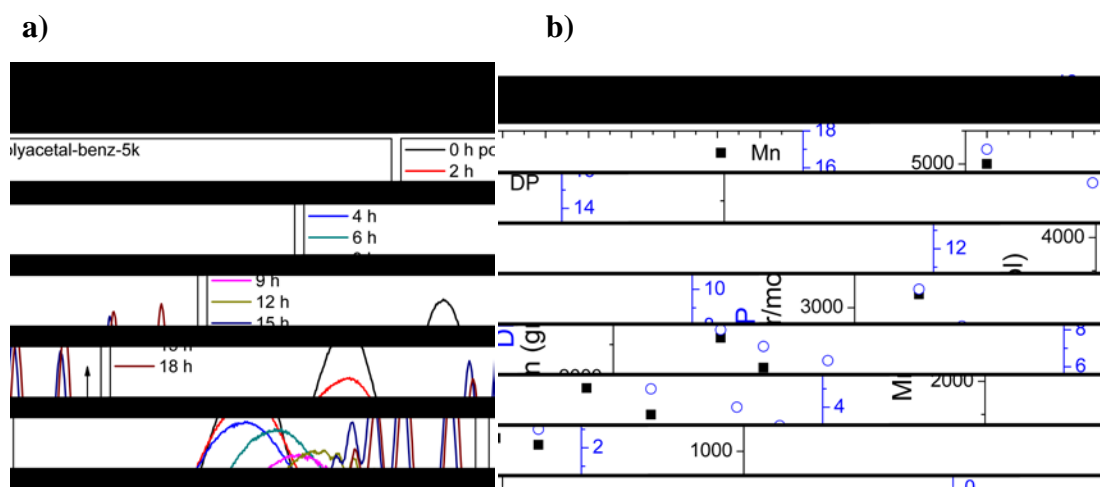


Figure 3.3: Ultrasonic degradation of PA-benz-5k in THF at 42 kHz and 0.23 W/cm² **a)** Degradation kinetics followed by GPC and **b)** Mn and DP as function of sonication time.

Next, the effect of the applied frequency on the degradation kinetics of the polyacetals was investigated. Samples of the two polymers (PA-benz-15k and PA-benz-5k) were prepared in THF at a concentration 20 mg/ml and were subjected to ultrasonic irradiation using 1 MHz ultrasound frequency. As mentioned in Chapter 1, the cavity effect (formation, growth and collapse of bubbles) is dominant at low ultrasound frequencies while at higher frequencies (above 2 MHz) fewer cavitation phenomena occur.

Figure 3.4 presents the degradation profile of PA-benz-15k and PA-benz-5k under 1 MHz irradiation. An incredibly fast initial degradation rate was observed for both polymers. In particular, the Mn of PA-benz-15k reduced from 15000 to around 8000 gr/mol in the first hour of treatment and reached a limiting Mn around of 2000 gr/mol after 11 h of sonication compared to 25 h ultrasound treatment required for the complete degradation at 42 kHz. Similar, the Mn of PA-benz-5k reduced from 5000 to 1000 gr/mol in only 4 h sonication which is almost 4 times lower to that used for its degradation at 42 kHz. Therefore, is obvious, that when increasing the ultrasound frequency the polymer chain scission increases for both the low and the high molecular weight polymers.

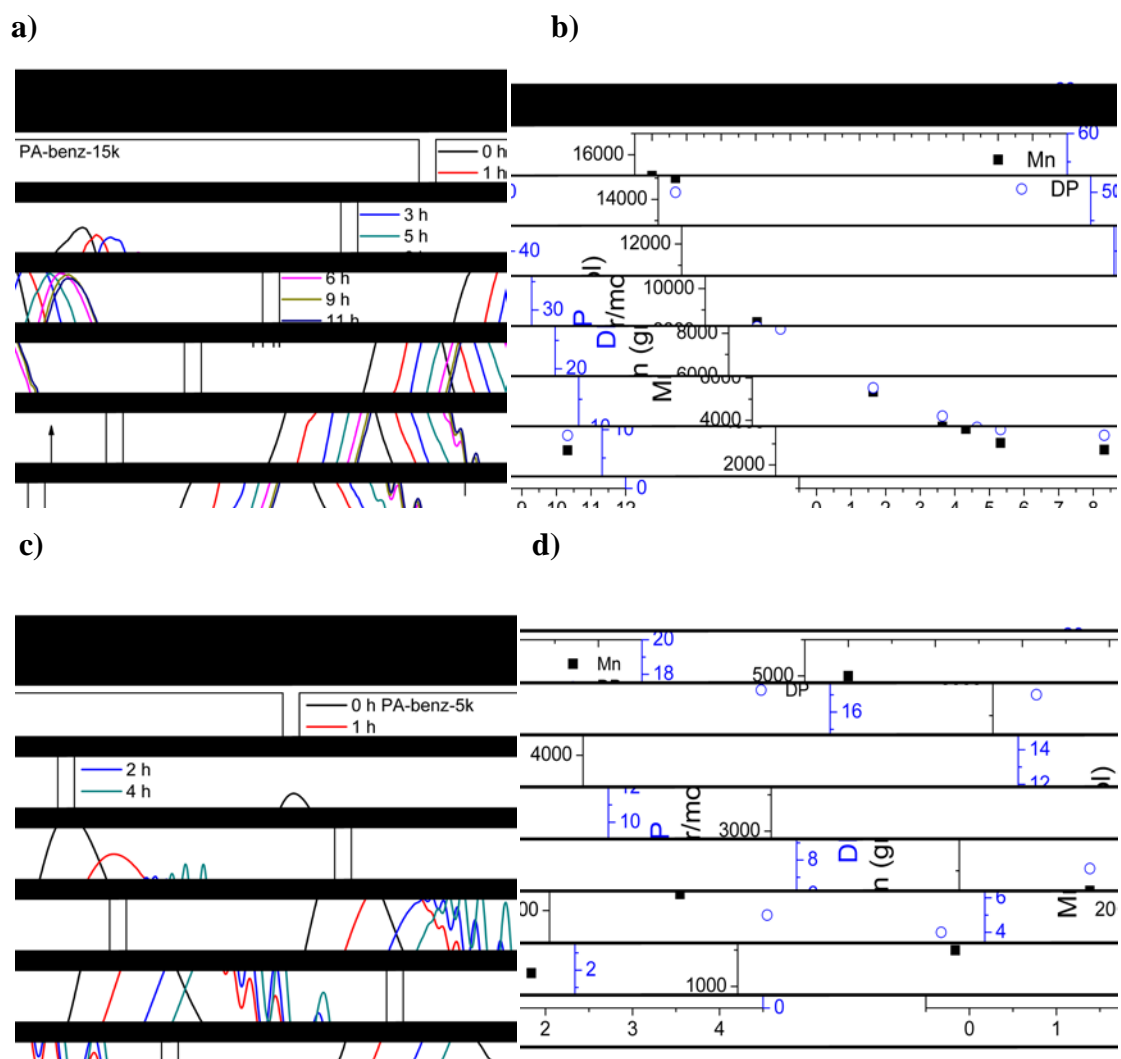


Figure 3.4: Degradation kinetics of PA-benz-15k and PA-benz-5k at 1 MHz ultrasound frequency and 0.083 W/cm^2 ultrasound intensity. **a)** GPC traces and **b)** Mn and DP as a function of sonication time for PA-benz-15k and **c)** GPC traces and **b)** Mn and DP as a function of sonication time for PA-benz-5k.

The degradation profiles for PA-benz-15k sonicated at two different frequencies (42 kHz and 1 MHz) are compared in **Figure 3.5**. In both cases, the Mn gradually decreases until a limiting molecular weight which is approximately the same. However, upon irradiation at 1 MHz, the degradation rate was faster at the first 3 h of sonication.

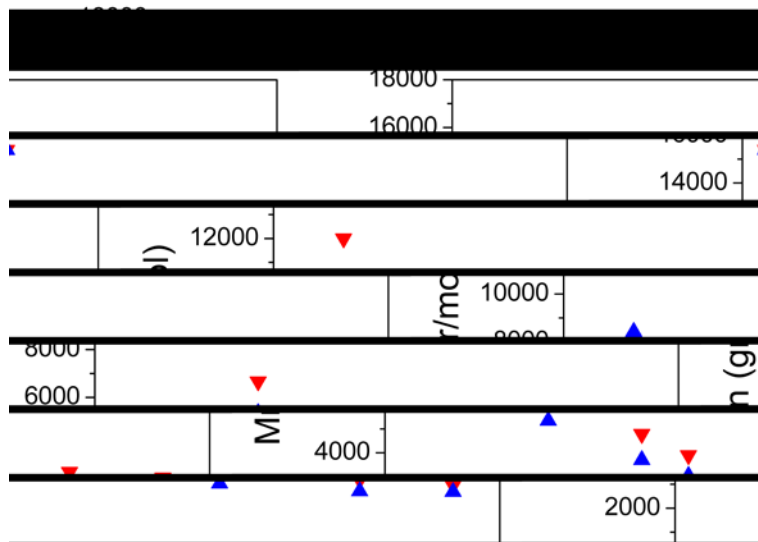


Figure 3.5: Molecular weight of PA-benz-15k as a function of sonication time (42 kHz (red down triangles) and 1 MHz (blue up triangles)).

On the other hand, significant differences were observed on the degradation profile of the low molecular weight PA-benz-5k. In Figure 3.6, it is clearly seen that the applied frequency affects significantly the degradation kinetics of the polymer. Only 4 h sonication are required at 1 MHz ultrasound frequency, while 18 h are need to reach a similar Mn at 42 kHz frequency.

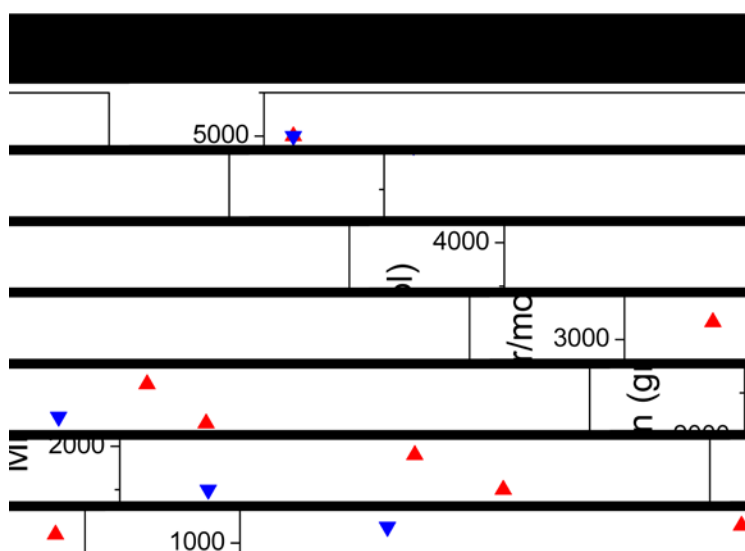


Figure 3.6: Molecular weight of PA-benz-5k as a function of sonication time (42 kHz (red up triangles) and 1 MHz (blue down triangles)).

As discussed in Chapter 1, the degradation of an acetal bond results in the production of an alcohol and an aldehyde molecule. For an efficient degradation, the presence of water molecules is important since the degradation of each acetal bond requires the presence of one water molecule to form the final degradation products. To confirm this hypothesis the degradation of PA-benz-15k was carried out in anhydrous THF as the solvent to minimize the presence of water and the degradation products were characterized by GPC.

In **Figure 3.7**, the degradation profile of the polymer upon sonication at 1 MHz frequency in regular THF and anhydrous THF is presented. The results suggest that when minimizing the water content of the solution the degradation rate reduces as expected, based on the discussion above. On the other hand, the presence of water plays a significant role in the cavitation effect. A small amount of water in an organic solvent decreases its viscosity which has been shown to influence the polymer degradation upon ultrasonication. At low viscosities the cavitation effect is more effective and the polymer chains move faster so that the produced shear forces can stretch the polymer backbone which facilitates bond cleavage.

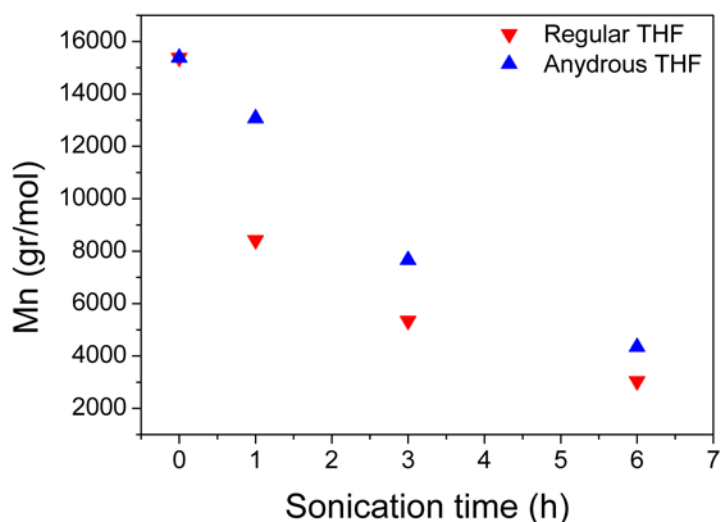


Figure 3.7: Degradation profile of the PA-benz-15k upon ultrasound irradiation at 1 MHz and 0.083 W/cm^2 intensity in regular THF (red triangles) and anhydrous THF (blue triangles).

The degradation mechanism was further studied by $^1\text{H-NMR}$ spectroscopy. For this, the sono-degradation of the high molecular weight PA-benz-15k was carried out in deuterated CDCl_3 using an ultrasound frequency of 42 kHz as described above. **Figure 3.8** shows the $^1\text{H-NMR}$ spectrum of the initial polymer before being subjected to sonication. The peaks assigned to all the corresponding protons of the polymer are observed and confirm the chemical structure of the polyacetal. The characteristic acetal proton appears at around 4.7 ppm.

Next, upon sonication, the integral of the characteristic acetal proton peak gradually decreased indicating the successful cleavage of the labile acetal bond (**Figure 3.9a, red arrow**) and the mechanically-induced main-chain scission of the polymer. In parallel, four new peaks appeared at 9.7, 4.9, 3.6 and 2.1 ppm (**Figure 3.9a, blue arrows**) indicating the formation of the sono-degradation products.

The peaks at 9.7 and 2.1 ppm were assigned to the protons of the acetaldehyde molecule and the peaks at 4.9 and 3.6 ppm were attributed to the hydroxyl protons of the two diols 1,4-benzenedimethanol and 1,4-cyclohexanedimethanol, respectively (**Figure 3.10**). Nevertheless, the characteristic peaks of the protons of the polymer were still present in the spectra and were used to calculate the %decrease of the acetal proton peak which corresponds to a %degradation of the polymer. From this data it was found that the polymer degradation is 50% after 10 h sonication which is in agreement with the GPC results (see figure 3.2) (**Figure 3.9b**). The slightly higher (~73%) degradation of the polyacetal after 10 h sonication found by GPC was attributed to the absence of water molecules in CDCl_3 facilitate the degradation process as discussed above.

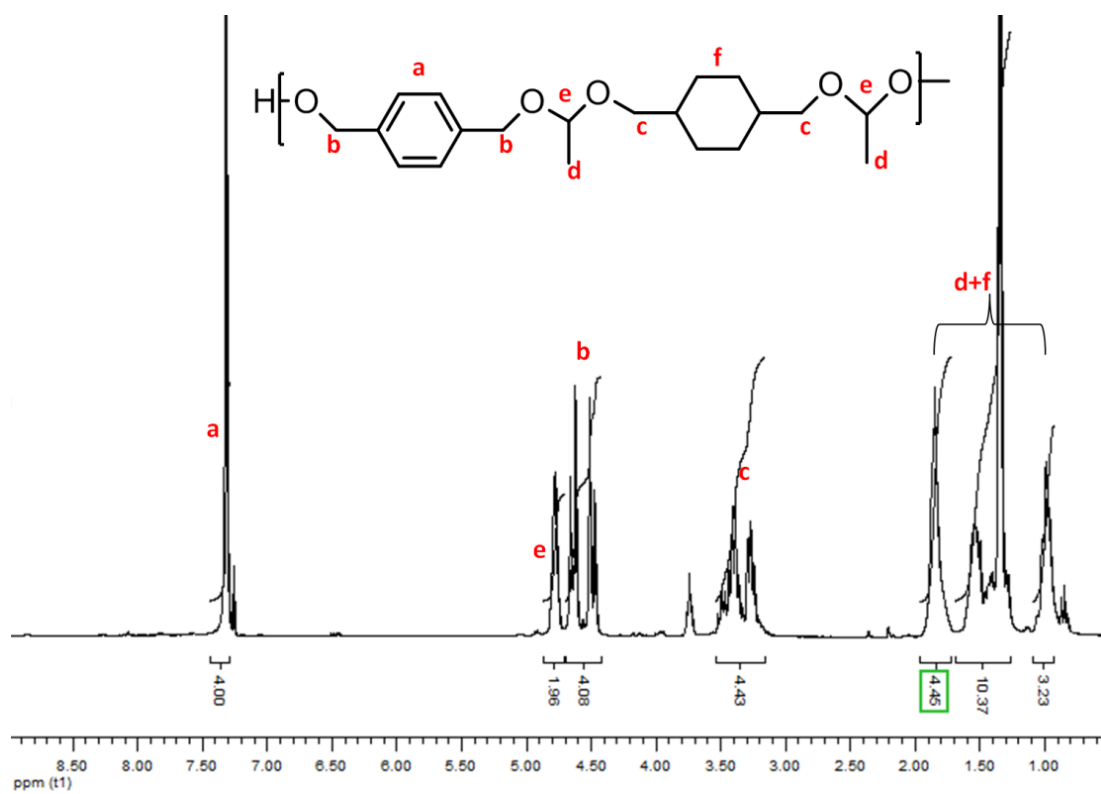
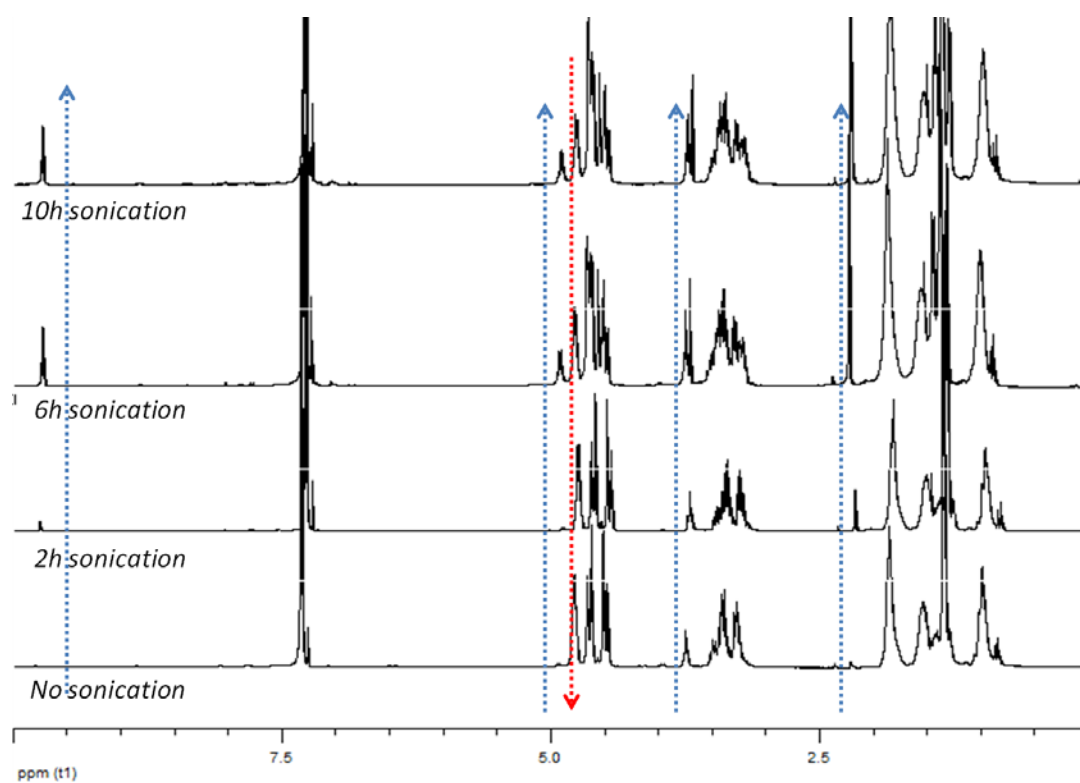


Figure 3.8: $^1\text{H-NMR}$ spectrum of PA-benz-15k in CDCl_3 .

a)



b)

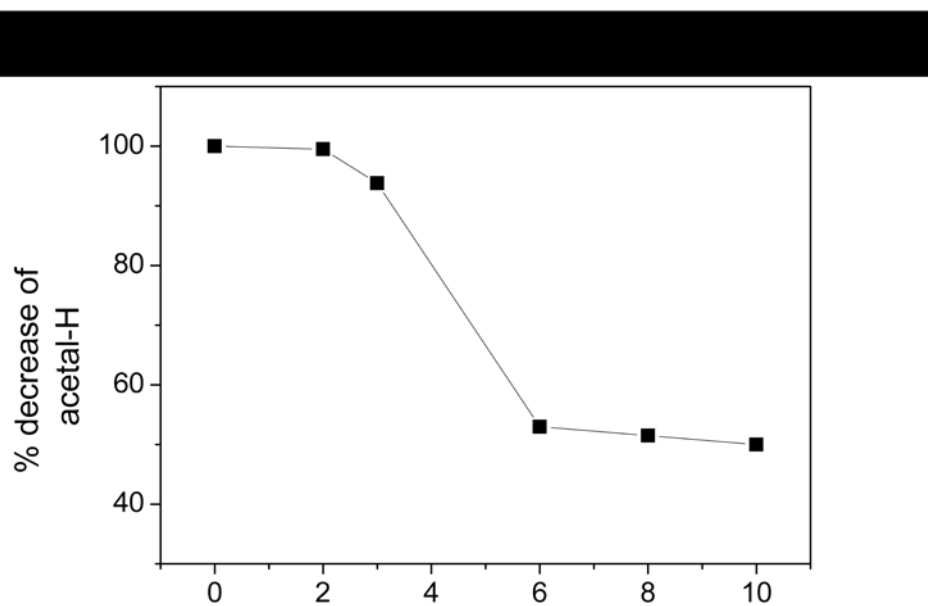


Figure 3.9: (a) $^1\text{H-NMR}$ spectra in CDCl_3 of PA-benz-15k during sonication at 42 kHz and (b) % decrease of the integral of the acetal proton found by $^1\text{H-NMR}$ as a function of sonication time.

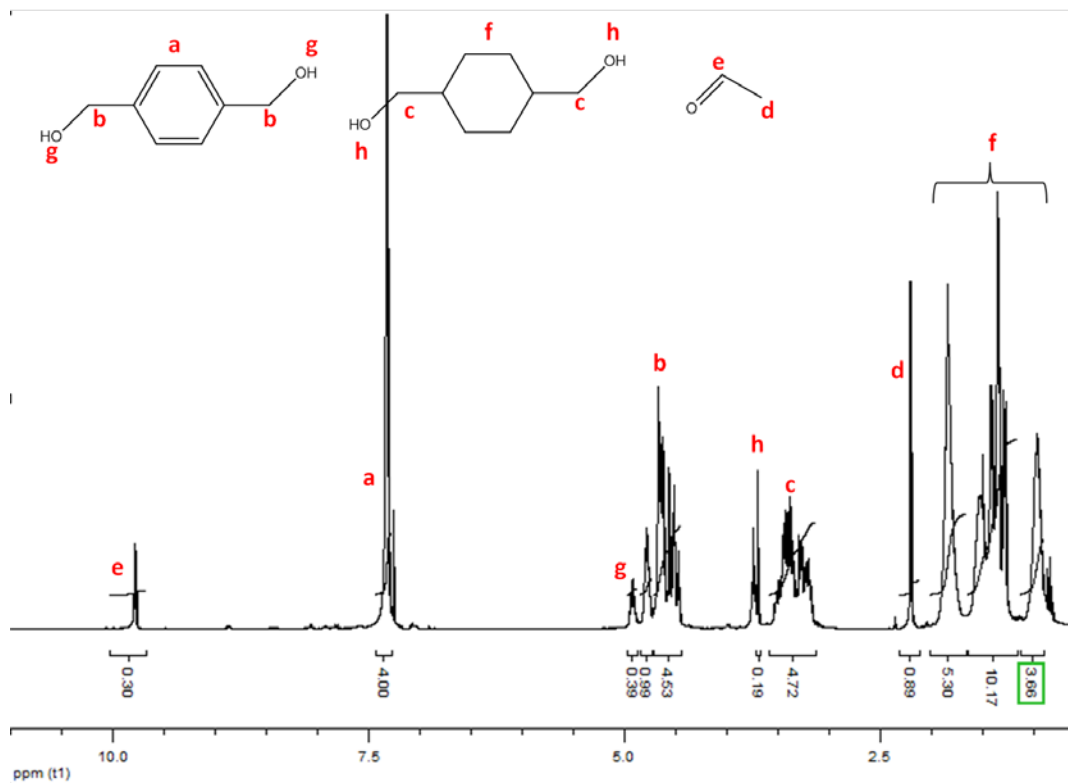


Figure 3.10: $^1\text{H-NMR}$ spectrum of PA-benz-15k after 10 h sonication at 42 kHz in CDCl_3 .

The ultrasonic scission of the polyacetals and the formation of the proposed degradation products were also studied by $^1\text{H-NMR}$ spectroscopy in deuterated THF. Following similar experimental protocol, PA-benz-15k was subjected to irradiation at 42 kHz ultrasound. No significant changes in the $^1\text{H-NMR}$ spectra of the polymer were found after 10 h sonication. Specifically, a $\sim 14\%$ decrease of the characteristic peak of the acetal group (4.7 ppm) which corresponds to $\sim 14\%$ degradation of the polymer was observed and the two peaks of the formed acetaldehyde molecule, at 2.1 and 9.7 ppm increased by $\sim 3.5\%$ and 0.9% , respectively. Furthermore, the peaks of the hydroxyl groups of the diols are not observed probably because of their very low concentration in the solution (**Figure 3.11**). The low polymer degradation in this case was attributed to the absence of water molecules in the solvent medium.

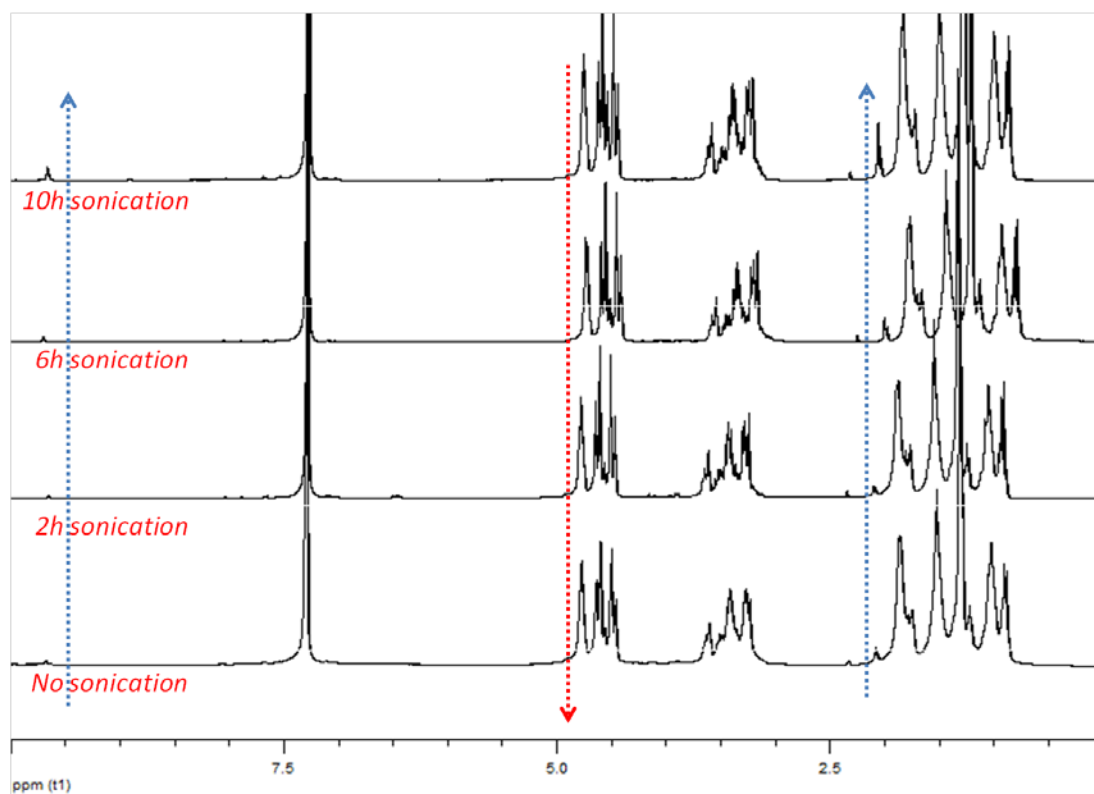


Figure 3.11: ^1H -NMR spectra in THF- d_8 of PA-benz-15k as a function of sonication time (42 kHz).

3.2.2 Ultrasonic degradation of PA-hex-15k and PA-hex-5k

Following the degradation studies of the aromatic PA-benz the effect of the chemical structure of the polymer on its degradation profile was investigated. For this purpose, PA-hex, which bears a six member aliphatic carbon chain instead of the aromatic benzene ring was employed.

Figure 3.12 shows the GPC traces of PA-hex-15k (**Figure 3.12a**) and PA-hex-5k (**Figure 3.12b**) after 6 h exposure to 1 MHz ultrasound frequency. In both cases, the GPC chromatograms did not change after 6 h irradiation suggesting that no polymer degradation has occurred. Similar results were obtained for PA-hex-15k after 6 h irradiation at 42 kHz suggesting that the irradiation frequency does not influence the polymer degradation (**Figure 3.12c**). It is noted that the degradation experiments were repeated at least twice and the results obtained were similar in all cases.

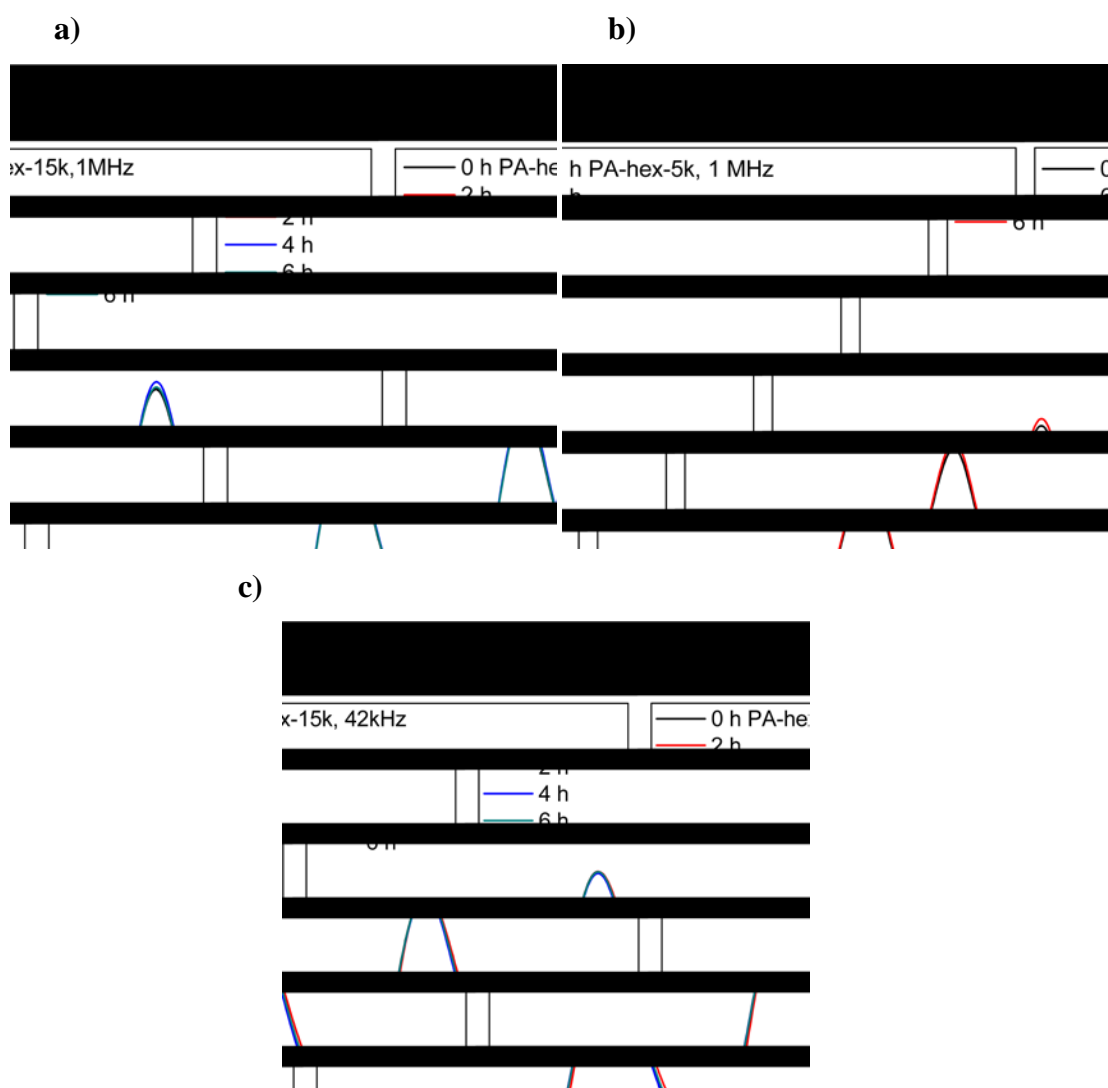


Figure 3.12: GPC traces of PA-hex-15k after 6 h exposure to 1MHz (a), PA-hex-5k after 6 h exposure to 1MHz (b) and PA-hex-15k after 6 h exposure at 42 kHz (c).

3.2.3 Influence of the chemical structure on the ultrasonic degradation of the polyacetals

From the above results it is obvious that the sono-degradation profile of the polyacetals is strongly affected by the chemical structure of the polymer. Homopolymer polyacetals bearing aromatic groups degrade into smaller molecules after exposure to ultrasound, whereas polyacetals bearing aliphatic chains do not undergo any change in their molecular weight under the same irradiation conditions. It is noted that in both cases the polymers were dissolved in a good solvent at a low

concentration (20 mg/ml) so the polymer chains could be considered to be swollen in the medium.

A crucial parameter that can affect the polymer degradation is the stiffness of the polymer which depends on the chemical structure of the polymer. Bulky groups such as aromatics result in more stiff structures and hinder the segmental motion of the polymer chain therefore increasing its fragility (**Figure 3.13a**). On the contrary, linear aliphatic groups are more flexible and hence the polymer is less fragile (**Figure 3.13b**). When ultrasound waves are applied, non-covalent intra- and inter- molecular bonds between the polymer chains are destroyed and the chains near the field of the collapsing bubbles become highly elongated. The polymer chains of the linear aliphatic polyacetals are flexible and can be substantially elongated without undergoing bond cleavage, whereas under the same irradiation conditions, linear polyacetals with aromatic groups become elongated up to a critical length above which the weakest bond becomes highly stretched leading to bond cleavage [72].

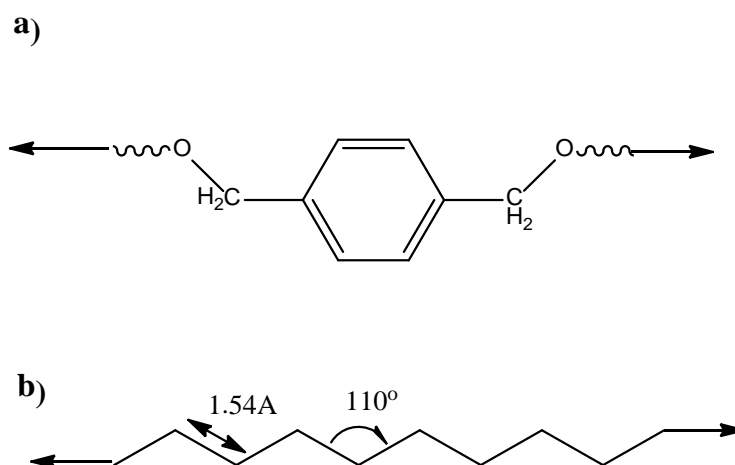


Figure 3.13: Schematic representation of the stretching of aromatic (**a**) and aliphatic (**b**) groups upon sonication.

3.2.4 Proposed mechanism for the sono-degradation of the polyacetals

Our study has shown that, both high and low molecular weight aromatic polyacetals can be degraded upon sonication using either high frequency (1 MHz) either low frequency (42 kHz) ultrasound at very low irradiation intensities (0.083 and 0.23 Watt/cm², respectively), two orders of magnitude lower than the intensities used for the sono-degradation of other polymer systems such as PEO-b-PTHPMA, polystyrene and carboxymethylcellulose [56], [68], [73]. Moreover, the degradation of polyacetals under ultrasound irradiation was efficient even at very low polymer molecular weights, around 2000 gr/mol, and extensive sonication resulted in a limiting molecular weight of around 1000 gr/mol signifying the high sensitivity of the acetal group to the ultrasonic field. This is in contrast to other polymer systems studied in the literature which showed a molecular weight dependence on their sonodegradation efficiency. For example, Schaefer et al, observed that polystyrene and brominated polystyrene with molecular weights around 13000gr/mol and 22000gr/mol respectively, exhibited no degradation [56]. However, they observed an effective degradation and decrease of the Mn in polystyrene and brominated polystyrene with molecular weights 42000 gr/mol and 70000 gr/mol.

Based on these results, a possible mechanism for the degradation of polyacetals is proposed, which employs the concept of cavitation and bubble explosion followed by mechanical effects such as shear forces and tension that lead to an elongation of the polymer chain and further stretching and cleavage of the most susceptible bonds (**Figure 3.14a**). The acetal bond is considered as the mechano-labile group located between the monomer repeated units along the polymer chain. When ultrasound irradiation is applied, the polymer chain becomes elongated and the O-C-O group which bears the most labile bond undergoes a zwitterionic cleavage similar to that proposed earlier by our group for the photo-degradation of the polyacetals [42], [44]. When the acetal bond is cleaved, the acetal carbon atom is positively charged while the oxygen atom is negatively charged leading to the formation of an aldehyde molecule and two polymer chains with lower molecular weight (**Figure 3.14b**). However, in contrast to other ultrasound-degradable polymers bearing one labile bond at the junction of the two blocks (e.g. PEG-S-S-PLA), it is possible that more than one acetal bond along the polymer chain is cleaved each time near the mid-point of the polymer chain. This would lead to the formation of acetaldehyde molecules, the two

diols, benzenedimethanol and cyclohexanedimethanol, and smaller polymer chains as the degradation products. This mechanism is supported by the GPC analysis of the degradation products which show the formation of monomeric species since the very early stages of the polymer degradation process (see Figures 3.2, 3.3, 3.4) in all the case of polyacetals.

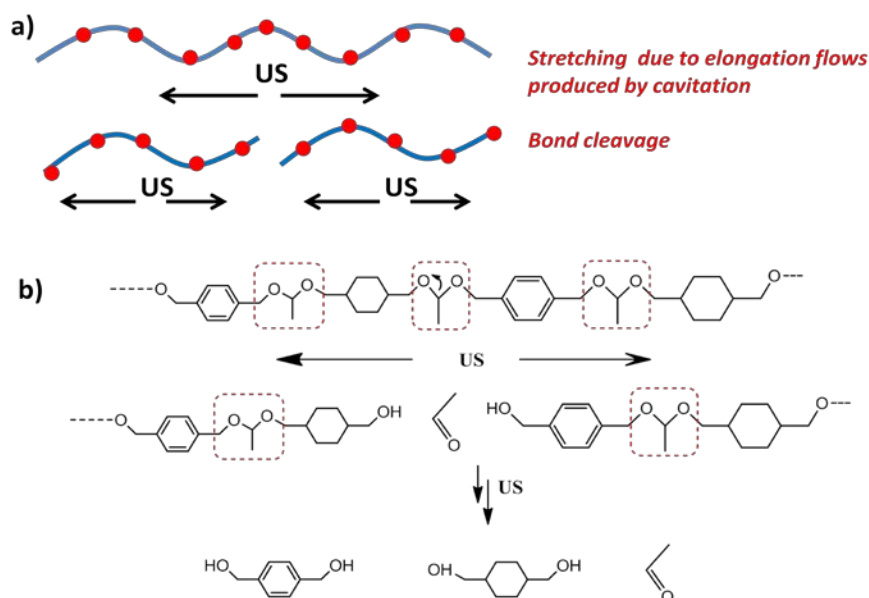


Figure 3.14: (a) Schematic illustration of the proposed mechanism of degradation of the polyacetals and (b) zwitterionic cleavage of the acetal bond during sonication and the degradation products.

3.3 PEG-*b*-polyacetal diblock copolymers

The successful sono-degradation of the polyacetal homopolymers under both high and low frequency ultrasound at incredibly low irradiation intensities has opened a new path towards the degradation of polyacetal-based amphiphilic diblock copolymers. Such amphiphilic block copolymers can self-assemble into core-shell micelles which are promising carriers for the controlled delivery and release of therapeutic agents. In this study, we have synthesized PEG-*b*-polyacetal diblock copolymers and investigated their degradation mechanism first in non-selective organic solvents and finally in water in the form of novel ultrasound-degradable polyacetal nanocarriers for the controlled release of active molecules.

3.3.1 Synthesis and characterization of the PEG-*b*-polyacetal diblock copolymers

Three different block copolymers were synthesized via a two-step acid catalyzed step-growth reaction. In the first step of the reaction the precursor polyacetal was synthesized by the condensation of a diol with a divinyl ether monomer at a 1:1.1 molar ratio. A monohydroxy PEG of 5000 gr/mol molecular weight was reacted in the second step at the vinyl ether ends of the homopolymer to afford the diblock copolymers. Three polyacetal homopolymers were synthesized using 1,4-benzenedimethanol, 1,6-hexanediol and 2-nitro-1,4-benzenedimethanol as the diol monomers and 1,4-cyclohexanedimethanol divinyl ether as ether monomers. The reaction kinetics were monitored by GPC. When the molecular weight of the precursor polyacetal block reached 5000-7000 gr/mol, a monohydroxy PEG with molecular weight 5000 gr/mol was added and was allowed to react with the vinyl ends of the polyacetal chains in the presence of the acid catalyst (1% PPTS). The chemical structures of the three block copolymers are shown in **Figure 3.15**.

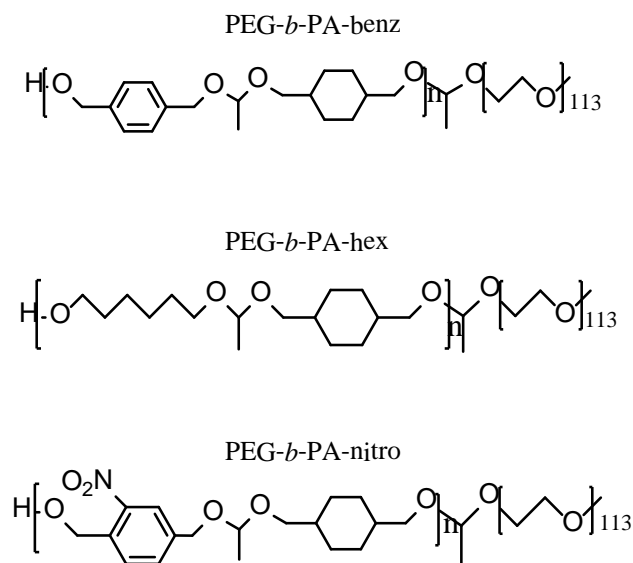


Figure 3.15: Chemical structures of the synthesized block copolymers

Figure 3.16 shows the GPC chromatograms for the three precursor polyacetals and the three respective PEG-*b*-polyacetal diblock copolymers. The chromatogram of PEG homopolymer is shown for comparison. The shift of the GPC curve to lower elution times upon the addition of PEG indicates the increase of the polymer

molecular weight and verifies the successful synthesis of the diblock copolymers. The %weight copolymer composition was selected to be similar for the two blocks in order to prevent the formation of undesired morphologies during the self-assembly process. The molecular weight characteristics of the final diblock copolymers, calculated by GPC, are summarized in Table 3.2. The M_n 's of the three copolymers are nearly equal to the sum of the PEG block and PA block as calculated by GPC. The polydispersity indices (M_w/M_n) range from 1.8 to 1.9, typical values for polycondensation reactions as discussed above.

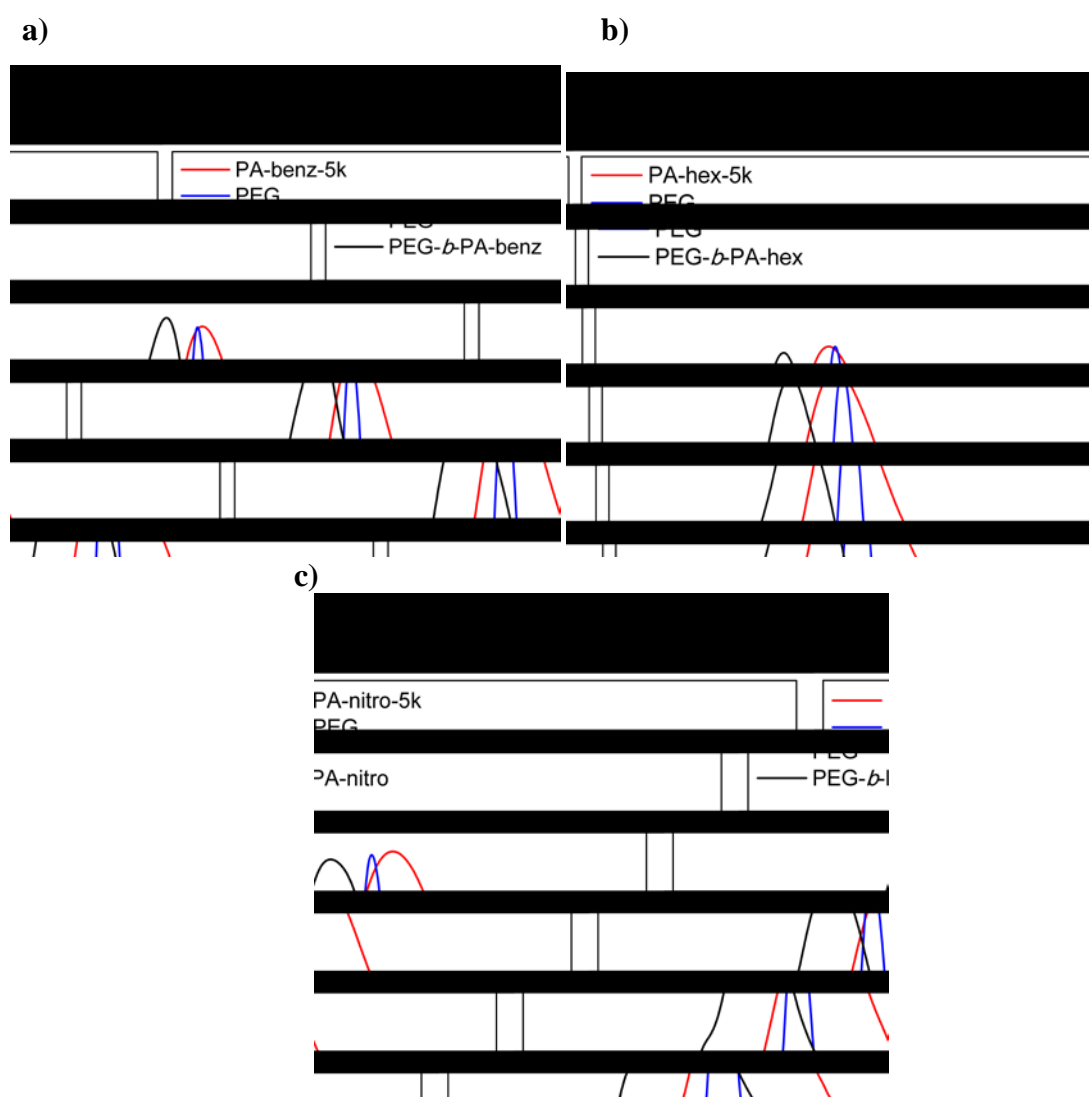


Figure 3.16: GPC traces for the polyacetal homopolymers and the respective diblock copolymers (a) PEG-*b*-PA-benz, (b) PEG-*b*-PA-hex and (c) PEG-*b*-PA-nitro. The GPC trace of PEG homopolymer is shown for comparison in each case.

Table 3.2: Molecular weight characteristics of the synthesized diblock copolymers by GPC.

Polymer	Mn PA	Mn PEG	Mn diblock copolymer	Mw/Mn block copolymer
PEG- <i>b</i> -PA-benz	7000	7000	16000	1.89
PEG- <i>b</i> -PA-hex	5500	7000	12100	1.79
PEG- <i>b</i> -PA-nitro	5000	7000	12400	1.91

3.3.2 Ultrasonic degradation of the block copolymers in organic media

After the synthesis, the sono-degradation of the diblock copolymers was investigated in non-selective organic solvents. Three fresh samples of the block copolymers were prepared in THF, which is a good solvent for both blocks, at a final concentration of 20 mg/ml. The samples were filtered to remove any un-dissolved polymer and were then transferred to the ultrasound set up. All samples were exposed to 1 MHz ultrasound frequency at 0.083 Watt/cm² intensity.

The ultrasonic degradation profile of the PEG-*b*-PA-benz copolymer was followed by GPC by collecting and analyzing samples of the polymer solution after exposure to ultrasound. **Figure 3.17a** shows the degradation profile of PEG-*b*-PA-benz diblock copolymer as a function of irradiation time. As seen in the figure, a gradual shift of the main polymer peak to higher elution times suggesting the decrease of the polymer molecular weight due to degradation was observed. Moreover, it is noteworthy that from the first hour of sonication a second peak appeared in the chromatogram which corresponds to the PEG block indicating the degradation of the block copolymer to the two constituent blocks. The bimodal distribution of the degraded polymer was more obvious after 4 h of ultrasonic treatment. The peak of the PEG block appears around 13.9 mins and is evident in all the GPC traces indicating that no degradation was occurred in this block whereas, the intensity of the second peak which corresponds to the polyacetal block gradually decreases and the peak is shifted to higher elution times, signifying the degradation of this block. Moreover, characteristic peaks appear at elution times above 17 mins suggesting the formation of oligomers. **Figure 3.17b** shows the decrease of the copolymer Mn as function of sonication time

calculated by the GPC data. The average molecular weight decreased from ~16000 gr/mol to ~8000 gr/mol after 1 h sonication which suggest that the block copolymer chains were cleaved at the midpoint between the two blocks. Moreover, the polymer reached a limiting Mn of ~1700 gr/mol after 4 h of sonication suggesting that no further degradation takes place.

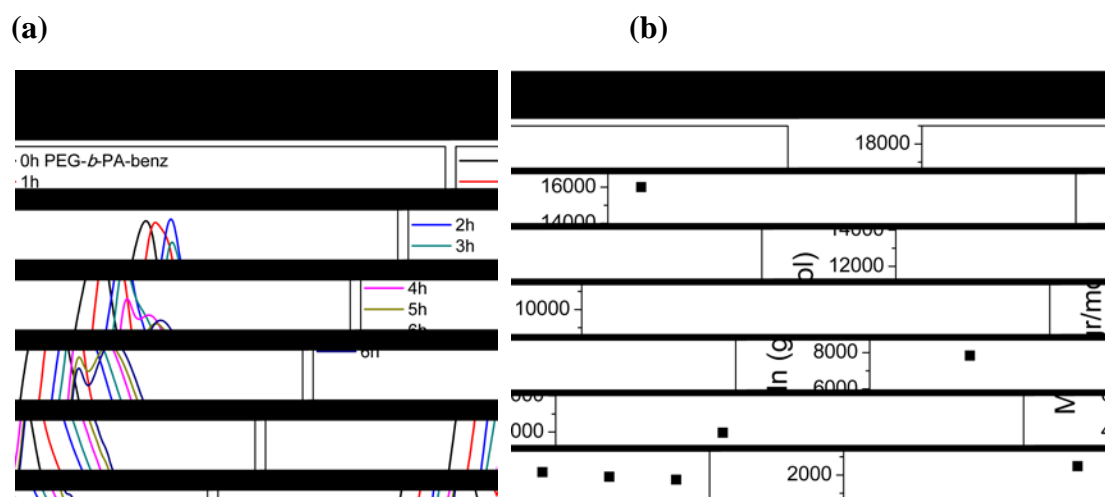


Figure 3.17: (a) GPC traces for PEG-*b*-PA-benz as function of sonication time at 1 MHz and (b) calculated Mn values as a function of sonication time.

Based on the mechanism proposed above for the sono-degradation of the homopolymer polyacetals, it was assumed that the most susceptible bond is near the mid-point of the PEG-*b*-polyacetal chains which connects the two blocks. However, in contrast to other block copolymer systems that have been proposed for ultrasound-controlled release application which undergo chain scission only in the middle of the chain (e.g. PEG-S-S-PLA) resulting in two long polymer chains after sonication, a major advantage of the PEG-*b*-polyacetal block copolymers studied herein is that they can be degraded into very low molecular weight products upon extensive sonication (**Figure 3.18**) [65].

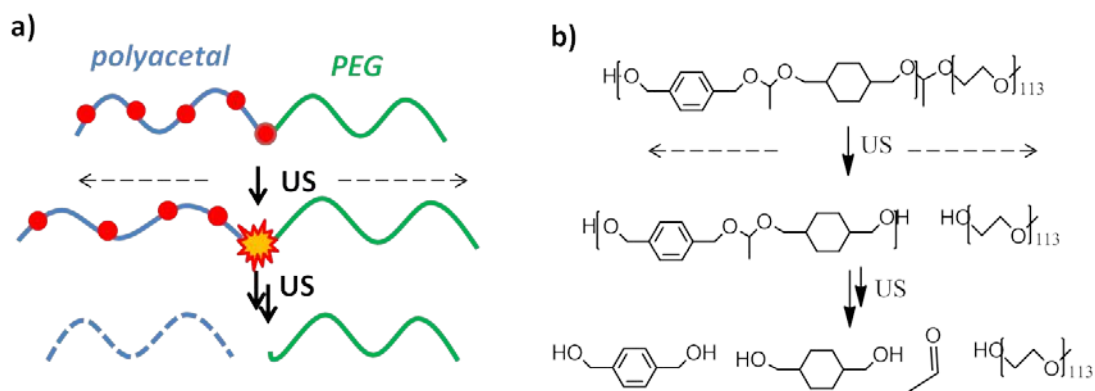


Figure 3.18: (a) Schematic illustration of the degradation of block copolymer polyacetals upon ultrasound irradiation and (b) sono-degradation of PEG-*b*-PA-benz and the degradation products.

The degradation products of the PEG-*b*-PA-benz block copolymer were characterized by $^1\text{H-NMR}$ spectroscopy. A fresh copolymer solution was prepared in CDCl_3 and was transferred into an NMR tube. $^1\text{H-NMR}$ spectra were recorded before ultrasonic treatment and after 4 h of sonication and are presented in **Figure 3.19**. The non exposed sample shows the characteristic peak of the acetal protons at ~ 4.7 ppm in a 1:4 ratio to the aromatic protons of the benzene ring which is in agreement with the chemical structure of the polymer. The PEG block appeared at around 3.6 ppm. After 4 hours of sonication, two new peaks appeared at 9.8 ppm and 2.2 ppm which correspond to formed acetaldehyde and at the same time the integral of the peak of the acetal proton decreased suggesting the cleavage of the acetal bond. The degradation in CDCl_3 after 4 h treatment was found around 45% which is lower compared to that found in THF and was attributed to the lower water content of the deuterated solvent.

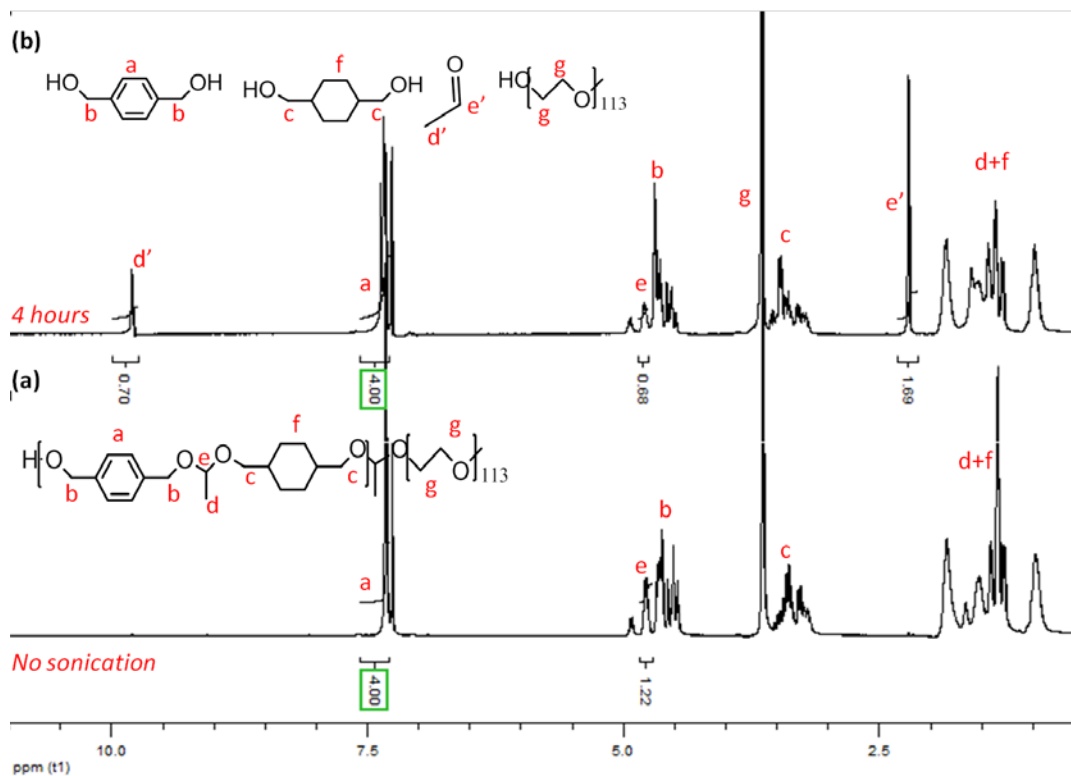


Figure 3.19: $^1\text{H-NMR}$ spectra of PEG-*b*-PA-benz block copolymer before (a) and after (b) 4 h ultrasonic treatment (1 MHz, 0.083 W/cm^2).

Next, the degradation profiles of the other two block copolymers, PEG-*b*-PA-nitro and PEG-*b*-PA-hex, were investigated in THF (20 mg/ml) at 1 MHz ultrasound frequency and 0.083 Watt/cm^2 intensity.

The PEG-*b*-PA-nitro block copolymer which had a similar chemical structure to the first block copolymer, bearing an $-\text{NO}_2$ group on the aromatic diol monomer, showed a similar degradation profile to the first block copolymer. The GPC chromatograms showed a clear shift of the polymer peak to higher elution times and the formation of a bimodal peak corresponding to the two blocks as discussed above for PEG-*b*-PA-benz (**Figure 3.20a**). The calculated average M_n decreased gradually indicating the cleavage of the acetal groups upon sonication (**Figure 3.20b**). Again a limiting molecular weight of $\sim 2000 \text{ gr/mol}$ was obtained after 4 h sonication.

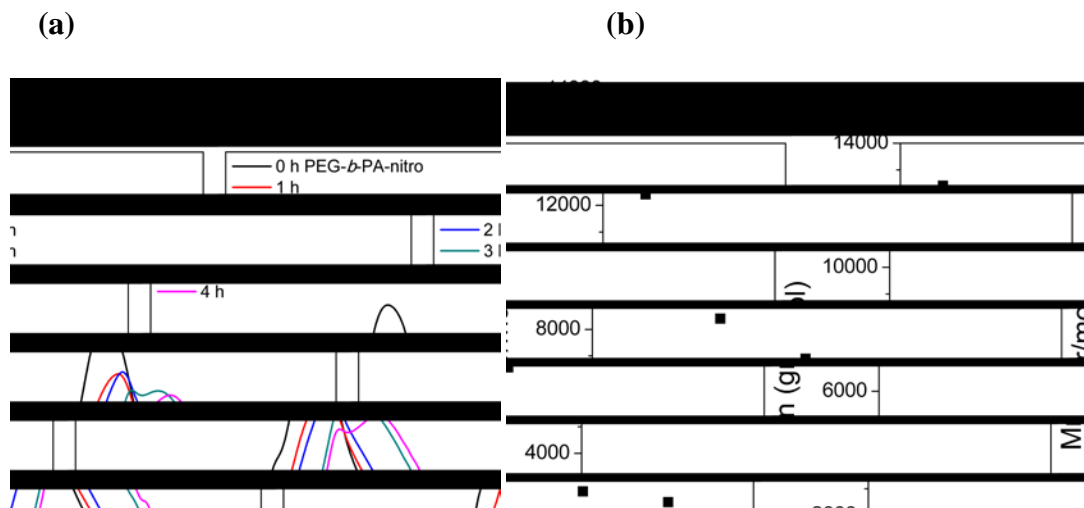


Figure 3.20: (a) GPC traces of PEG-*b*-PA-nitro as a function of sonication time and (b) the calculated Mn values as function of sonication time.

Finally, the effect of ultrasound irradiation on the aliphatic PEG-*b*-PA-hex block copolymer was investigated under similar irradiation conditions. As shown in **Figure 3.21**, the GPC chromatograms for this polymer remained unchanged for all the irradiated samples indicating that no polymer degradation occurs similar to the results for PA-hex homopolymer, verifying that the chemical structure of the polyacetal is a critical factor which dominates its sono-degradation behavior.

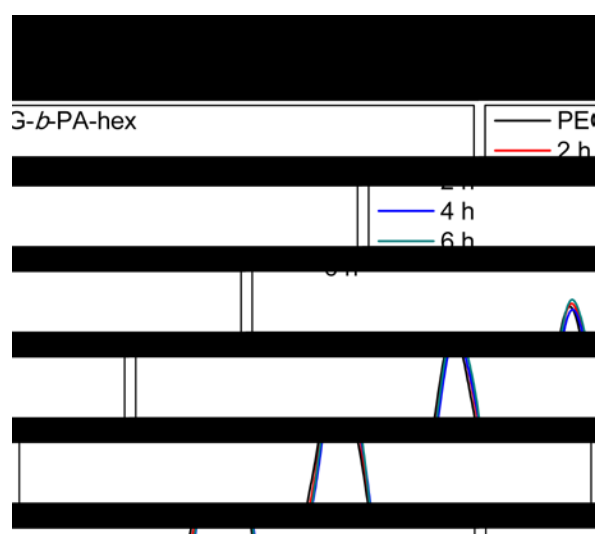
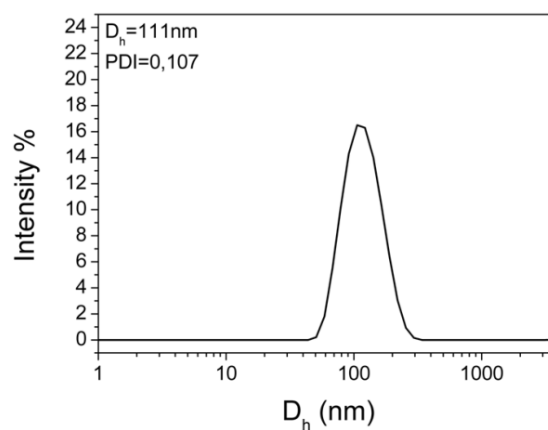
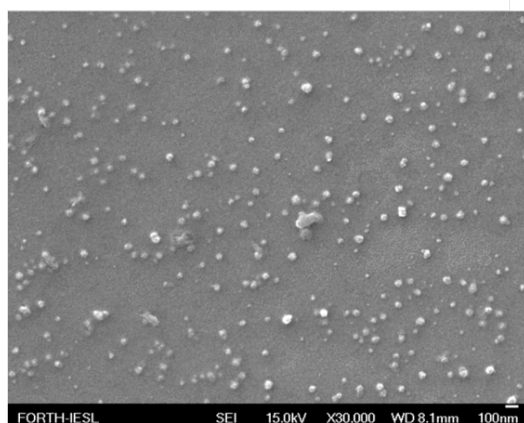


Figure 3.21: GPC traces of PEG-*b*-PA-hex block copolymer as a function of sonication time (1 MHz, 0.083 W/cm²).

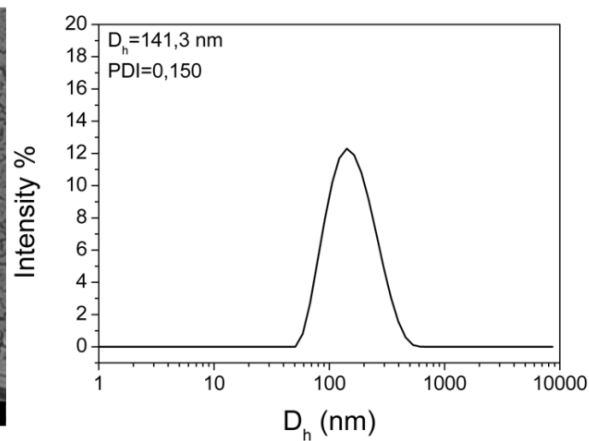
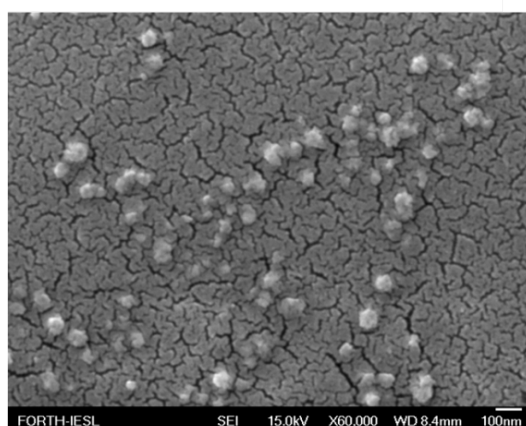
3.4 Self-assembly of the PEG-*b*-polyacetal block copolymers in water

The three PEG-*b*-PA di-block copolymers synthesized were used for the preparation of polymer micelles in water at a polymer concentration 0.2 mg/ml. The block copolymers were first dissolved in THF and next neutral water (pH 7.4) was slowly added to induce the micelle formation. The size and the morphology of the polyacetal micelles were characterized by DLS and SEM, respectively. As shown in **Figure 3.22**, all the block copolymer micelles had a spherical and uniform shape and their size ranged from ~100 to ~180 nm for the three block copolymers. In general, such sizes in the range of 10-100 nm are preferred for controlled drug delivery applications [74].

a)



b)



c)

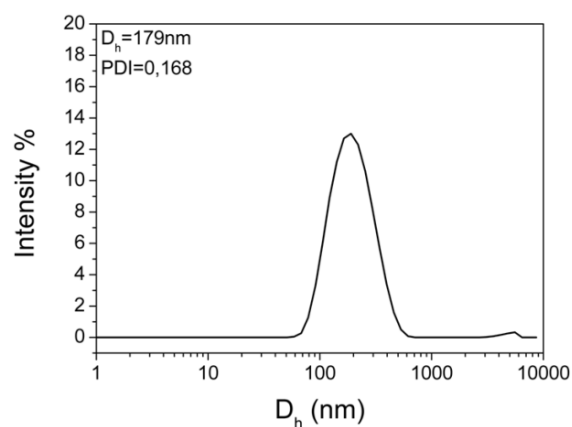
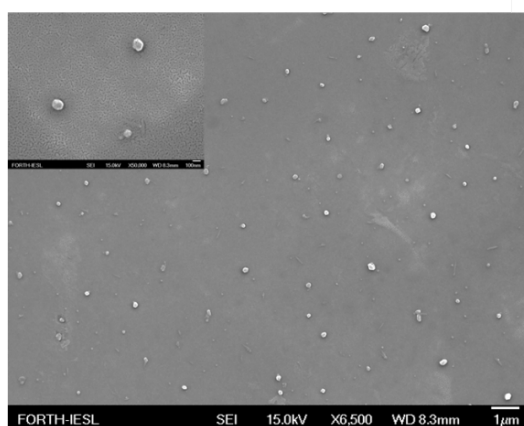


Figure 3.22: SEM images and DLS measurements for **a)** PEG-*b*-PA-benz block copolymer micelles, **b)** PEG-*b*-PA-hex block copolymer micelles and **c)** PEG-*b*-PA-nitro block copolymer micelles.

3.5 Ultrasound-induced morphological changes of the PEG-*b*-polyacetal block copolymer micelles

The ultrasound-triggered main-chain degradation of the PEG-*b*-polyacetal block copolymers into small hydrophilic molecules has provided an excellent platform to study the effect of ultrasound irradiation on the micellar structures of these polymers. Polymer micelles of the PEG-*b*-PA-benz block copolymer were prepared and were used as a model system to study the changes in the micellar structure after exposure to ultrasound irradiation. DLS and SEM were used to observe the possible changes in the size and the morphology of the micelles, respectively.

Figure 3.23a, shows the DLS results for the PEG-*b*-PA-benz polyacetal micelles in water, after exposure to ultrasound irradiation (1 MHz, 0.083 Watt/cm²). A shift of the size distribution to higher values after sonication was observed by DLS suggesting that structural changes have taken place which increase the size of the scatters. Therefore, it was clear that the initial block copolymer micelles were disrupted leading to the formation of larger species with average size around 200 nm. Ultrasonication of the micellar suspension can lead to an initial swelling of the polymer micelles in the early stages of exposure and next to the degradation of the polymer chains. Taking into account the sono-degradation results of the block copolymers in organic media discussed above, it is expected that the block copolymer micelles break first in the middle of the chains upon irradiation which results in the formation of two individual blocks, a PEG and a polyacetal block, and extensive sonication is required for the formation of low molecular weight species such as oligomers and monomers. The degradation products which are rich in aromatic benzene groups possibly lead to the formation of the larger size aggregates. To verify this hypothesis, the sample which was irradiated for 4 h was measured by DLS following filtration through a 0.2 μm pore size filter. The curve appears at very low hydrodynamic diameters ($\sim 13\text{nm}$) it corresponds to the coil of the hydrophilic PEG block. However, a second curve at around 160 nm remained after filtration which is attributed to some remaining non degraded polymer micelles as well as aggregates formed by the degraded polymer chains in the solution. **Figure 3.23b** presents the characteristic increase of the hydrodynamic diameter (D_h) as function of sonication time. D_h gradually increases from ~ 110 to 220 nm as discussed above.

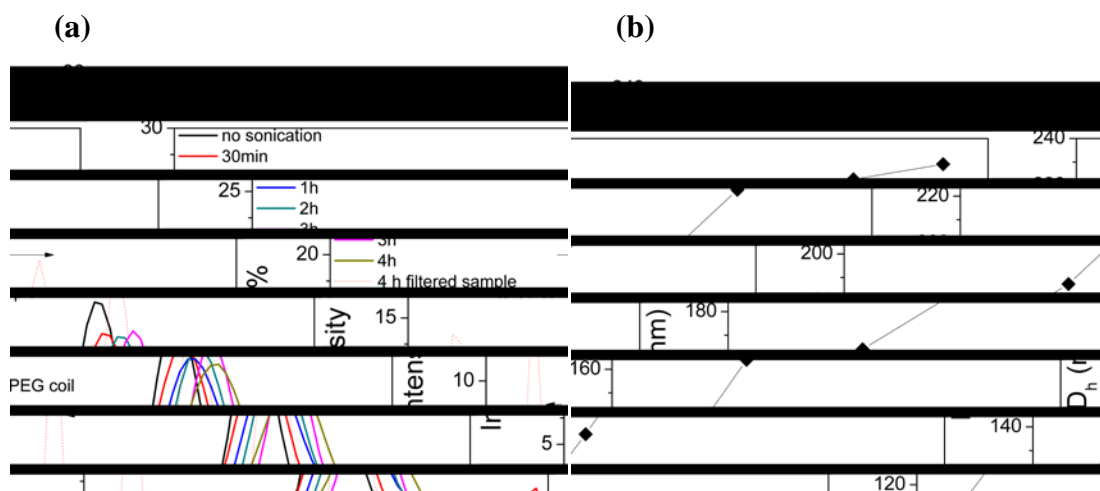
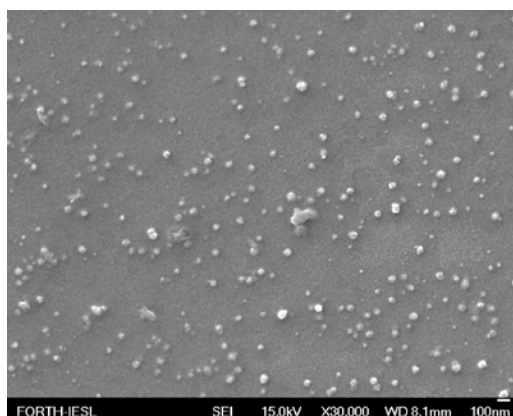


Figure 3.23: (a) Evolution of the intensity average size distribution of the PEG-*b*-PA-benz micelles with ultrasound irradiation time and (b) Mean hydrodynamic diameter (D_h) versus sonication time for the PEG-*b*-PA-benz micelles (ultrasound frequency 1 MHz, intensity 0.083 Watt/cm²).

In order to obtain further insights of the shape of the block copolymer micelles after exposure to ultrasound irradiation, SEM images were taken before and after ultrasonic treatment. As shown in **Figure 3.24a**, before exposure the micelles have spherical shape and uniform size and are well dispersed on the substrate. After 4 h of total sonication (**Figure 3.24b**) the polymer micelles were completely disrupted leading to the formation of a polymer film onto the substrate. Moreover, a few larger polymer aggregates were observed which possibly correspond to the aggregated degradation products which are in good agreement with the DLS results.

a)



b)

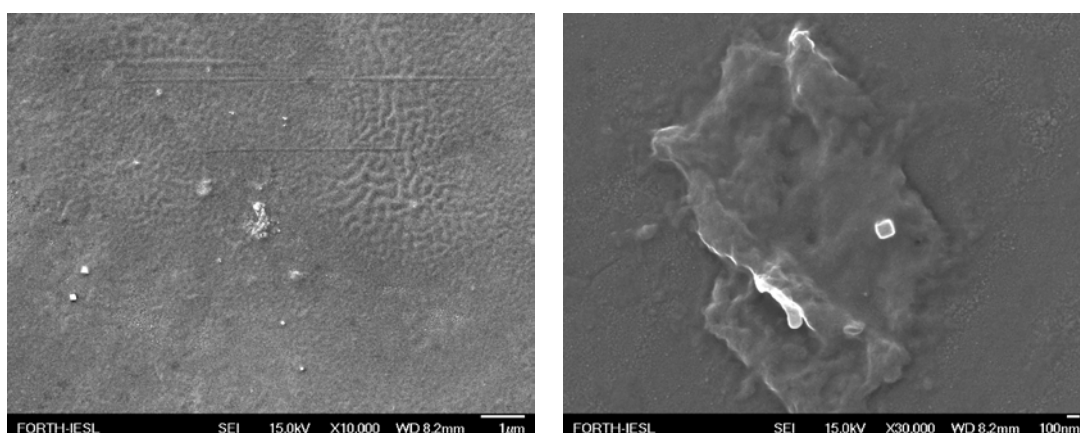


Figure 3.24: SEM images of the PEG-*b*-PA-benz micelles a) before and b) after 4h ultrasonic treatment at 1 MHz and 0.083 Watt/cm².

The effect of ultrasound irradiation on the shape and the morphology of the PEG-*b*-PA-hex diblock copolymer micelles was also investigated. SEM images were obtained before and after 4 h ultrasonic treatment. As seen in **Figure 3.25**, the spherical shape of the micelles is preserved after sonication. A few larger aggregates were observed which is expected due to prolonged sonication. These results are in agreement with the GPC results for the PEG-*b*-PA-hex diblock copolymer in THF and verify the effect of the chemical structure of the polyacetal on its sono-degradation behavior.

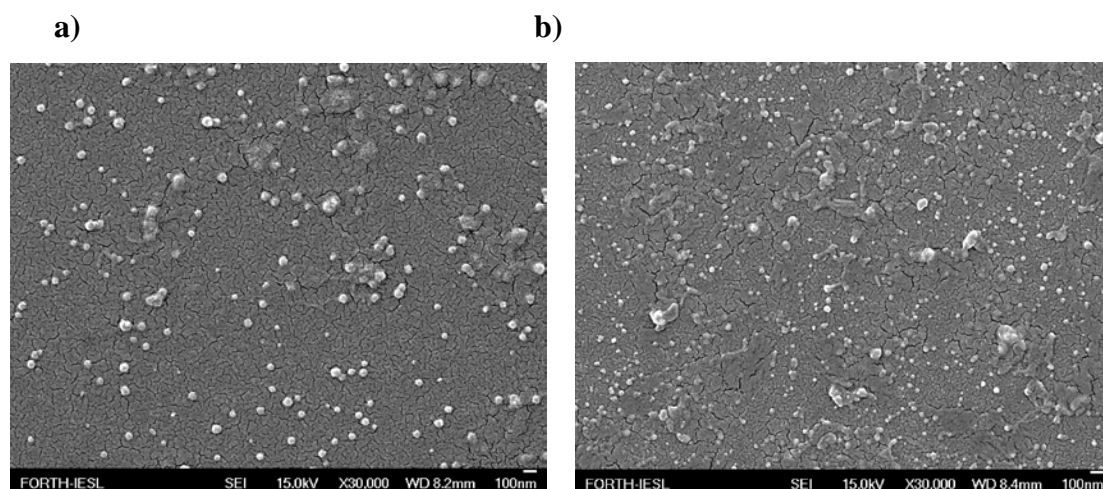


Figure 3.25: SEM images of the PEG-*b*-PA-hex diblock copolymer micelles (a) before and (b) after 4 h ultrasonic treatment at 1 MHz and 0.083 Watt/cm².

3.6 In vitro release studies

Stimuli-controlled drug release from polymeric nanocarriers has attracted significant interest over the past decades. As discussed in Chapter 1, ultrasound is a powerful external stimulus which can be utilized as an effective trigger to induce the release of bioactive species from polymeric micelles in a spatiotemporally controlled manner. Moreover, ultrasound irradiation can effectively penetrate deep into the human body, it is non-invasive and it can be harmless depending on the applied intensity and frequency. For controlled drug delivery application, ultrasound at 1 MHz frequency is usually preferred. The effect of ultrasound irradiation on the release profile of encapsulated molecules from the polyacetal block copolymer micelles was investigated. Moreover, the synergistic effect of ultrasound and low solution pH on the degradation and release profile of dye loaded PEG-*b*-polyacetal micelles is examined.

3.6.1 Influence of frequency on the ultrasound-induced disruption of the PEG-*b*-polyacetal micelles and the release of the encapsulated dye molecules

The ultrasound induced main chain degradation of the PEG-*b*-polyacetal diblock copolymers and the subsequent disruption of the polyacetal micelles provided the basis for the ultrasound-controlled release of encapsulated molecules from the copolymer micelles. To examine this behavior, copolymer micelles loaded with the hydrophobic dye sudan red were prepared from the PEG-*b*-PA-benz diblock copolymer. The dye loaded micelles were prepared by first dissolving both the block copolymer and the dye in THF followed by the dropwise addition of an excess of neutral water to induce the micelle formation and the slow evaporation of THF under vacuum. The addition of water leads to the self-assembly of the amphiphilic block copolymers into core-shell micelles hydrophobic dye molecules encapsulated into the micellar cores.

A polymer micelle suspension (0.2 mg/ml, 5ml) was prepared and irradiated at 1 MHz and a second solution was sonicated at 3 MHz frequency. These two frequencies were used for the release studies because they are the most common ones used in medical application [45], [46]. A control sample (untreated micelles) was kept under the same environmental conditions (stirring at 37°C) without irradiation. The degradation of the copolymer micelles and the release of the encapsulated dye as function of sonication time were monitored by UV-Vis spectroscopy. The dye molecules incorporated within the hydrophobic cores of the micelles absorb strongly at around 550 nm and therefore can be detected by UV/Vis spectroscopy whereas the released hydrophobic dye molecules precipitate in water and cannot be detected by UV/Vis.

Figure 3.26 shows the UV-Vis spectra of the sudan red loaded PEG-*b*-PA-benz diblock copolymer micelles as function of sonication time. The maximum absorbance of the dye, located at 550 nm, gradually decreases after exposure to 1 MHz ultrasound frequency (**Figure 3.26a**) indicating the disruption of the micelles and the release of the cargo in the water medium. At the same time, the UV-Vis spectra of the micellar solution used as the control (non-irradiated micelles, **Figure 3.26b**), shows that the absorbance does not change in 4 h, signifying the stability of the dye loaded-micelles at pH 7.4. Finally, when 3 MHz ultrasound frequency was applied to the micellar solution, no significant changes in the UV-Vis spectra were observed (**Figure 3.26c**) signifying the minimal dye release from the micelles at this irradiation frequency.

Figure 3.27a shows the % released dye molecules from the micellar cores after exposure to ultrasound irradiation at 1 MHz, 3 MHz and the untreated micellar solution as a function of exposure time. Almost quantitative release of the loaded cargo (~95%) was achieved when applying 1 MHz ultrasound for 4 h. Moreover, it is important to note that in the first 2 h around 30% of the loaded dye was released while after that the release rate increased rapidly reaching 95% in 4 h. This release profile can be explained by the degradation profile of the copolymer in the micelles. As discussed above, the mid-chain acetal bond which connects the polyacetal block with the PEG block is cleaved first leading to the release of dye molecules that were physically entrapped between the PEG chains in the outer shell of the micelles. Next, the polyacetal chains in the micellar cores are degraded leading to the release of the larger amount of loaded cargo from the cores. The successful degradation of the micelles and the release of the dye could also be observed by naked eye. It is clear that as the irradiation time increased, the pink color of the micellar solution faded gradually and after 4 h irradiation a clear solution was obtained. This provides direct evidence that the encapsulated dye molecules were released into the aqueous solution under ultrasound irradiation (**Figure 3.27b**).

Next, following irradiation at even higher frequencies, 3 MHz, the release of the dye was significantly reduced leading to only 10% released dye was after 4 h ultrasonication. This was attributed to the low cavitation effect at such high frequencies and justifies the use of lower frequencies (~1 MHz) for controlled drug delivery applications. Finally, the untreated micelles showed a minimal release of the dye justifying the use of the polyacetal nanocarriers for the stimuli controlled release of drugs or other bioactive species.

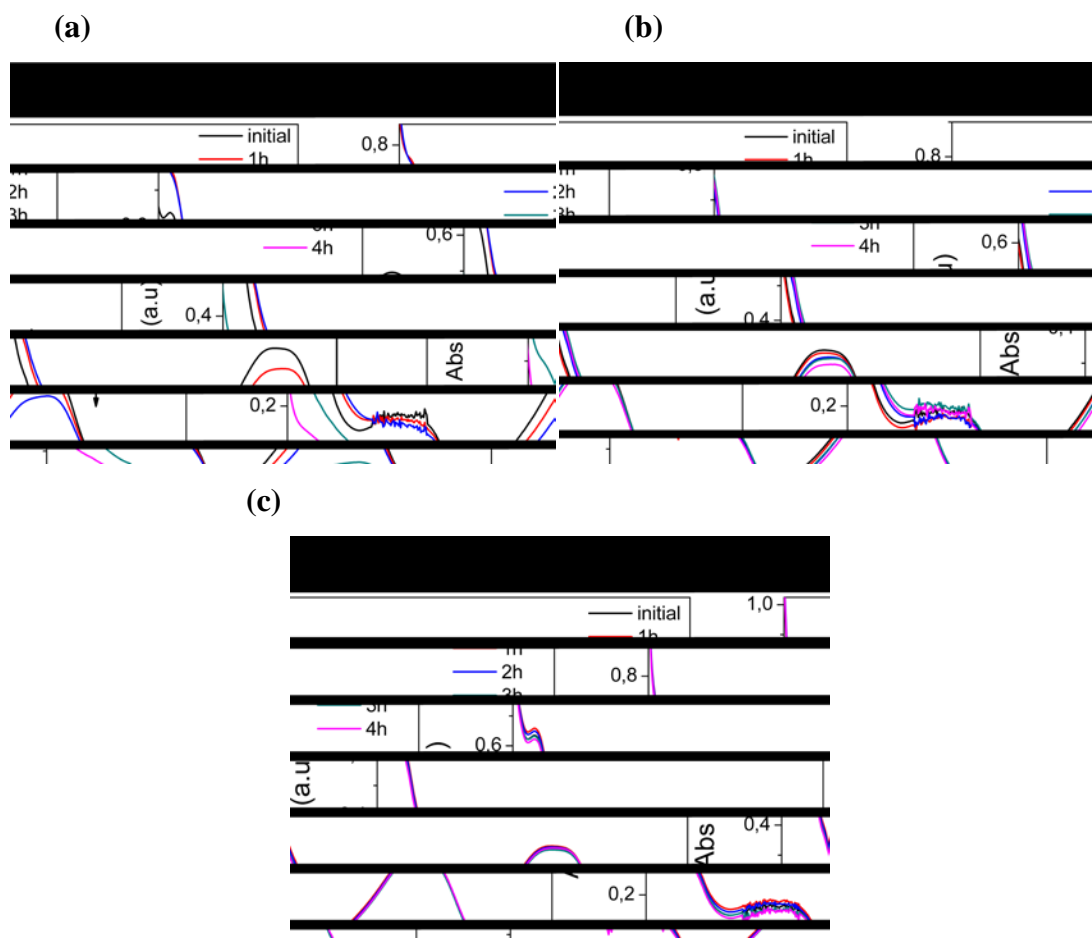


Figure 3.26: UV-Vis spectra of the SR-loaded PEG-*b*-PA-benz copolymer micelles as function of sonication time. Irradiation at (a) 1 MHz, (b) 3MHz and (c) control micelles.

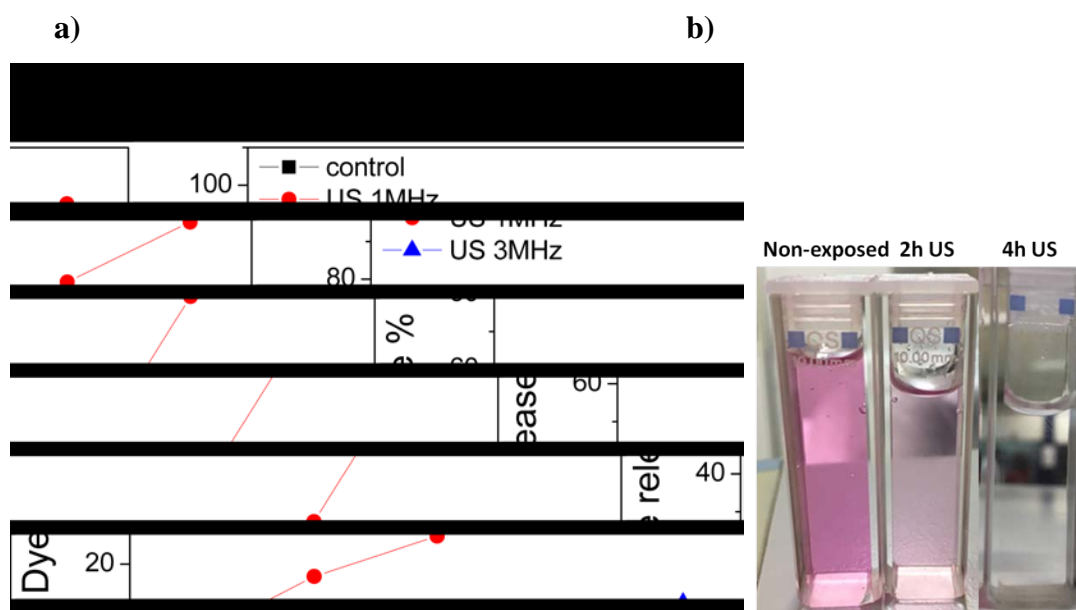


Figure 3.27: (a) Sudan red release profiles from the PEG-*b*-PA-benz block copolymer micelles upon 1 MHz ultrasound irradiation (red circles), 3 MHz ultrasound irradiation (blue triangles) and the non-exposed micelles (black squares). (b) Digital photos of the non exposed sample and the same sample after 2 h and 4 h exposure to ultrasound.

Finally, the release kinetics of the encapsulated dye molecules from the polyacetal block copolymer micelles for different polymer concentrations were studied. A systematic decrease of the release rate in particular at longer irradiation times was found upon increasing the polymer concentration from 0.2 mg/ml to ~1 mg/ml and to 2 mg/ml (**Figure 3.28**). In general, the cavitation effect is stronger in solutions of lower concentration or else in liquids with low viscosities. When the polymer micelle concentration increases the cavitation effect decreases and thus the release rate is slower.

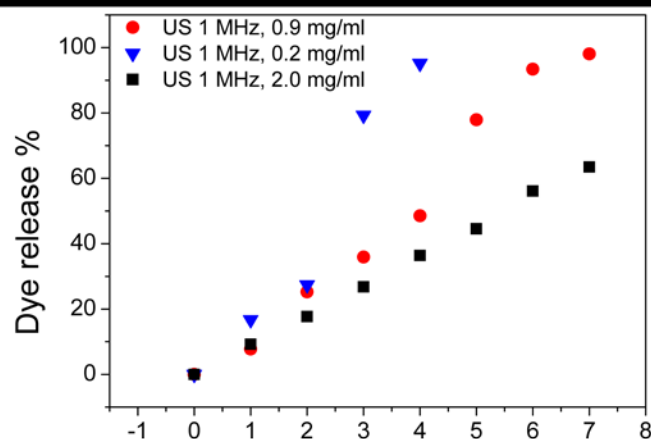


Figure 3.28: Release of sudan red from the PEG-*b*-PA-benz micelles as a function of sonication time for different polymer concentrations: 0.2 mg/ml (blue triangles), 0.9 mg/ml (red circles) and 2 mg/ml (black squares).

The effect of the ultrasound intensity on the release rate of the cargo was also tested. The micellar solution (0.2 mg/ml) was irradiated at 1 MHz ultrasound frequency and at intensity 3 watt/cm². **Figure 3.29** shows the release profiles for the exposed and the non-exposed micelles. Comparing these results with the release rate found for the PEG-*b*-PA-benz micelles upon exposure to 0.083 W/cm², it is clear that upon increasing the ultrasound intensity the release rate becomes significantly higher with around 80% release of the cargo in the first thirty minutes of exposure.

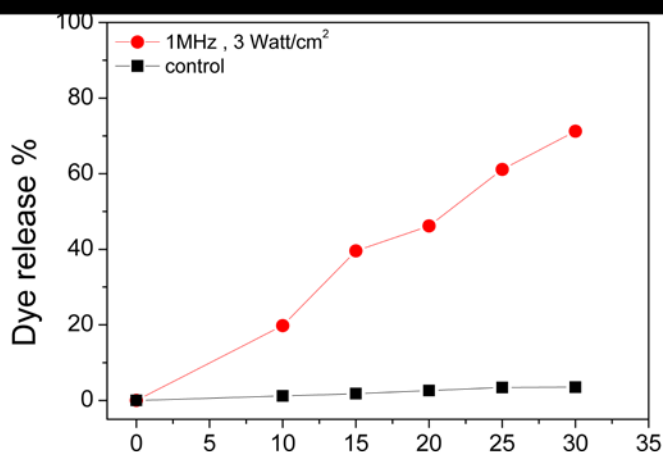


Figure 3.29: Release profiles of the dye from the polyacetal micelles as function of sonication time for ultrasound intensity 3 W/cm² (red circles) and the control micelles (black squares).

3.8 The synergistic effect of ultrasound and low solution pH on the degradation of the PEG-*b*-polyacetal micelles and the release of the encapsulated loads

Ultrasound irradiation is among of the most promising triggers for the controlled release of active compounds from nanocarriers such as polymeric micelles. As discussed above, ultrasound at 1 MHz frequency and 0.083 W/cm² intensity can effectively degrade the PEG-*b*-polyacetal block copolymer micelles into small compounds and release the encapsulated cargo on a controlled manner. However, it is also well-known that polyacetals undergo mild hydrolysis at acidic pH (~5.0), while they rapidly degrade at very acidic conditions (pH<4). Herein, the combination of two external stimuli that is ultrasound and low solution pH, was employed in the controlled release of the cargo from the PEG-*b*-PA-benz block copolymer micelles.

As seen in **Figure 3.30**, no significant difference was observed in the release profiles of the untreated micelles and the polymer micelles which were incubated for 4 h at pH 5.0. In both cases the release was below 5%. On the other hand, the synergistic effect of low solution pH and ultrasound irradiation is impressive. Around 80% of the encapsulated dye was released in the first 2 h of irradiation at pH 5.0 which is significantly higher than the 30% released dye when ultrasound was used as a single stimulus. At higher irradiation time the differences are smaller because the sample exposed to the synergistic stimuli has already released >95% of the dye.

The enhanced release upon the application of the synergistic stimuli was attributed to the cavitation effect. More specifically, when ultrasound is applied alone to the micellar solution, mechanical effects are produced by cavitation which cause the swelling of the polymer micelles. The swelling of the micelles results in a more effective penetration of the protons from the solution into the core of the micelles which leads to a more effective hydrolysis of the acetal bonds and the release of the encapsulated cargo. It is also worth to emphasize that the release of the dye from the micelles was irreversible which indicates the absence of re-encapsulation events of the dye into the micellar core. This supports further the chemical degradation of the block copolymer upon the application of the two different stimuli.

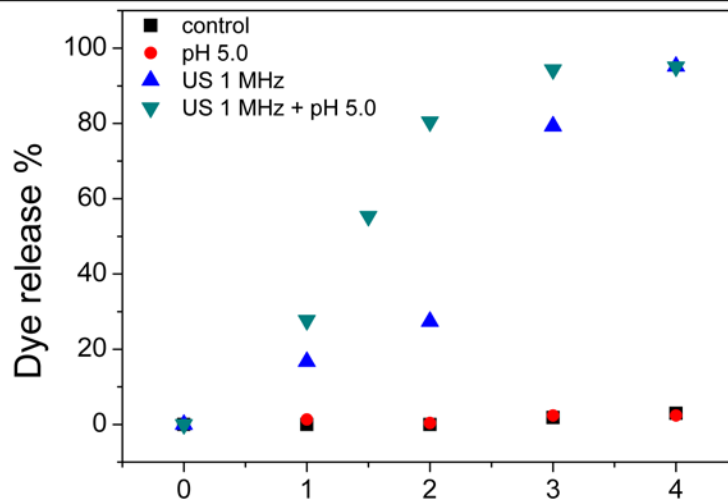


Figure 3.30: Release profiles of sudan red dye from the PEG-*b*-PA-benz block copolymer micelles as a function of time for untreated micelles (black squares), micelles at pH 5.0 (red circles), micelles irradiated at 1 MHz (blue up triangle) and micelles treated at both pH and ultrasound (green down triangle).

Chapter 4

Conclusions

Cancer is the second leading cause of death worldwide for both men and women and attacks even very young ages. Nowadays, the most commonly used treatments involve the administration of anticancer drugs, which are usually hydrophobic, directly into the bloodstream via injection. This approach suffers from important disadvantages which include low drug solubility, non-specific accumulation of the drug in healthy tissues and other side toxicities. This is a major common problem in anticancer therapies as well as other genetic diseases which require the administration of high doses of very toxic drugs. The main objective in this master thesis was the development of a novel stimuli-responsive drug release system which could encapsulate hydrophobic molecules and release them in a controlled manner following its exposure to an external stimulus. Ultrasound, is a very attractive stimulus which has been used both to trigger drug release from nanocarriers and for tumor ablation. In this work, a novel, dual-sensitive nanocarrier based on amphiphilic PEG-*b*-polyacetal diblock copolymers was developed.

First, polyacetal homopolymers bearing either aromatic or aliphatic groups were successfully synthesized using a simple step-growth polycondensation reaction of an appropriate diol with a divinyl ether. The diols with aromatic groups that were used were 1,4-benzenedimethanol and 2-nitro-1,4-benzenedimethanol and the aliphatic was 1,6-hexanediol. A series of low and high molecular weight polyacetals were synthesized. Next, the degradation profile of these polymers under ultrasonic irradiation was investigated. It was found that polyacetals bearing aromatic groups along their backbone can easily undergo main-chain scission into low molecular weight products at ultrasound frequencies of 42 kHz or 1 MHz both at very low irradiation energies which to the best of our knowledge are two orders of magnitude lower than those used in other ultrasound degradable systems. It was verified that the mechano-labile bond that undergoes cleavage because of the mechanical tension produced by the cavitation effect, is the acetal bond. The mechanism of degradation was proposed to proceed first via the bonds located near the center of the polymer chain followed by the scission of the new chains produced to give the initial monomers and polyacetal oligomers. It was also found that at 1 MHz ultrasound frequency the degradation rate of the polymers was faster. Another important

parameter which affected the degradation rate was the amount of water in the solution. When decreasing the amount of water a decrease in the degradation rate of the polymers was found. An important influence of the polyacetal chemical structure on its degradation profile was found with the aliphatic polymers exhibiting no degradation upon irradiation. This was attributed to the flexibility of the linear aliphatic polymer chains in contrast to the rigid chains which contain stiff aromatic rings.

Based on the above results, polyacetals were employed as an excellent platform for the development of sono-degradable block copolymers. The amphiphilic diblock copolymers comprising a hydrophilic PEG block and a hydrophobic polyacetal block were synthesized following a two-step polycondensation reaction. In the first step the polyacetal block with molecular weight ranging from 5000-7000 gr/mol was synthesized and next the second block consisting of a commercially available methoxy PEG with molecular weight 5000 gr/ml was linked to the first block. Three different block copolymers were synthesized by varying the diol monomer. All the block copolymers were subjected to ultrasound irradiation at 1 MHz and intensity 0.083 W/cm^2 in organic media. The two block copolymers bearing aromatic groups exhibited a similar degradation profile with first the cleavage of the junction between the two blocks followed by the main-chain degradation of the polyacetal block to product low molecular weight molecules.

In the next step, the synthesized amphiphilic PEG-*b*-polyacetal block copolymers were employed for the preparation of micelles, comprising of a hydrophobic polyacetal core and a hydrophilic PEG shell, in water. Spherical micelles with size between 100 and 180 nm were obtained for all the copolymers. DLS and SEM were employed to confirm the disruption of the polymer micelles, following ultrasound irradiation of the micellar solution in water, attributed to the degradation of the hydrophobic polyacetal blocks.

The release behavior of a hydrophobic model dye, sudan red, from the PEG-*b*-PA-benz micelles upon ultrasound treatment was investigated. The effect of ultrasound frequency (1 MHz and 3 MHz) on the release profile showed that upon 1MHz ultrasound irradiation around 80% of the encapsulated cargo was released in the first 3 h of treatment. Moreover, it was found that when increasing micelle concentration in the solution the release rate of the cargo was decreased with an effective release rate obtained at 0.2 mg/ml. The ultrasound intensity had a significant effect on the

release rate with a 6-fold increase found when the intensity increased from 0.083 to 3 W/cm². At this high intensity, an effective 80% release of the dye was found at 30 mins of irradiation. Finally, the synergistic effect of ultrasound irradiation and low solution pH on the degradation rate of the polyacetal micelles and the release profile of the payload was verified. A faster release was observed when both stimuli were applied with the solution pH adjusted at 5.0, compared to application of the two stimuli alone. These results provided strong evidence of the potential of the developed nanocarriers in external stimuli controlled drug release.

REFERENCES

- [1] R. L. Siegel, K. D. Miller, and A. Jemal, "Cancer statistics, 2018," *CA. Cancer J. Clin.*, vol. 68, no. 1, pp. 7–30, 2018.
- [2] T. Nanotheranostics, *SPRINGER BRIEFS IN APPLIED SCIENCES AND Nanomedicine for Cancer Therapy From Chemotherapeutic to Hyperthermia-Based Therapy*. .
- [3] K. Strebhardt and A. Ullrich, "Paul Ehrlich 's magic bullet concept : 100 years of progress," *Nat. Rev. cancer*, vol. 8, no. june, pp. 473–480, 2008.
- [4] D. Peer, J. M. Karp, S. Hong, O. C. Farokhzad, R. Margalit, and R. Langer, "Nanocarriers as an emerging platform for cancer therapy," *Nat. Nanotechnol.*, vol. 2, no. 12, pp. 751–760, 2007.
- [5] J. Shi, P. W. Kantoff, R. Wooster, and O. C. Farokhzad, "Cancer nanomedicine: Progress, challenges and opportunities," *Nat. Rev. Cancer*, vol. 17, no. 1, pp. 20–37, 2017.
- [6] Y. Matsumura and H. Maeda, "A new concept for macromolecular therapeutics in cancer chemotherapy: mechanism of tumor-tropic accumulation of proteins and the antitumor agents Smancs," *Cancer Res.*, vol. 46, no. 12 Pt 1, pp. 6387–6392, 1986.
- [7] J. Fang, H. Nakamura, and H. Maeda, "The EPR effect: Unique features of tumor blood vessels for drug delivery, factors involved, and limitations and augmentation of the effect," *Adv. Drug Deliv. Rev.*, vol. 63, no. 3, pp. 136–151, 2011.
- [8] F. Danhier, O. Feron, and V. Préat, "To exploit the tumor microenvironment: Passive and active tumor targeting of nanocarriers for anti-cancer drug delivery," *J. Control. Release*, vol. 148, no. 2, pp. 135–146, 2010.
- [9] J. W. Nichols and Y. H. Bae, "EPR: Evidence and fallacy," *J. Control. Release*, vol. 190, pp. 451–464, 2014.
- [10] F. Danhier, "To exploit the tumor microenvironment: Since the EPR effect fails in the clinic, what is the future of nanomedicine?," *J. Control. Release*, vol. 244, pp. 108–121, 2016.
- [11] M. Juweid *et al.*, "Micropharmacology of Monoclonal-Antibodies in Solid Tumors - Direct Experimental Evidence for a Binding-Site Barrier," *Cancer Res.*, vol. 52, no. 19, pp. 5144–5153, 1992.
- [12] J. M. Klotz and W. C. W. Chan, "Quantum Dots in Biological and Biomedical Research: Recent Progress and Present Challenges," *Adv. Mater.*, vol. 18, no. 15, pp. 1953–1964, 2006.
- [13] I. I. Slowing, B. G. Trewyn, S. Giri, and V. S. Y. Lin, "Mesoporous silica nanoparticles for drug delivery and biosensing applications," *Adv. Funct. Mater.*, vol. 17, no. 8, pp. 1225–1236, 2007.
- [14] M. Mahmoudi, S. Sant, B. Wang, S. Laurent, and T. Sen, "Superparamagnetic iron oxide nanoparticles (SPIONs): Development, surface modification and applications in chemotherapy," *Adv. Drug Deliv. Rev.*, vol. 63, no. 1–2, pp. 24–46, 2011.
- [15] R. Duncan, "The dawning era of polymer therapeutics," *Nat. Rev. Drug Discov.*, vol. 2, no. 5, pp. 347–360, 2003.
- [16] H. Cabral and K. Kataoka, "Progress of drug-loaded polymeric micelles into clinical studies," *J. Control. Release*, vol. 190, pp. 465–476, 2014.
- [17] D. Bobo, K. J. Robinson, J. Islam, K. J. Thurecht, and S. R. Corrie,

- “Nanoparticle-Based Medicines: A Review of FDA-Approved Materials and Clinical Trials to Date,” *Pharm. Res.*, vol. 33, no. 10, pp. 2373–2387, 2016.
- [18] D. Press, “Clinical development of liposome-based drugs : formulation , characterization , and therapeutic efficacy,” pp. 49–60, 2012.
- [19] S. Senapati, A. K. Mahanta, S. Kumar, and P. Maiti, “Controlled drug delivery vehicles for cancer treatment and their performance,” *Signal Transduct. Target. Ther.*, vol. 3, no. 1, p. 7, 2018.
- [20] A. Kumari, S. K. Yadav, and S. C. Yadav, “Biodegradable polymeric nanoparticles based drug delivery systems,” *Colloids Surfaces B Biointerfaces*, vol. 75, no. 1, pp. 1–18, 2010.
- [21] F. Abedi-Gaballu *et al.*, “PAMAM dendrimers as efficient drug and gene delivery nanosystems for cancer therapy,” *Appl. Mater. Today*, vol. 12, pp. 177–190, 2018.
- [22] J. S. Choi, K. Nam, J. Y. Park, J. Bin Kim, J. K. Lee, and J. S. Park, “Enhanced transfection efficiency of PAMAM dendrimer by surface modification with l-arginine,” *J. Control. Release*, vol. 99, no. 3, pp. 445–456, 2004.
- [23] A. Kakkar, G. Traverso, O. C. Farokhzad, R. Weissleder, and R. Langer, “Evolution of macromolecular complexity in drug delivery systems,” *Nat. Rev. Chem.*, vol. 1, pp. 1–18, 2017.
- [24] T. Smart, H. Lomas, M. Massignani, M. V Flores-merino, L. R. Perez, and G. Battaglia, “Block copolymer nanostructures One of the most important classes of synthetic systems for creating,” *Rev. Lit. Arts Am.*, vol. 3, no. 3, pp. 38–46, 2008.
- [25] K. Knop, R. Hoogenboom, D. Fischer, and U. S. Schubert, “Poly(ethylene glycol) in drug delivery: Pros and cons as well as potential alternatives,” *Angew. Chemie - Int. Ed.*, vol. 49, no. 36, pp. 6288–6308, 2010.
- [26] Y. Mai and A. Eisenberg, “Self-assembly of block copolymers,” *Chem. Soc. Rev.*, vol. 41, no. 18, pp. 5969–5985, 2012.
- [27] M. Karayianni and S. P. Pispas, *Fluorescence Studies of Polymer Containing Systems*, vol. 16, 2016.
- [28] G. Gaucher, M. H. Dufresne, V. P. Sant, N. Kang, D. Maysinger, and J. C. Leroux, “Block copolymer micelles: Preparation, characterization and application in drug delivery,” *J. Control. Release*, vol. 109, no. 1–3, pp. 169–188, 2005.
- [29] M. Karimi *et al.*, *Smart micro/nanoparticles in stimulus-responsive drug/gene delivery systems*, vol. 45, no. 5. Royal Society of Chemistry, 2016.
- [30] T. Manouras and M. Vamvakaki, “Field responsive materials: photo-, electro-, magnetic- and ultrasound-sensitive polymers,” *Polym. Chem.*, vol. 8, no. 1, pp. 74–96, 2017.
- [31] S. Manchun, C. R. Dass, and P. Sriamornsak, “Targeted therapy for cancer using pH-responsive nanocarrier systems,” *Life Sci.*, vol. 90, no. 11–12, pp. 381–387, 2012.
- [32] S. Binauld and M. H. Stenzel, “Acid-degradable polymers for drug delivery: a decade of innovation,” *Chem. Commun.*, vol. 49, no. 21, p. 2082, 2013.
- [33] V. V. Pchelintsev, A. Y. Sokolov, and G. E. Zaikov, “Kinetic principles and mechanisms of hydrolytic degradation of mono- and polyacetals-A review,” *Polym. Degrad. Stab.*, vol. 21, no. 4, pp. 285–310, 1988.
- [34] R. F. Heller, J., Penhale, D. W. H. and Helwing, “Preparation of Polyacetals By the Reaction of Divinyl Ethers and Polyols,” *J. Polym. Sci. B Polym. Lett. Ed*, vol. 18, no. 4, pp. 293–297, 1980.

- [35] R. Tomlinson, M. Klee, S. Garrett, J. Heller, R. Duncan, and S. Brocchini, "Pendent chain functionalized polyacetals that display pH-dependent degradation: A platform for the development of novel polymer therapeutics," *Macromolecules*, vol. 35, no. 2, pp. 473–480, 2002.
- [36] R. Tomlinson, J. Heller, S. Brocchini, and R. Duncan, "Polyacetal-Doxorubicin Conjugates Designed for pH-Dependent Degradation," *Bioconjug. Chem.*, vol. 14, no. 6, pp. 1096–1106, 2003.
- [37] M. J. Vicent, R. Tomlinson, S. Brocchini, and R. Duncan, "Polyacetal-diethylstilboestrol: A polymeric drug designed for pH-triggered activation," *J. Drug Target.*, vol. 12, no. 8, pp. 491–501, 2004.
- [38] E. Schacht, V. Toncheva, K. Vandertaelen, and J. Heller, "Polyacetal and poly(ortho ester)-poly(ethylene glycol) graft copolymer thermogels: Preparation, hydrolysis and FITC-BSA release studies," *J. Control. Release*, vol. 116, no. 2 SPEC. ISS., pp. 219–225, 2006.
- [39] M. J. Heffernan and N. Murthy, "Polyketal Nanoparticles: A New pH-Sensitive Biodegradable Drug Delivery Vehicle," *Bioconjug. Chem.*, vol. 16, no. 6, pp. 1340–1342, 2005.
- [40] S. D. Khaja, S. Lee, and N. Murthy, "Acid-degradable protein delivery vehicles based on metathesis chemistry," *Biomacromolecules*, vol. 8, no. 5, pp. 1391–1395, 2007.
- [41] S. E. Paramonov *et al.*, "Fully acid-degradable biocompatible polyacetal microparticles for drug delivery," *Bioconjug. Chem.*, vol. 19, no. 4, pp. 911–919, 2008.
- [42] G. Pasparakis, T. Manouras, A. Selimis, and M. Vamvakaki, "Laser-Induced Cell Detachment and Patterning with Photodegradable Polymer Substrates," 2011.
- [43] G. Pasparakis, T. Manouras, P. Argitis, and M. Vamvakaki, "Photodegradable polymers for biotechnological applications," *Macromol. Rapid Commun.*, vol. 33, no. 3, pp. 183–198, 2012.
- [44] G. Pasparakis, T. Manouras, M. Vamvakaki, and P. Argitis, "Harnessing photochemical internalization with dual degradable nanoparticles for combinatorial photo-chemotherapy," *Nat. Commun.*, vol. 5, p. 3623, 2014.
- [45] V. S. Dogra, M. Zhang, and S. Bhatt, "High-Intensity Focused Ultrasound (HIFU) Therapy Applications," *Ultrasound Clin.*, vol. 4, no. 3, pp. 307–321, 2009.
- [46] L. G. Merckel *et al.*, "First clinical experience with a dedicated MRI-guided high-intensity focused ultrasound system for breast cancer ablation," *Eur. Radiol.*, vol. 26, no. 11, pp. 4037–4046, 2016.
- [47] R. L. Manthe, S. P. Foy, N. Krishnamurthy, B. Sharma, and V. Labhasetwar, "reviews Tumor Ablation and Nanotechnology," *Mol. Pharm.*, no. 3, pp. 1034–1044, 2010.
- [48] S. Kentish and M. Ashokkumar, "The Physical and Chemical Effects of Ultrasound," pp. 1–12, 2011.
- [49] T. Leong, M. Ashokkumar, and S. Kentish, "THE FUNDAMENTALS OF POWER ULTRASOUND – A REVIEW."
- [50] P. C. Lyon *et al.*, "Clinical trial protocol for TARDOX: A phase I study to investigate the feasibility of targeted release of lyso-thermosensitive liposomal doxorubicin (ThermoDox®) using focused ultrasound in patients with liver tumours," *J. Ther. Ultrasound*, vol. 5, no. 1, pp. 1–8, 2017.
- [51] J. O. S. M. J. Paulusse and R. P. Sijbesma, "Ultrasound in Polymer Chemistry :

- Revival of an Established Technique,” vol. 44, pp. 5445–5453, 2006.
- [52] E. W. Flosdorf and L. A. Chambers, “the Chemical Action of Audible Sound,” *J. Am. Chem. Soc.*, vol. 55, no. 7, pp. 3051–3052, 1933.
- [53] H. W. Melville and A. J. R. Murray, “The Ultrasonic Degradation of Polymers,” *Trans. Faraday Soc.*, vol. 46, no. 996, pp. 996–1009, 1950.
- [54] P. R. Gogate and A. L. Prajapat, “Depolymerization using sonochemical reactors: A critical review,” *Ultrason. Sonochem.*, vol. 27, pp. 480–494, 2015.
- [55] M. M. Caruso *et al.*, “Mechanically-Induced Chemical Changes in Polymeric Materials,” pp. 5755–5798, 2009.
- [56] M. Schaefer, B. Icli, C. Weder, M. Lattuada, A. F. M. Kilbinger, and Y. C. Simon, “The Role of Mass and Length in the Sonochemistry of Polymers,” 2016.
- [57] K. L. Berkowski, S. L. Potisek, C. R. Hickenboth, and J. S. Moore, “Ultrasound-induced site-specific cleavage of azo-functionalized poly(ethylene glycol),” *Macromolecules*, vol. 38, no. 22, pp. 8975–8978, 2005.
- [58] J. Li, C. Nagamani, and J. S. Moore, “Polymer Mechanochemistry: From Destructive to Productive,” *Acc. Chem. Res.*, vol. 48, no. 8, pp. 2181–2190, 2015.
- [59] J. N. Brantley, K. M. Wiggins, and C. W. Bielawski, “Polymer mechanochemistry : the design and study of mechanophores,” no. June 2012, pp. 2–12, 2013.
- [60] C. E. Diesendruck *et al.*, “low-ceiling-temperature polymer,” no. April, 2014.
- [61] N. Munshi, N. Rapoport, and W. G. Pitt, “Ultrasonic activated drug delivery from Pluronic P-105 micelles,” *Cancer Lett.*, vol. 118, no. 1, pp. 13–19, 1997.
- [62] A. Marin, H. Sun, G. A. Husseini, W. G. Pitt, D. A. Christensen, and N. Y. Rapoport, “Drug delivery in pluronic micelles: Effect of high-frequency ultrasound on drug release from micelles and intracellular uptake,” *J. Control. Release*, vol. 84, no. 1–2, pp. 39–47, 2002.
- [63] N. Rapoport, “Ultrasound Interactions with Polymeric Micelles and Viable Cells,” pp. 161–174, 2004.
- [64] H. Zhang, H. Xia, J. Wang, and Y. Li, “High intensity focused ultrasound-responsive release behavior of PLA-b-PEG copolymer micelles,” *J. Control. Release*, vol. 139, no. 1, pp. 31–39, 2009.
- [65] Y. Li, R. Tong, H. Xia, H. Zhang, and J. Xuan, “High intensity focused ultrasound and redox dual responsive polymer micelles,” *Chem. Commun.*, vol. 46, no. 41, p. 7739, 2010.
- [66] R. Tong, H. Xia, and X. Lu, “Fast release behavior of block copolymer micelles under high intensity focused ultrasound/redox combined stimulus,” *J. Mater. Chem. B*, vol. 1, no. 6, pp. 886–894, 2013.
- [67] R. Tong, X. Lu, and H. Xia, “A facile mechanophore functionalization of an amphiphilic block copolymer towards remote ultrasound and redox dual stimulus responsiveness,” *Chem. Commun.*, vol. 50, no. 27, pp. 3575–3578, 2014.
- [68] J. Wang, M. Pelletier, H. Zhang, H. Xia, and Y. Zhao, “High-frequency ultrasound-responsive block copolymer micelle,” *Langmuir*, vol. 25, no. 22, pp. 13201–13205, 2009.
- [69] J. Xuan, M. Pelletier, H. Xia, and Y. Zhao, “Ultrasound-induced disruption of amphiphilic block copolymer micelles,” *Macromol. Chem. Phys.*, vol. 212, no. 5, pp. 498–506, 2011.
- [70] Y.-K. Lin, Y.-C. Yu, S.-W. Wang, and R.-S. Lee, “Temperature, ultrasound

- and redox triple-responsive poly(N-isopropylacrylamide) block copolymer: synthesis, characterization and controlled release,” *RSC Adv.*, vol. 7, no. 68, pp. 43212–43226, 2017.
- [71] H. Zhang and E. Ruckenstein, “Self-polyaddition of hydroxyalkyl vinyl ethers,” *J. Polym. Sci. Part A Polym. Chem.*, vol. 38, no. 20, pp. 3751–3760, 2000.
- [72] K. Kunal, C. G. Robertson, S. Pawlus, S. F. Hahn, and A. P. Sokolov, “Role of chemical structure in fragility of polymers: A qualitative picture,” *Macromolecules*, vol. 41, no. 19, pp. 7232–7238, 2008.
- [73] A. Grönroos, P. Pirkonen, and O. Ruppert, “Ultrasonic depolymerization of aqueous carboxymethylcellulose,” *Ultrason. Sonochem.*, vol. 11, no. 1, pp. 9–12, 2004.
- [74] H. Cabral *et al.*, “Accumulation of sub-100 nm polymeric micelles in poorly permeable tumours depends on size,” *Nat. Nanotechnol.*, vol. 6, no. 12, pp. 815–823, 2011.

APPENDIX: Characterization Techniques

1) Gel Permeation Chromatography (GPC)

Gel permeation chromatography (GPC) or size exclusion chromatography (SEC), is a well-known polymer separation method that allows determination of the polymer molecular characteristics such as average molecular weight and molecular weight distribution. In general GPC is an important analytical tool used to evaluate molecular characteristic of natural or synthetic polymers and proteins. In a GPC instrument are usually involved a pump, a detector (e.g. UV or RI or both) and one, two or more separating columns (**Figure 1A**). The columns or the stationary phase are filled with porous bead such as polystyrene gels (**Figure 1B**). The beads are made with a variety of pore size that span the range of the sizes of the macromolecules to be separated. The pump circulates solvent (mobile phase) through the gel columns resulting in swollen of the gel material into the column. A small amount of diluted polymer solution in the same solvent with the mobile phase is injected into the flowing solvent entering the columns. As the polymer solution passes through the columns, the largest polymer coils are excluded from all but the largest pores and elute from the column first. Right after, smaller polymer coils can pass through smaller pores and excluded later from the columns (**Figure 1C**). Thus, to be more precise, GPC separates molecules by their size in solution which is their hydrodynamic volume (V_h). After separation, the solution passes through the detectors that are used in the system and are analyzed upon proper calibration with narrow molar mass distribution standards.

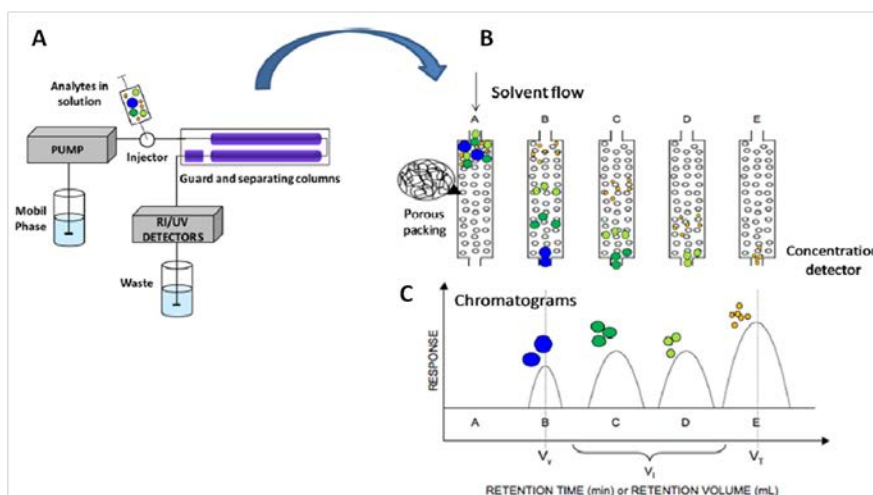


Figure 1: Schematic illustration of GPC instrument. **A)** Main parts of a GPC, **B)** separation columns and **C)** representative retention time of a polymer depending on its size.

2) ^1H -NMR spectroscopy

NMR spectroscopy is a very useful and common technique for the determination of the chemical structure of chemical compounds. ^1H -NMR and ^{13}C -NMR are the most commonly used for the characterization of materials. NMR is a spectroscopic technique to observe local magnetic fields around atomic nuclei. The sample with the material is placed in a magnetic field and the NMR signal is produced by excitation of the nuclei of the sample with radio waves into nuclear magnetic resonance which is detected with sensitive radio receivers (**Figure 2**).

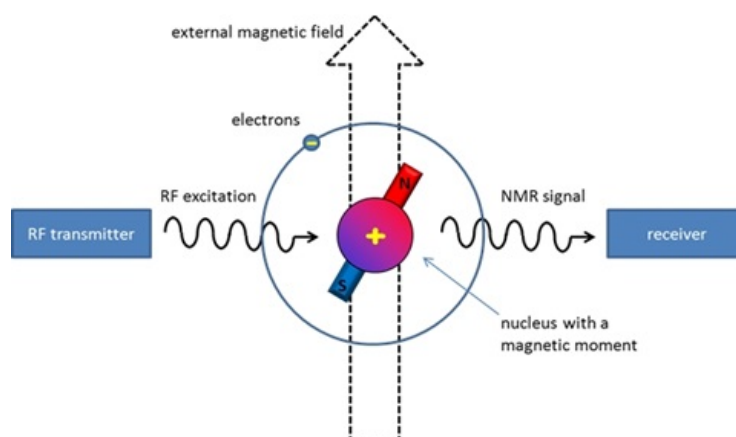


Figure 2: The nuclear magnetic resonance phenomenon.

Different nuclei absorb electromagnetic irradiation at different wavelength depending on the chemical and electronic environment. The position and the pattern of the NMR signal provide the required information regarding the environment of the nuclei. The exact field strength (in ppm) of a nucleus comes into resonance relative to a reference standard, usually the signal of the deuterated solvent used. Electron clouds shield the nuclei from the external magnetic field causing them to absorb at higher energy (lower ppm) while the neighboring functional groups “deshield” the nuclei causing them to absorb at lower energy (higher ppm). Chemically and magnetically equivalent nuclei resonate at the same energy and give a single signal or pattern. Protons on adjacent carbons interact and split each other’s resonances into multiple peaks following the n+1 rule with coupling constant J. Spin-spin coupling is commonly observed between nuclei that are one, two and three bonds apart. The area under an NMR resonance is proportional to the number of nuclei that give rise to that resonance, thus by integration the protons of that resonance can be calculated.

3) Ultraviolet-Visible spectroscopy (UV/Vis)

UV/Vis spectroscopy is a commonly used technique for the characterization and analysis of both organic and inorganic materials. Also, it is used for the quantitative determination of loaded molecules into nanoparticles. The range of wavelengths that are corresponded to UV/Vis spectrum is from 200 to 800 nm, from which 200-400 nm is the ultraviolet region 400-800 nm is the visible region. When molecules that contain π -electrons are strike by UV/Vis light then the molecules absorb this energy and electronical transitions are occurred. The absorbance A can be defined by the Beer-Lambert law that correlates the absorption with the concentration of the absorbing species as shown in the below equation:

$$A = \log_{10} (I_0/I) = \epsilon * L * c$$

Where (I_0) is the intensity of the incident light, (I) is the intensity of the transmitted light, (ϵ) is the absorption coefficient, which is constant for a specific substance and depends on the wavelength, the solvent and the temperature, (L) is the path length through the sample and (c) the concentration of the sample.

A typical UV/Vis spectrometer is shown in **Figure 3**. A beam of light from a light source is separated into its component wavelengths by a prism or diffraction grating. Each monochromatic (single wavelength) beam in turn is split into two equal intensity beams by a beam splitter. One beam, the sample beam, passes through a small the cuvette containing a solution of the compound being studied in a transparent solvent. The other beam, passes through an identical cuvette containing only the solvent. The intensities of these light beams are then measured by electronic detectors and compared. The intensity of the reference beam, which should have suffered little or no light absorption, is defined as I_0 . The intensity of the sample beam is defined as I . Over a short period of time, the spectrometer automatically scans all the component wavelengths in the manner described.

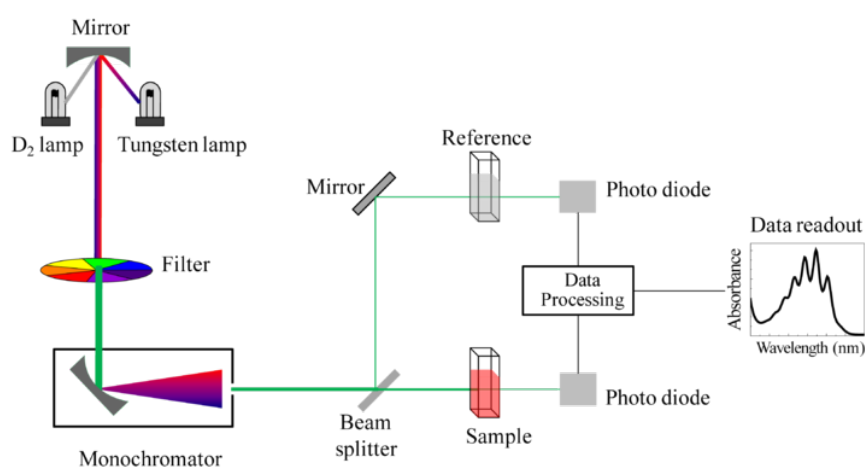


Figure 3: Schematic representation of a UV/Vis spectrophotometer.

4) Scanning electron microscopy (SEM)

Scanning electron microscopy is designed to provide high-resolution images of a sample placed on a surface. A tungsten filament emits electrons, which are focused by an electron optical system. The electron beam can scan the sample surface and can provide composition at a point, along a line or over a rectangular area, by scanning the beam across the surface in a series of parallel lines. The sample is mounted on a stage that can be accurately moved in all three directions (x, y and z), normal to the plane of the sample.

The instrument generally operates in a high vacuum a very dry environment in order to produce the high energy beam of electrons needed for imaging. Thus, most specimens destined for study in the SEM are poor conductors. In the SEM, the

imaging system depends on the specimen being sufficiently electrically conductive to ensure that the bulk of the incoming electrons go to ground. The formation of the image depends on collecting the different signals that are scattered as a consequence of the high electron beam interacting with the sample. The two principal signals used to form images are backscattered and secondary electrons generated within the primary beam-sample interactive volume. The backscattered electron coefficient increases with increasing atomic number of the specimen, whereas the secondary electron coefficient is relatively insensitive to atomic number. This fundamental difference in the two signals has an important effect on the way samples may need to be prepared. The use of scanning electron microscopy may be considered when being able to interpret the information obtained from the SEM and attempt to relate the form and structure of the two-dimensional images and identity, validity and location of the chemical data back to the three-dimensional sample from which the information was derived. A schematic representation of a SEM instrument is shown in **Figure 4**.

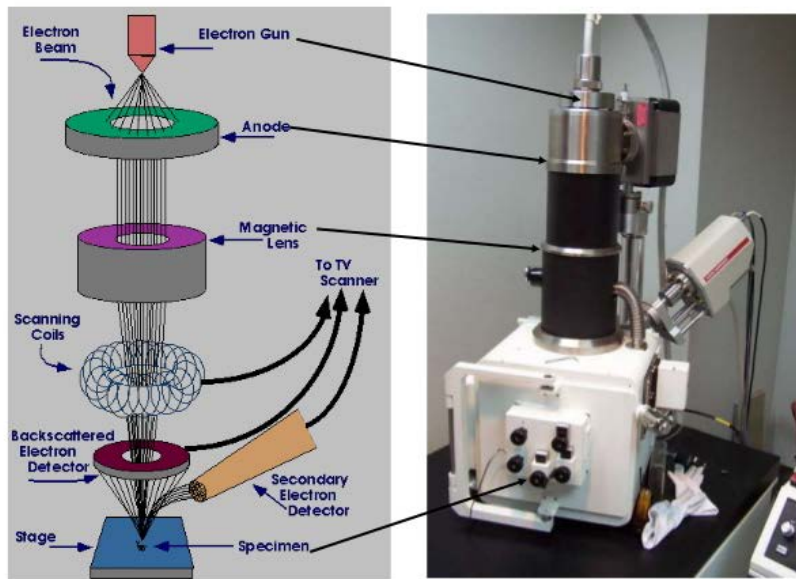


Figure 4: A typical SEM setup.

5) Dynamic light scattering (DLS)

Light scattering is a powerful tool for the characterization of the size of polymer nanoparticles in a solution. The monochromatic, coherent laser beam hits the particles, which is scattered and due to the Brownian motion of the particles that changes their distance in the solution a time-dependant fluctuation of the scattering intensity is observed. Changing the observation angle (θ) and thus the scattering vector (q) a measure of the size is provided. The form factor that is the interference pattern of the scattered light is characteristic of the size and shape of the scatterer. The larger the particle is the slower the Brownian motion. Accuracy and stability of the temperature during the entire measurement is essential since the viscosity of the liquid is related to the temperature (**Figure 5**).

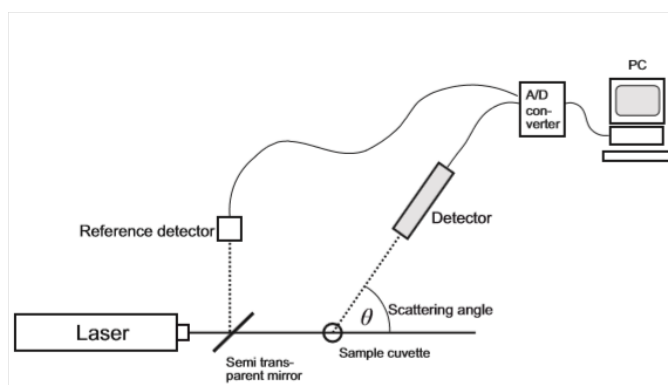


Figure 5: Schematic representation of the experimental setup of the dynamic light scattering technique.

The velocity of the Brownian motion is defined by the translational diffusion coefficient (D). The Stocks-Einstein equation is used in order to calculate the particles size based on the translational diffusion coefficient:

$$R_h = \frac{k_B T}{6\eta\pi D}$$

Where, (R_h) is the hydrodynamic radius, (η) is the viscosity of the solvent, (k_B) is the Boltzmann constant and (T) is the temperature.

The hydrodynamic radius refers to how the particle diffuses within the liquid solvent and is the same as that of a hard sphere with the same translation diffusion coefficient (D) as the particle. The translation diffusion coefficient depends on various factors such as the size of the particle, the surface structure, the concentration of the sample and the type of ions in the medium. As shown in **Figure 6** for a system of particles under constant, random Brownian motion a speckle pattern is observed. The phase addition from the moving particles is constantly evolving and forming new patterns. These intensity fluctuations of the scattered light are depending on the size of the particles and the time. Small particles cause the intensity to fluctuate more rapidly than larger ones.

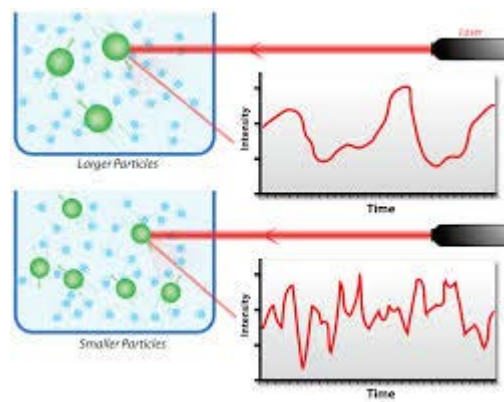


Figure 6: Schematic illustrations of the intensity fluctuations of larger and smaller particles.

For a large number of monodisperse particles in Brownian motion, the correlation function (G) is an exponential decaying function of the correlator time delay (τ):

$$G(\tau) = A[1 + B \exp(-2\Gamma\tau)]$$

Where (A) is the baseline of the correlation function, (B) is the intercept of the correlation function and (Γ) is given by the equation:

$$\Gamma = Dq^2$$

Where (D) is the translational diffusion coefficient and the wavevector (q) is given by the equation:

$$q = \frac{4\pi n}{\lambda} \sin\left(\frac{\theta}{2}\right)$$

Where (n) is the refractive index of the dispersant, (λ) is the wavelength of the laser and (θ) is the scattering angle.